NTNU

Norwegian University of
Science and Technology

Design, numerical modelling and analysis of a spar floater supporting the DTU 10MW wind turbine

Wenfei Xue

Marine Technology
Submission date: June 2016
Supervisor: Zhen Gao, IMT

Norwegian University of Science and Technology
Department of Marine Technology

NTNU – Trondheim
Norwegian University of
Science and Technology

Design, numerical modelling and analysis of a spar floater supporting the DTU 10MW wind turbine

XUE, WENFEI

JUNE 2016

MASTER THESIS

Department of Marine Technology

Norwegian University of Science and Technology

Approved by:

Supervisor:
Prof. Zhen Gao

PREFACE

Nowadays, wind energy is one of the most promising, sustainable and clean energy solutions for the future. The wind industry in Europe experiences a very fast development these years, moving from onshore to offshore in shallow water and then in deep water. A floating wind turbine is an offshore wind turbine mounted on a floating structure that allows the turbine to generate electricity in water depths where bottom-fixed towers are not accessible.

However, the offshore wind energy still has its shortcoming, i.e. the high cost. The most effective way to reduce the cost of energy is to use a larger wind turbine, which can absorb more wind power. So a new design of offshore wind turbine need to be considered.

In this thesis, a new spar-buoy concept was developed based on the "OC3-Hywind" concept which developed by National Renewable Energy Laboratory (NREL), to support the DTU 10MW reference wind turbine. An initial design is performed by upscaling of an existing 5MW spar platform design, then checked against buoyancy, stability, hydrodynamic and strength criteria. In addition, a spread catenary mooring system has been designed for the spar concept.

Then the SIMO-RIFLEX-AeroDyn model is established include viscous drag elements. It is found that the blade pitch controller can excite large platform resonant motion at above rated wind speeds during turbulent wind test, which could be possibly reduced by changing the PI gains of the controller.

Finally, time domain coupled dynamic analysis of the spar floating wind turbine is performed by using the SIMO-RIFLEX-AeroDyn code. Characteristic responses of the spar floating wind turbine are studied and compared to other two floating wind turbine concepts. It is found that spar has the largest surge oscillations among three concepts, yet the semi has largest pitch mean value and standard deviation than others. Due to the taut mooring system, all the motions for the TLP is much smaller as compared to the spar and the semi.

ACKNOWLEDGMENTS

Foremost, I would like to express my sincere gratitude to my advisor Prof. Zhen Gao at Norwegian University of Technology and Science (NTNU) for the continuous support of my master study and research, for his patience, motivation, enthusiasm, and immense knowledge. His guidance helped me in all the time of research and writing of this project thesis. He is actually a good advisor and mentor for my master study in NTNU.

My sincere thanks also goes to PhD candidate Chenyu Luan, for his encouragement, insightful comments, and kindness in helping me with the thesis work. His help means a lot for me.

Besides, I would like to thank Associate Professor Erin Bachynski, who gave me considerable help during the coupled dynamic analysis of floater wind turbine.

I am thankful to master students Xiaoshuang Tian and Touhidul Islam for their selfless help and support during the master thesis work. I enjoyed the time when we worked together.

Finally, I would like to thank my family, for their understanding, support and love.

Trondheim, Norway Xue, Wenfei

June 9, 2016

TABLE OF CONTENTS

LIST OF TABLES

Table Page

LIST OF FIGURES

Figure Page

LIST OF ABBREVIATIONS

1P	Rotational frequency of turbine blade
3P	Blade passing frequency for a three bladed wind turbine
BEM	Blade Element Momentum
CM	Center of Mass
COB	Centre of Buoyancy
COG	Centre of Gravity
DNV	Det Norske Veritas
DOF	Degree of Freedom
DTU	Technical University of Denmark
FFT	Fast Fourier Transform
GDW	Generalized Dynamic Wake
GM	Metacentric Height
NREL	National Renewable Energy Laboratory
rpm	Revolutions per minute
RWT	Reference Wind Turbine
SRA	SIMO-RIFLEX-AeroDyn
SS	Semi-Submersible
SWL	Still Water Level
TLP	Tension Leg Platform
ULS	Ultimate Limit State
VCG	Vertical center of gravity

1 CHAPTER I: INTRODUCTION

1.1 Background

Energy is the topic of most concern for human society. Traditional energy source like oil and gas still play a dominant role in energy consumption but also be connected with many environmental problems, such as greenhouse effects and air pollution. To deal with that, much attention has been drawn to renewable energy, e.g. the wind energy.

Nowadays, there is a consensus that wind energy is one of the most promising, sustainable and clean energy solutions for the future. The wind resource is renewable and the process of using wind energy has very little CO2 emissions compared to other sources of electrical power. So the wind energy is seen as a good method to reaching the European Union's Renewables Directive: at least 20% of the member countries' total energy consumption should be covered by renewable sources of energy within the year 2020. [21]

The wind industry in Europe experiences a very fast development these years, moving from onshore to offshore in shallow water and then in deep water. This trend is mainly due to the limitations in available wind farm sites on land; and the higher wind speeds, less turbulent wind patterns, less noise and visual effects for human living area of offshore wind turbines, compared to the land-based wind turbines [1][2].

The offshore wind energy already plays a significant role in the European power sector, since the success of the first offshore wind farm at Vindeby in Denmark in 1991. In 2015, the wind industry installed 3,019 MW in the EU - more than gas and coal combined, as shown in *Figure 1-1*. The wind energy today can cover 1.5% of EU's total electricity demand with a cumulative capacity of 11,027 MW at the end of 2015. In total, there are 84 offshore wind farms in 11 European countries by now, including the sites under construction. [22]

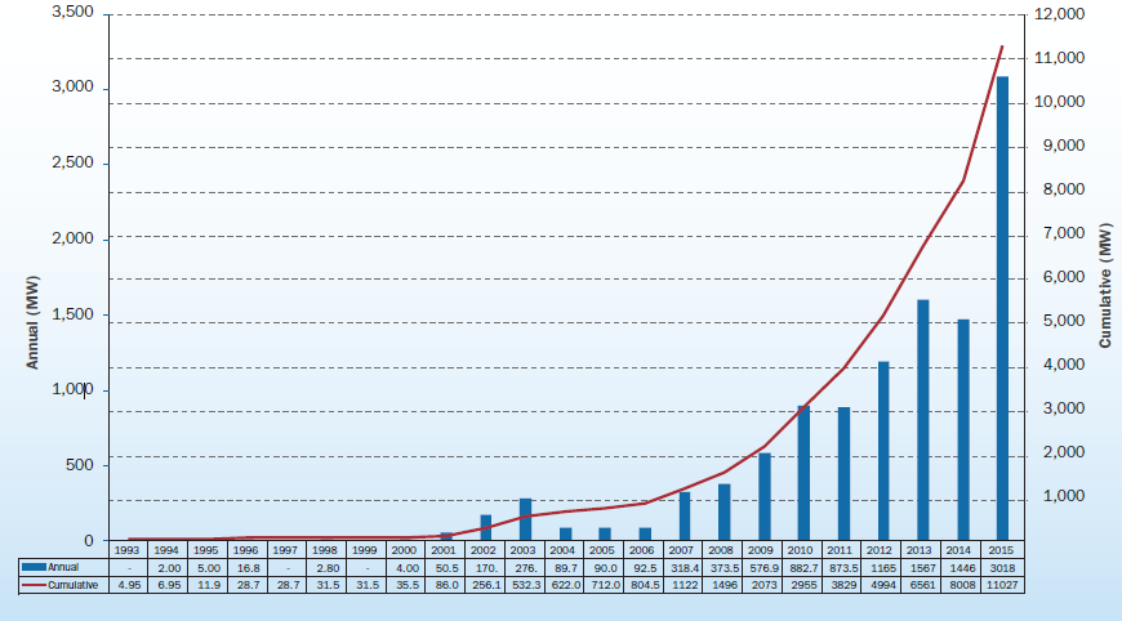

	1993	1994	1995	1996	1997	1998	1999	2000	2001	2002	2003	2004	2005	2006	2007	2008	2009	2010	2011	2012	2013	2014	2015
Annual	-	2.00	5.00	16.8	-	2.80	-	4.00	50.5	170.	276.	89.7	90.0	92.5	318.4	373.5	576.9	882.7	873.5	1165	1567	1446	3018
Cumulative	4.95	6.95	11.9	28.7	28.7	31.5	31.5	35.5	86.0	256.1	532.3	622.0	712.0	804.5	1122	1496	2073	2955	3829	4994	6561	8008	11027

Figure 1-1: Cumulative and annual offshore wind installations (MW) ([22])

However, the offshore wind energy still has its shortcoming, i.e. the high cost. Cost reduction is one of the main challenges for offshore wind turbines, in particular for floating concepts. The most effective way to reduce the cost of energy is to use a larger wind turbine, which can absorb more wind power. So a new design of offshore wind turbine need to be considered. This is the key motivation for this thesis work.

1.2 Floating Wind Turbine Concepts

A floating wind turbine is an offshore wind turbine mounted on a floating structure that allows the turbine to generate electricity in water depths where bottom-fixed towers are not accessible [4]. The first concept of floating wind turbine system was introduced in 1970s by professor Heronemus from the University of Massachusetts at Amherst [5]. It was not until the mid-1990s, after the commercial wind industry was well established, that the concept was taken up again by the mainstream researchers [6]. After decades of development, a wide variety of floating wind turbine concepts have already been proposed, such as spar, semi-submersible, and tension leg platforms (TLP). In 2008, the first scaled prototype, Blue H, was installed at the water depth of 113 m offshore Italy.

By now, two full-scale floating wind turbines, which are the Spar-type Hywind (Bratland, 2009) and the Semi-submersible-based WindFloat (Weinstein, 2009), had been installed for concept demonstrations.[23] In addition to that, several scaled prototype floating wind turbines have also been installed for testing.

Currently, most commercial offshore wind turbine projects are limited to a water depth less than 50m with bottom fixed structures – such as monopile, gravity, or jacket structures – and already came into service. However, in order to access a larger wind resource and move the noise and visual effects to farther offshore area, wind turbine support platforms for intermediate water depth (45 - 150 m) and deep water (> 150 m) are necessarily being considered. At these depths, floating platforms will have lower design and installation costs than gravity and monopile foundations, although fixed jacket structures may be appropriate for some intermediate depths (45 - 80 m) [3].

The stability of the floating wind turbine is a big challenge, since the typical large top mass and large thrust force acting at a height more than 80m above the sea level. Generally there are three different strategies of solution to this challenge, based on how the structure reach the stability in pitch/roll [8]:

- Gravity-based, with the center of gravity under center of buoyancy. Spar is a typical gravity-based platform.

- Waterplane area based, with a large free surface area to achieve large moment of inertia. Semi-submersible belongs to this kind of platforms.

- External constrain based, with large external mooring forces to keep the platform stable, such as the tension-leg platform (TLP).

Here all the three strategies are briefly discussed in the following [7][8]:

Spar: A gravity stabilized structure which usually has a very large draft. That’s why spar usually has good stability and small heave motions. What’s more, the deep draft design of spars makes them less affected by wind, wave and current. However, it cannot be used in

less than 100m of water depth, due to the necessary draft. And the large draft may make it difficult for major maintenance of structure.

Semi-submersible: A waterplane area moment of inertia stabilized structure with flexible draft capability. It obtains its buoyancy from ballasted, watertight pontoons located below the ocean surface and wave action. The structure can operate in different draft, allows it to be completely assembled in shipyard and then towed to its installation site. A main problem is that semi-submersible may experience large heave motions in waves.

Tension-leg platform: The platform is permanently moored by devices like tethers or tendons grouped at each of the structure's corners. The motion of the platform is limited due to the external tendons or tethers. However, there are difficulties with the natural frequency similarities and the potential of structural coupling between the wind turbine and the tendons. And it also hard to tow-back for a major maintenance.

The examples of the three types of floating wind turbine platforms are shown in *Figure 1-2*.

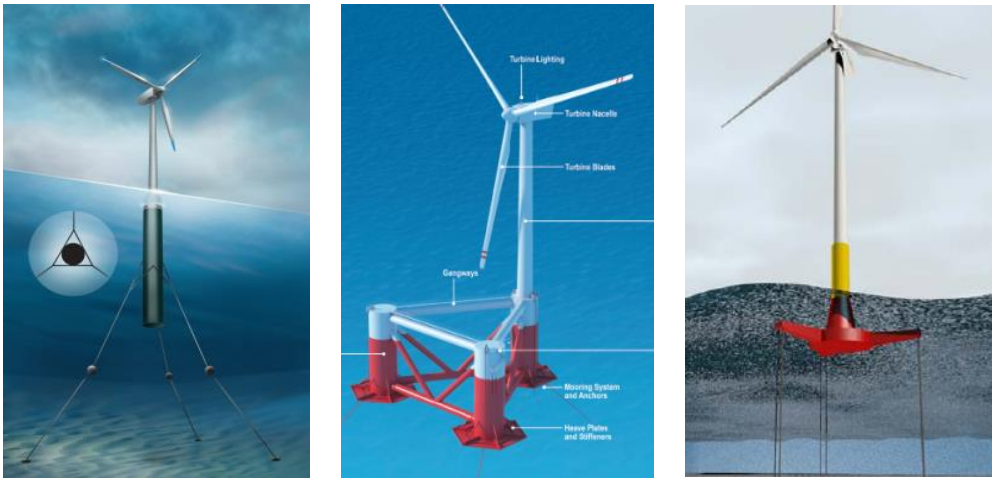

Figure 1-2: Floating wind turbine platforms (left to right: spar, semi-submersible, TLP)

Numerous floating platform concepts are accessible for offshore wind turbines, including the three types above and also hybrid concepts of them, which have different advantages

and disadvantages respectively. When considering a floating structure for an offshore wind turbine, several logistical and economic considerations need to be evaluated.

1.3 Research in Spar Wind Turbine Concepts

In this thesis, the spar-buoy concept named "Hywind", developed by Statoil of Norway, was chosen for the upscaling and modeling activities. Hywind is the first floating wind turbine that reached the stage of full-scale prototype testing. It combines known technologies in a completely new setting and has a vast potential for future development. As shown in *Figure 1-3*, the Hywind concept consists of a concrete or steel cylinder with ballast. The floater draft is 120 m and a 3-point catenary mooring system is used for station-keeping. This concept was known for its simplicity in design, suitability to modeling, and potential prospect to commercialization [9]. A general introduction of Hywind concept can be found in Gjørv (2006) and Larsen (2008) [23].

Figure 1-3: The Hywind concept

Based on the Hywind concept, several studies were further carried out to assess the load and response characteristics of floating wind turbines. It was selected by the IEA Wind Task 23 Offshore Code Comparison Collaboration (OC3) for software tool comparisons. Based on the concept design data, the Hywind concept was modified in order to support the NREL 5-MW baseline offshore wind turbine. The new modified Hywind was known "OC3-Hywind", which was the original case for this thesis work. The detail of "OC3-

Hywind" can be seen in "Final Technical Report - IEA Wind Task 23 Offshore Wind Technology and Deployment" [25].

There are also several other concepts for the spar floater, for example, the SWAY concept. The SWAY concept consists of a deep draft column with ballast in the bottom. Similar to the Hywind concept, the center of gravity of the SWAY concept is designed to be far below the center of buoyancy of the column to provide sufficient stability and the required hydrodynamic characteristics [23]. The floater is anchored to the seabed by a tendon and a suction anchor [23]. The detail of SWAY concept is in below:

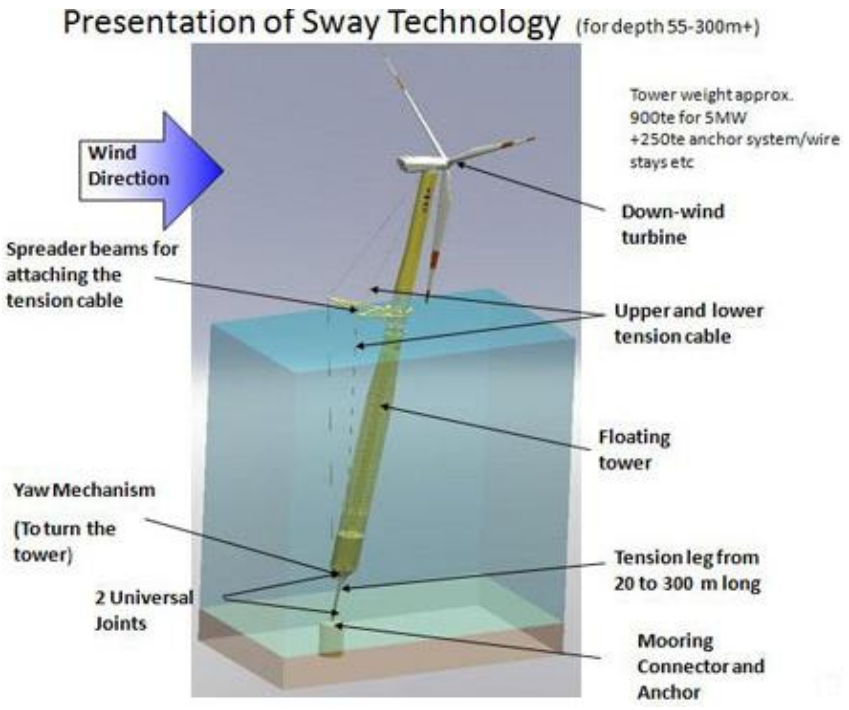

Figure 1-4: The SWAY concept

1.4 Mooring System

All floating structures (Semi-submersible, Spar, and TLP) are positioned by a station-keeping system. Mooring systems and thrusters are the traditional ways of sea-keeping, but for floating wind turbines, the particular choice until now is the mooring system. A mooring system consists of several cables with their upper ends attached to different

positions of the floater and their lower ends anchored at the seabed [15]. There are three typical types of mooring systems [24]:

Catenary Line Mooring

The oldest and still most common mooring systems, which obtains restoring force mainly by lifting and lowering the weight of mooring line. In a spread mooring system, several pre-tension anchor lines are arrayed around the structure to keep it in the wanted location. For this system, a large part of the anchor line need to lie on the sea bed, to ensure that the anchors are kept in position.

Taut Line Mooring

The mooring system has a pattern of taut, light-weight lines radiating outward, and gets its restoring force primarily from elastic stretch of the line itself. The lines have a low net submerged weight, so that the catenary action can be eliminated. Synthetic fibers are most common for this type of mooring.

Tension Leg Mooring

Specially be used for tension leg platforms (TLP). The buoyancy of the platform exceeds its weight and a net downward force is supplied by the vertically tensioned mooring, secured by deadweight or anchor piles at seabed.

Many studies have been carried out for the characteristics of these mooring systems above. For the catenary line mooring system and taut line mooring system, clump weights or buoys can be attached to the mooring lines to improve the performance of system [26]. The detail about criteria, technical requirements and guidelines on design and construction of mooring systems can be found in the design code DNV-OS-E301[27].

For a spar floater, a spread mooring system composed of either a chain-wire-chain or chain-polyester-chain configuration is usually applied [28]. The floater is permanently anchored to the seabed by its mooring lines. The Statoil's Hywind platform applied a system consists of three catenary lines. In order to increase the system's yaw stiffness,

these lines are attached to the platform via a so-called “crowfoot” (delta connection). What’s more, each line consists of multiple segments of varying properties and a clump weight[9]. [9]

1.5 Tool for Coupled Dynamic Analysis of Floating Wind Turbines

A floating wind turbine system includes rotor, nacelle, tower, platform and mooring system. Uncoupled dynamic analysis is suited for a fixed wind turbine system, but not for a floating wind turbine system. Karimirad [38] points out that the coupling of the top-side and the floater is important for a floating wind turbine system. So it’s necessary to combine the nonlinear, dynamic response of wind turbine with floater and mooring system, which requires a nonlinear stochastic time-domain analysis tools that can be used with hydro-elastic-aero-servo simulations. Until now, several numerical tools are available for the coupled dynamic analysis of floating wind turbines, such as FAST, HAWC2 and SIMO/RIFLEX.

In this paper, a numerical code named “SIMO-RIFLEX-AeroDyn” is applied for the analysis. SIMO is a time domain simulation program developed by MARINTEK for multi-body system [39]. RIFLEX is a non-linear FEM program also developed by MARINTEK for static and dynamic analysis of slender marine structures [40]. SIMO-RIFLEX is the state-of-the-art tool for dynamic response analysis of moored offshore structures.

Besides, RIFLEX is extended with AeroDyn code by Bachynski to include the aerodynamic forces on elastic structural members. It consists of the aerodynamic loads and the control system implementation for blade pitch and electrical torque for power extraction. Taken together with the coupled SIMO code, the extension to RIFLEX yields the coupled SIMO-RIFLEX-AeroDyn (SRA) code, which can do the time domain simulation for offshore wind turbine. The SRA code is well applied by Bachynski for the analysis of TLP floating wind turbines, which is detailed documented in her PhD thesis [41].

1.6 Thesis Overview

The aim of this thesis is to study the theoretical feasibility of supporting a DTU 10MW wind turbine by a spar-type platform. The thesis is organized in the following way:

Chapter 1: the general background of offshore wind energy and the literature review of floating wind turbine, mooring system and coupled dynamic analysis tool.

Chapter 2: the theoretical background of floater hydrostatics, linear and nonlinear floater hydrodynamics, as well as the aerodynamics and operating performance of wind turbine.

Chapter 3: the introduction of DTU 10MW reference wind turbine and comparison with the NREL 5MW baseline turbine. In addition, a reference site is chosen and three operational load cases and one extreme load case has been selected.

Chapter 4: a brief summary of previous project about the initial design of spar floater. The design is made by upscaling of an existing 5MW OC3-Hywind design, then checked against buoyancy, stability and hydrodynamic performance within frequency domain.

Chapter 5: the preliminary mooring system design. Free decay test has been performed to determine the characteristic of the mooring system. In addition, an extreme condition test with ULS check has also been performed.

Chapter 6: the SIMO-RIFLEX-AeroDyn model is made, several tests have been performed to check the model. Coupled dynamic analysis has been performed for the floating wind turbine system under different load conditions. Characteristic responses of the spar floating wind turbine are studied.

Chapter 7: the comparison of dynamic analysis result with another two concepts (TLP and Semi-submersible). A brief discussion of the three concepts' performance is made.

Chapter 8: Conclusions of the thesis work and recommendations for future work.

CHAPTER I: INTRODUCTION

2 CHAPTER II: THEORETICAL BACKGROUND

Spar floating wind turbines are complex systems, which must be analyzed in a multidisciplinary context, including at structural mechanics, hydrodynamics, aerodynamics, and controller.

This thesis is mainly focus on the structure's motions, hydrostatic stability, hydrodynamic and aerodynamic performance, so the relevant theoretical background for analysis is discussed in this chapter.

2.1 Rigid-body Motions and Basic Assumption

Any ships and ocean structures in the relevant sea conditions (waves, current & wind), will subject to the induced loads and motions. It requires a definition of the motions because different types of motions can be relevant for different marine structures.

In case of large motions, it is natural to find them in a reference frame moving with the body. In the linear seakeeping, the oscillatory translational and rotational motions are defined in the inertial reference frame Earth-fixed or translating with the vessel speed if any, and then the motions can be found by applying directly the Newton's second law. In the linear system, the oscillatory translational and rotational motions are defined respectively as: surge, sway, heave, roll, pitch and yaw (*Figure 2-1*) [17].

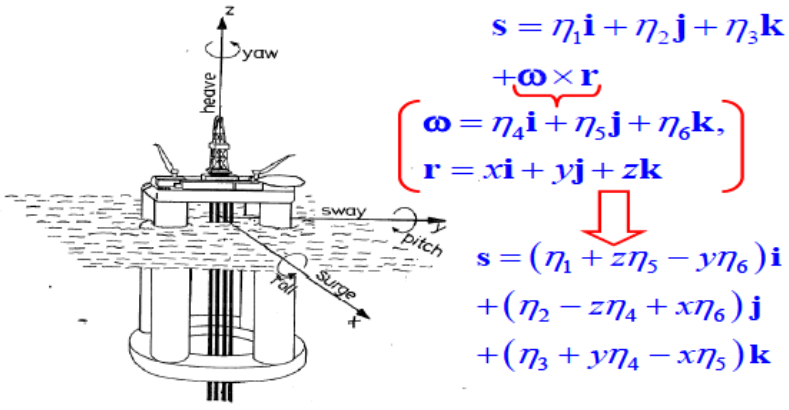

Figure 2-1: Coordinate system & Rigid-body motions

The definition of degrees of freedom for floating wind turbines by DNV is shown in *Table 2-1* below:

Degree of freedom	Description
Surge	Translation along the longitudinal axis (main wind direction), x-axis
Sway	Translation along the lateral axis (transversal to main wind direction), y-axis
Heave	Translation along the vertical axis, z-axis
Roll	Rotation about the longitudinal axis, x-axis
Pitch	Rotation about the lateral axis, y-axis
Yaw	Rotation about the vertical axis, z-axis

Table 2-1: Definition of degrees of freedom

Strip Theory

Strip theory is a linear, approximate theory and it is useful for estimating loads on ships and elongated parts of ocean structures.[17]

The basic assumption behind strip theory is that we are dealing with a slender body, i.e. long and thin (2D and no end effects). The body is divided into many thin strips, and the loads are calculated for each strip independently. Finally, the loads are integrated along the x-axis to compute the 3D loads.

If there is no forward speed, then the strip theory can be used for the radiation problem and the frequency of the oscillations corresponds to wave length that has the same order of magnitude as the cross-sectional dimension in the (y, z)-plane. In the case, flow variations occur mostly in the (y, z)-plane, and the 3D problem can be treated as a sum of 2D problems. But it's not suit for the structure with a non-zero forward speed, or the waves are larger than the mentioned limit. [17]

For the diffraction problem, strip theory is applicable if the order of magnitude of the wave lengths are large relative to the cross-section in the (y, z)- plane. In this case, the flow variations occur mainly along the x-axis, and crossflow is less important.[17]

2.2 Floater Hydrostatics

Hydrostatics is a branch of physics which generally deals with the characteristics of fluids at rest and especially with the pressure distribution in a fluid or exerted by a fluid on an immersed body. There are no shearing stresses represented, and the pressure (p) depends only on depth z [14]. For an incompressible fluid with density ρ,

$$dp/dz = -\rho g \tag{2.1}$$

where g is the acceleration due to gravity.

The distribution of hydrostatic pressure gives rise to the mean loading on the hull of the structure, which is an important load component for detailed design. What's more, hydrostatic pressure can affect the stability of free-floating structures according to recent criteria for offshore structures [15][16].

Considering the spar platform as a rigid body, the hydrostatic stiffness depends only on the waterplane geometry, the overall center of buoyancy (z_B) and the overall center of gravity (z_G). The expressions below [15] can be used to determine the nonzero terms in the hydrostatic stiffness matrix for a body with x-z symmetry.

$$C_{33} = \rho g A_w \tag{2.2}$$

$$C_{35} = C_{53} = -\rho g \int_{A_w} x dS \tag{2.3}$$

$$C_{44} = \rho g V(\int_{A_w} y^2 dS + z_B + z_G) = \rho g V \overline{GM_T} \tag{2.4}$$

$$C_{55} = \rho g V(\int_{A_w} x^2 dS + z_B + z_G) = \rho g V \overline{GM_L} \tag{2.5}$$

In expressions above, A_w is the waterplane area and V is the displacement volume. The waterplane inertia moment (I_T) is the same about all axes. For a Spar with circular waterplane and diameter D:

$$C_{35} = C_{53} = 0 \tag{2.6}$$

$$A_w = \pi D^2/4 \tag{2.7}$$

$$I_T = \pi D^4/64 \tag{2.8}$$

For hydrostatics, the intact stability is an important requirement for the initial design of an offshore structure. Taking a vessel as an example, from *Figure 2-2* we can see that point *B* is the center of buoyancy, point *G* is the center of gravity, point *F* is the center of flotation, points M_T is the metacenter of roll and GM_T is the metacentric height of roll. *GZ* is the righting arm.

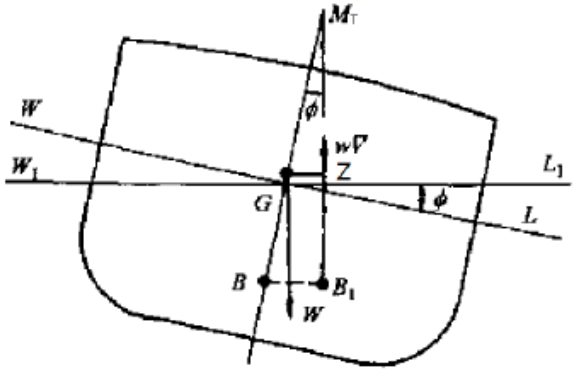

Figure 2-2: Metacenter and metacentric height in roll

Take roll motion as an example, under the conditions of tilting of a small angle, the righting moment can be expressed as

$$M_R = \Delta\overline{GZ} = \Delta\overline{GM_T}\sin\varphi = \rho\nabla\overline{GM_T}\sin\varphi \tag{2.9}$$

Where ρ is the density of seawater, ∇ is the volume of displacement and φ is the angle of transverse inclination. If M_R is positive, the structure can return to its initial balanced position when the external force disappears. Otherwise, the structure will not return to its initial balanced position.

$$\overline{GM} = \overline{BM} - \overline{BG} \tag{2.10}$$

$$\overline{BM} = \frac{I_T}{\nabla} \tag{2.11}$$

Where BM is metacentric radius, I_T is the moment of waterplane area about ox axis which depends on water plane area and radii of gyration.

2.3 Floater Hydrodynamics

The majority of the calculations and analysis in this project are based on potential theory. The most of details are taken from the book "*Sea Loads on Ships and Offshore Structures*" written by Prof. Faltinsen [15].

2.3.1 Governing Equations

In potential flow theory, the basic assumptions are that the fluid is inviscid, irrotational and incompressible. Combining these assumptions with linear theory, the linear wave body interaction problem simplifies to find the velocity potential ϕ which is shown as:

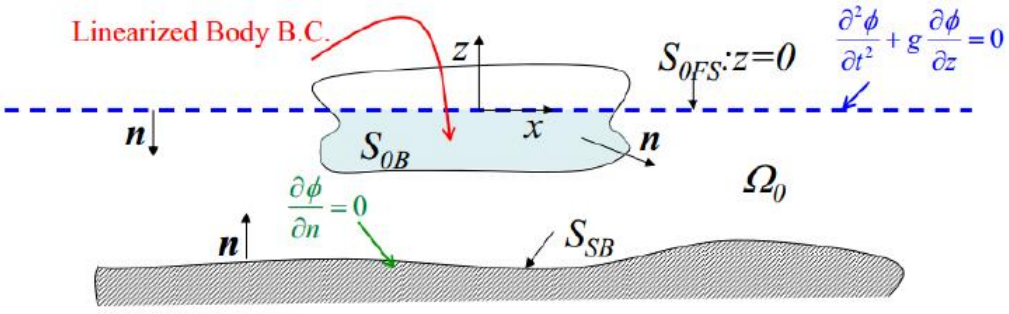

Figure 2-3: Linear wave body interaction problem ([17])

where n is the normal vector pointing into the fluid, $S_{0FS}$is mean free surface, S_{SB} is seabed surface, S_{0B} is mean body wetted surface, Ω_0 is the mean fluid volume and V_B is body velocity.

The governing equation:

$$\nabla^2\phi = 0 \qquad in\ \Omega_0 \tag{2.12}$$

Sea bottom boundary condition:

$$\frac{\partial\phi}{\partial n} = 0 \qquad on\ S_{SB} \tag{2.13}$$

Body boundary condition:

$$\frac{\partial\phi}{\partial n} = \boldsymbol{V_B}\cdot\boldsymbol{n} \qquad on\ S_{0B} \tag{2.14}$$

Combined free surface condition:

$$\frac{\partial^2\phi}{\partial t^2} + g\frac{\partial\phi}{\partial z} = 0 \qquad on\ z = 0 \tag{2.15}$$

Equation (2.12) to (2.15) together with a far field condition that the waves are outgoing form the whole system's governing equations for the linear wave body interaction problem, which be applied as the basis for frequency domain analysis.

2.3.2 Equations of Motions

Based on Newton's second law, the equations of motion for the structure could be written as:

$$\sum_{k=1}^{6} M_{jk}\ddot{\eta}_k(t) = F_j(t) \qquad j = 1,\dots,6 \tag{2.16}$$

where M_{jk} is one of components in the mass matrix $\boldsymbol{M}$, $\ddot{\eta}_k$ is one of components in the body acceleration vector $\ddot{\boldsymbol{\eta}}$ and F_j is one of components in the force vector $\boldsymbol{F}$, j indicates the degree of freedom. The external load could be calculated by integration of pressure, combining with the linear Bernoulli equation. With the dynamic pressure being integrated on the mean body surface S_{0B} and the static pressure being integrated on the instantaneous body surface S_B, we get:

$$F_j(t) = \int_{S_{0B}} -\rho\frac{\partial\phi}{\partial t}\boldsymbol{n}dS + \int_{S_B} -\rho g z\boldsymbol{n}dS \qquad j = 1,\dots,6 \tag{2.17}$$

Due to linearity, the superposition principle is valid and the potential ϕ can be decomposed in terms of the fundamental physical effects involved in the fluid-body interaction.

So the linear wave body interaction problem could be split into two sub-problems [15]:

- Diffraction problem, when the body is fixed and interacting with incident waves;
- Radiation problem, the body is forced to oscillate in its six dofs, no incident waves.

By linear theory, the velocity potential ϕ in Equation (2.17) could be written as:

$$\phi(x,y,z,t) = \phi_0(x,y,z,t) + \phi_D(x,y,z,t) + \phi_R(x,y,z,t) \qquad (2.18)$$

where the ϕ_0 is the potential of incident wave, ϕ_D is the potential due to diffraction and ϕ_R is the potential due to radiation.

The diffraction problem is involved with ϕ_0 and ϕ_D, the integration of which gives the wave excitation loads. The radiation problem is involved with ϕ_R and hydrostatic pressure, the integration of which gives the added mass, damping and restoring force.

Introducing the following equation:

$$\phi_R(x,y,z,t) = \Re\{\sum_{k=1}^{6} \dot{\eta}_k \varphi_k(x,y,z)\} \qquad (2.19)$$

where $\varphi_k(x,y,z)$ is the complex spatial velocity potential for the body oscillating with unitary speed in the *k*th dof. Then the Equation (2.17) could be rewritten into:

$$F_j(t) = \sum_{k=1}^{6} F_j^{exc}(t) - A_{jk}\ddot{\eta}_k(t) - B_{jk}\dot{\eta}_k(t) - C_{jk}\eta_k(t) \quad j = 1, \dots 6 \quad (2.20)$$

where A_{jk} is the is the added mass coefficient, B_{jk} is the damping coefficient and C_{jk} is the linear restoring coefficient.

$$A_{jk} = \Re\left[\rho \int_{S_{0B}} \varphi_k n_j dS\right] \quad and \quad B_{jk} = -\omega\Im\left[\rho \int_{S_{0B}} \varphi_k n_j dS\right] \quad (2.21)$$

Then the equations of motions for the linear wave structure interaction problem can be written as:

$$\sum_{k=1}^{6}[(M_{jk} + A_{jk})\,\ddot{\eta}_k(t) + B_{jk}\dot{\eta}_k(t) + C_{jk}\eta_k(t)] = F_j^{exc}(t) \quad j = 1, \dots 6 \quad (2.22)$$

With matrix form:

$$\big(\boldsymbol{M} + \boldsymbol{A}(\omega)\big)\ddot{\boldsymbol{\eta}} + \boldsymbol{B}(\omega)\dot{\boldsymbol{\eta}} + \boldsymbol{C}\boldsymbol{\eta} = \boldsymbol{F} \quad (2.23)$$

In a linear system at steady state condition, the response oscillates with the frequency of the excitation and the amplitude of response is proportional to the excitation.

Therefore, it reasonable to assume the excitation loads F is proportional to the incident wave amplitude ξ_a and oscillate with frequency ω, written into complex form:

$$\boldsymbol{F}(t) = \Re\{\xi_a \boldsymbol{X}(\omega, \beta)e^{i\omega t}\} \quad (2.24)$$

The response can also be written as complex form:

$$\boldsymbol{\eta}(t) = \Re\{\boldsymbol{\eta}_a(\omega)e^{i\omega t}\} \quad (2.25)$$

Substitute the two equations above into Equation (2.23) and neglect the time dependence, we can get the equation of motion in frequency domain:

$$\big(-\omega^2\big(\boldsymbol{M} + \boldsymbol{A}(\omega)\big) + i\omega\boldsymbol{B}(\omega) + \boldsymbol{C}\big)\boldsymbol{\eta}_a(\omega) = \xi_a \boldsymbol{X}(\omega, \beta) \quad (2.26)$$

The response amplitude operator (RAO) is then defined as:

$$RAO = |H(\omega, \beta)| = |\boldsymbol{\eta}_a(\omega)/\xi_a| = \big[-\omega^2\big(\boldsymbol{M} + \boldsymbol{A}(\omega)\big) + i\omega\boldsymbol{B}(\omega) + \boldsymbol{C}\big]\boldsymbol{X}(\omega, \beta) \quad (2.27)$$

2.3.3 Eigenvalue Analysis

For an undamped system with no excitation loads, Equation (2.26) could be simplified into the eigenvalue problem:

$$\big(-\omega^2\big(\boldsymbol{M} + \boldsymbol{A}(\omega)\big) + \boldsymbol{C}\big)\boldsymbol{\eta}_a(\omega) = 0 \quad (2.28)$$

Eigenfrequency for the six degree of freedom could be obtained by setting:

$$\det\left(-\omega^2\left(\boldsymbol{M}+\boldsymbol{A}(\omega)\right)+\boldsymbol{C}\right)=0 \tag{2.29}$$

The expression for natural frequencies of the six dofs:

$$\omega_{nj}=\sqrt{\frac{C_{jj}}{M_{jj}+A_{jj}}} \qquad j=1,\dots,6 \tag{2.30}$$

2.3.4 Viscous Damping

The damping term in equation of motion (Equation (2.22)), only includes the potential linear damping, which is connected with the ability of wave generation. The linear wave-radiation damping is associated with the wave energy radiated from the body and so is the square of the amplitude of the generated waves. However, for long incident waves, the wave generated by the wave-body interaction is rather small, which means that the potential linear damping is small and less important. According to Equation (2.27), there will be large amplification of the motion at resonance. In this condition, as shown in *Figure 2-4*, viscous forces will become significant.

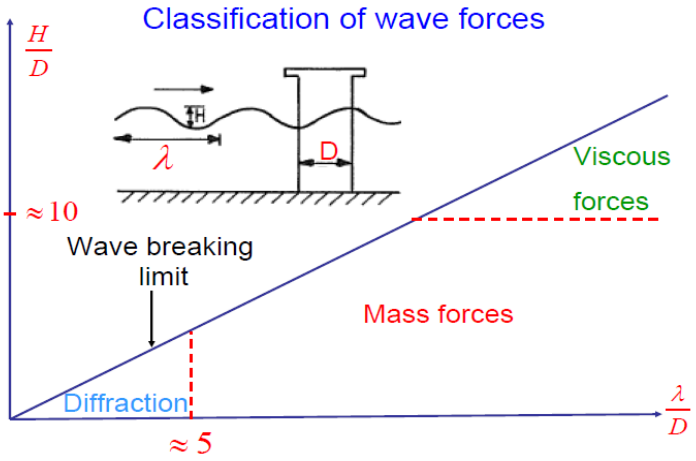

Figure 2-4: Classification of wave forces ([17])

One of the main sources of viscous damping is the drag force acting on the structure which is not considered by potential theory. An alternative method, Morison's equation is

often used for slender structures where the diameter *D* is small compared to the wavelength λ (in general, $D < \lambda/5$) [15]. According to Morison's equation, the drag force for a fixed cylinder with a diameter of *D* could be written as:

$$dF_{drag} = \frac{1}{2}\rho C_D D|u - \dot{\eta}|\,(u - \dot{\eta}) \tag{2.31}$$

From the equation above, we can see that the drag force is a quadratic function of the relative velocity between the wave particle velocity u and the structure velocity $\dot{\eta}$. So the linearization of damping coefficient is necessary before it could be used in the frequency domain analysis.

Linearization of viscous damping

Assuming a regular wave with velocity:

$$u = u_a \sin(\omega t) \tag{2.32}$$

Then the response of the structure will also be harmonic and with the same frequency, but may be not in phase with the wave velocity:

$$\eta = \eta_1 \cos(\omega t) + \eta_2 \sin(\omega t) \tag{2.33}$$

Then the relative velocity can be written as:

$$u_r = u - \dot{\eta} = A\cos(\omega t + \phi) \tag{2.34}$$

where

$$A = \sqrt{(u - \omega\eta_2)^2 + (\omega\eta_1)^2} \tag{2.35}$$

Here the phase angle ϕ in Equation (2.34) is neglected, then the nonlinear drag force can be written as:

$$dF_{drag,NL} = \frac{1}{2}\rho C_D D A^2 |\cos(\omega t)|\cos(\omega t) \tag{2.36}$$

Rewriting the expression above into the linearized drag force with the following form, and with a coefficient K_L:

$$dF_{drag,L} = \frac{1}{2}\rho C_D D K_L A\cos(\omega t) \tag{2.37}$$

The linear coefficient K_L can be found by setting the work done by nonlinear drag force and linear drag force over one period equal:

$$\int_0^T \left(dF_{drag,L} - dF_{drag,NL}\right) u_r dt = 0 \tag{2.38}$$

From the equation above, the coefficient K_L can be solved:

$$K_L = \frac{A\int_0^T |\cos(\omega t)|\cos^2(\omega t)dt}{\int_0^T \cos^2(\omega t)dt} = \frac{8A}{3\pi} \tag{2.39}$$

The linearized drag force can be obtained by:

$$dF_{drag,L} = \frac{4\rho C_D DA}{3\pi}(u - \dot{\eta}) \tag{2.40}$$

In the equation above, the term in front of the relative velocity can be written as the viscous damping coefficient for the linearized drag force, and then to be written to the left side of the equation of motion:

$$B_{viscous} = \frac{4\rho C_D DA}{3\pi} \tag{2.41}$$

where A is from Equation (2.35) and depends on the motion of the structure. Therefore, an iteration is needed to determine the linearized damping coefficient.

2.4 Aerodynamics of Wind Turbines

M. Hansen has provided a detailed insight into wind turbine aerodynamics and aeroelasticity in his book “Aerodynamics of Wind Turbines” [31]. Some basic theory of aerodynamics for wind turbines will be introduced in the section [32].

2.4.1 One-dimensional Momentum Theory and Betz Limit

Before introducing the Blade Element Momentum method, it is useful to examine a simple one-dimensional (1-D) model for an ideal disk model.

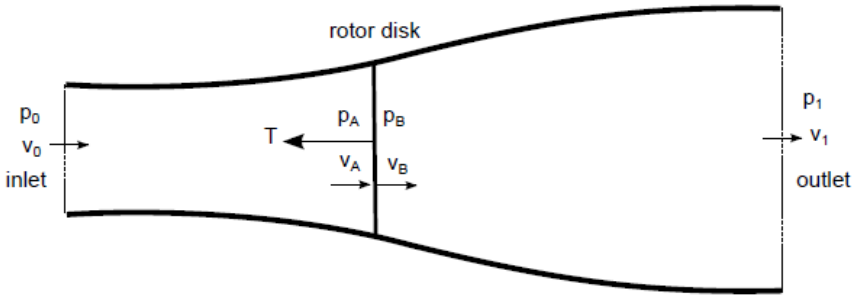

Figure 2-5: One-dimensional disk rotor model

The flow in *Figure 2-5* does not across the tube boundaries, so two control volumes account: from the inlet to side A, and from side B to the outlet. The flow only travels from inlet to outlet and through the rotor. P_0 is the inlet pressure and V_0 is inflow velocity, the corresponding quantities for the two sides of the rotor disk are shown above. T is the thrust force from the disk.

According to the conservation of momentum from the inlet to the outlet, accounting for the momentum changed by the thrust force T and the fluid density ρ:

$$T = v_0(\rho A_0 v_0) - v_1(\rho A_1 v_1) \tag{2.42}$$

Then introduce the conservation of mass through the control volumes. The $\dot{m}$ is the mass flow rate.

$$\rho A_0 v_0 = \rho A_1 v_1 = \dot{m} \tag{2.43}$$

Combining the two equations above,

$$T = \dot{m}(v_0 - v_1) \tag{2.44}$$

Assuming that there is a discontinuity in the pressure across the rotor, then applying Bernoulli's equation on both sides of the rotor.

$$P_0 + \frac{1}{2}\rho {v_0}^2 = P_A + \frac{1}{2}\rho {v_A}^2 \tag{2.45}$$

$$P_B + \frac{1}{2}\rho {v_B}^2 = P_1 + \frac{1}{2}\rho {v_1}^2 \tag{2.46}$$

There is no flow discontinuity across the rotor, $v_A = v_B$. Furthermore, by assuming that the pressure is equal to ambient pressure far from the disk, $P_0 = P_1$. Then the pressure drop across the rotor disk can be expressed as:

$$P_A - P_B = \frac{1}{2}\rho {v_0}^2 - \frac{1}{2}\rho {v_1}^2 \tag{2.47}$$

The thrust force is equal to the pressure drop multiplied by the rotor disk area A.

$$T = \frac{1}{2}\rho A({v_0}^2 - {v_1}^2) \tag{2.48}$$

According to Eq. (2.44) and (2.48),

$$\dot{m}(v_0 - v_1) = \frac{1}{2}\rho A({v_0}^2 - {v_1}^2) \tag{2.49}$$

And the mass flow is also constant across the rotor,

$$\dot{m} = \rho A v_A = \rho A v_B \tag{2.50}$$

Then can get,

$$v_A = \frac{1}{2}(v_0 + v_1) \tag{2.51}$$

If introduce the axial induction factor as

$$a = \frac{v_0 - v_A}{v_0} \tag{2.52}$$

Then can get $v_A = v_0(1 - a)$ and $v_B = v_0(1 - 2a)$.

In order to determine the power, two equivalent formulations for power could be considered: the change in kinetic energy or the thrust multiplied by velocity. According to the formula above, the power can be expressed in terms of the induction factor:

$$P = \frac{1}{2}\rho A {v_0}^3 4a(1-a)^2 \tag{2.53}$$

The power coefficient is defined as the ratio between the power extracted by the rotor disk and the power in the incoming wind (with speed v_0) in the area of the rotor disk.

$$C_P = P/\frac{1}{2}\rho A {v_0}^3 \tag{2.54}$$

From Eq. (2.53) and (2.54),

$$C_P = 4a(1-a)^2 \tag{2.55}$$

When $a = 1/3$, it gives the maximum power coefficient, which is known as the Betz limit: $C_{Pmax} = 16/27$.

2.4.2 Blade Element/Momentum Theory (BEM)

As Hansen pointed out in his book, "The BEM method is simple but very fast and will therefore very likely be used for many years to come."[31] Until now, most of the coupled dynamic simulation codes for floating wind turbines are based on BEM theory, include the SIMO-REFLEX-AeroDyn (SRA) code which be used in this thesis.

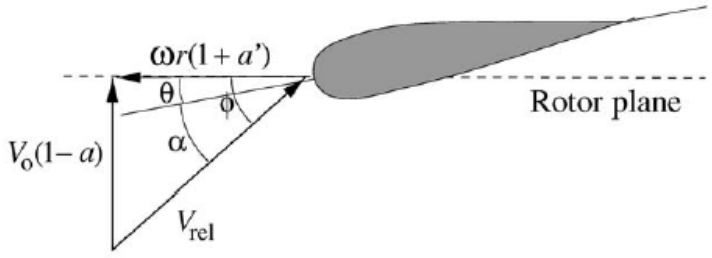

Figure 2-6: Velocities at the rotor plane ([31])

The *Figure 2-6* shows an airfoil section, where θ is local pitch of the blade (the local angle between the chord and the plane of rotation), r is the distance to the center of rotation and ω is the angular velocity. The wind velocity v_0 is perpendicular to the rotor plane. The lift and drag coefficients are:

$$C_l = \frac{f_l}{0.5\rho {V_{rel}}^2 c} \tag{2.56}$$

$$C_d = \frac{f_d}{0.5\rho {V_{rel}}^2 c} \tag{2.57}$$

where f_l and f_d are lift and drag loads on the airfoil respectively, ρ is air density, c is chord length of the section, V_{rel} is relative wind velocity, ϕ is the flow angle and α is the angle of attack which is defined as:

$$\alpha = \phi - \theta \tag{2.58}$$

$$\tan\phi = \frac{(1-a)V_0}{(1+a')\omega r} \tag{2.59}$$

where a and a' are axial and rotational induction factors respectively, given by:

$$a = \left[1 + \frac{4\mathrm{Sin}^2\phi}{\sigma C_n}\right] \tag{2.60}$$

$$a' = \left[-1 + \frac{4\sin\phi\cos\phi}{\sigma C_t}\right]^{-1} \tag{2.61}$$

Here the normal force coefficient $C_n = C_l\cos\phi - C_d\sin\phi$ and tangential force coefficient $C_t = C_l\sin\phi - C_d\cos\phi$. And the solidity σ is defined as the fraction of the annular area in the control volume which is covered by blades:

$$\sigma = \frac{cB}{2\pi r} \tag{2.62}$$

where *B* is the number of blades.

The Eq. (2.60) and (2.61) are for the unknown a and a', however, the ϕ, C_n and C_t depend on a and a'. So an iteration solution may need:

1. Guess starting values for a and a'.
2. Calculate ϕ and consequently α, C_l and C_d.
3. Update a and a' by Eq. (2.60) and (2.61).
4. Check for convergence within a given tolerance, if not, repeat.

The equations for the BEM method above need some important corrections. First is the Prandtl correction, which is a correction of tip loss due to the finite number of blades. Another is the Glauert correction which is used for large induction factors, for $a > 0.4$. The reason is that the BEM theory is not valid for induction factors greater than 0.5, since the wind velocity in the far wake would be negative. [32]

2.4.3 Generalized Dynamic Wake (GDW)

An alternative method to find the induced velocities and aerodynamic loads is the Generalize Dynamic Wake (GDW) method which also can be used in the SRA code. So far, the theory is suitable for lightly loaded rotors. But for wind speed below 8 m/s, this method should not be used [32].

GDW is based on a potential flow solution to Laplaces equation. This method includes inherent models of dynamic wake, tip loss and skewed wake effects. It is better suited for dynamic inflow, yawed inflow and high wind speeds. What's more, GDW doesn't need iteration [32].

2.5 Operating Performance of Wind Turbines

When operating a wind turbine, the general target is to minimize the operational cost while maximize the power production. The operational cost depends on the conditions under which the wind turbine produces the power, and here is a conceptual power and rotor speed curve of a variable-speed pitch-regulated wind turbine in *Figure 2-7*.

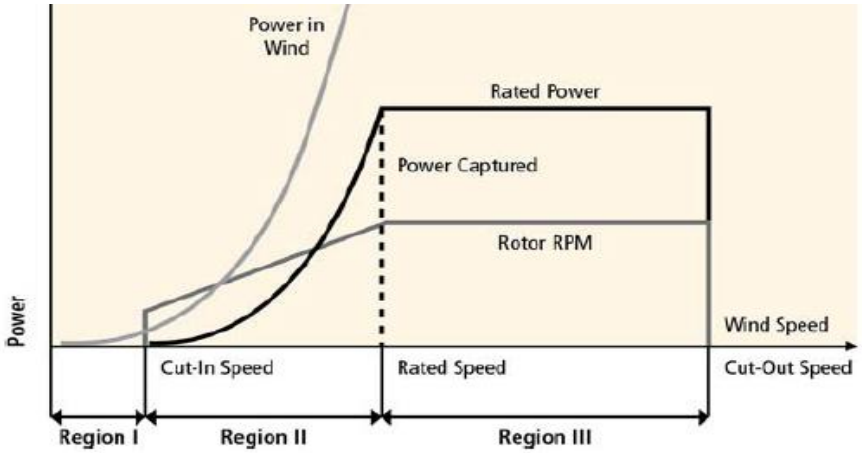

Figure 2-7: Conceptual performance of a variable-speed pitch-regulated wind turbine

There are three regions of the curve, Region II and III denote the partial load region and the full load region. When the wind speeds below the cut-in speed, the wind turbine does not produce any energy since the operational cost exceeds the value of the produced power. And also there is no energy produced when wind speeds exceed the cut-out wind speed, since the wind turbine is shut down to protect the systems from wind overloads. The detail about what happens in the two regions of power production is:

Region II: The partial load region is located between the cut-in wind speed and the rated wind speed. In this region the wind turbine is controlled to generate as much power as possible. To achieve the maximum power coefficient, by increasing the rotor speed for increasing wind speed.

Region III: The full load region is located between the rated wind speed and the cut-out wind speed. It implies that the produced power is kept at a rated value to minimize structural loads and thereby reduce fatigue damages.

In order to control the power output and loads, the wind turbine uses blade pitch to adjust the rotation speed. While operating, the control system of wind turbine adjusts the blade pitch to keep the rotor speed within operating limits whenever the wind speed exceeds the maximum rated speed. This control system called Pitch-regulated and it plays an important role to maximize the energy capture and to minimize the loads.

CHAPTER II: THEORETICAL BACKGROUND

3 CHAPTER III: WIND TURBINE & ENVIRONMENT CONDITION

3.1 DTU 10MW Reference Wind Turbine

3.1.1 General Introduction

Since 1970's, the scale of offshore wind turbines has become larger and larger, due to the motivation to reduce the cost of energy from the offshore wind turbines.

Until now, the largest wind turbines which already on the market are in the order of 7MW. Moreover, the department of Wind Energy at Technical University of Denmark (DTU) has already developed a concept of 10MW reference wind turbine which may be more reliable, efficient and cost effective. In this thesis work, the DTU 10MW reference wind turbine was used for the upscaling, modeling and analysis. It is shown in *Figure 3-1* below.

Figure 3-1: The DTU 10MW wind turbine ([18])

The detail information about the DTU 10MW reference wind turbine can be found from the DTU Wind Energy Report [18].

3.1.2 Properties of DTU 10MW and NREL 5MW Wind Turbines

The NREL 5MW RWT which developed by National Renewable Energy Laboratory is used as the reference wind turbine for the upscaling of the DTU 10MW RWT [29]. A general comparison between the DTU 10MW RWT and NREL 5MW RWT are shown in below:

Properties	DTU 10MW	NREL 5MW
Rating	10 MW	5 MW
Configuration	Upwind, 3 blades	Upwind, 3 blades
Control	Collective pitch	Collective pitch
Drivetrain	Multiple stage gearbox	Multiple stage gearbox
Cut-in, Rated, Cut-out wind speed	4 m/s, 11.4 m/s, 25 m/s	3 m/s, 11.4 m/s, 25 m/s
Cut-in, Rated rotor speed	6 rpm, 9.6 rpm	6.9 rpm, 12.1 rpm
Rated tip speed	90 m/s	80 m/s
Maximum Thrust	1500 kN	~750 kN
Rotor, Hub diameter	178.3 m, 5.6 m	126 m, 3m
Hub height	119 m	90 m
Tower height	115.63 m	87.6 m
Overhang, Shaft tilt	7.1 m, 5°	5m, 5°
Pre-cone	-2.5°	-2.5°
Rotor mass	230.7 t	110 t
Nacelle mass	446.0 t	240 t
Tower mass	628.4 t	347.5 t
Total mass	1305.1 t	697.5 t
Overall CM	(-0.3 m, 0 m, 85.5 m)	(-0.2 m, 0 m, 64.0 m)

Table 3-1: Comparison between DTU 10MW and NREL 5MW RWTs

From *Table 3-1*, it could be seen that the DTU 10MW RWT is an upscaled design mainly based on NREL 5MW RWT with the same rated wind speed and an upscale rotor. The resulting overall tower mass is 628,442kg, and the tower's center of mass is located at

47.6m above the still water level (SWL). Besides, the overall mass of rotor (blades and hub) and nacelle is 230,667kg and 446,036kg, respectively. So the total mass of the DTU 10MW wind turbine is 1,305,145kg (1305.145t).

The corresponding mechanical power and thrust curves for DTU 10MW wind turbine are shown below:

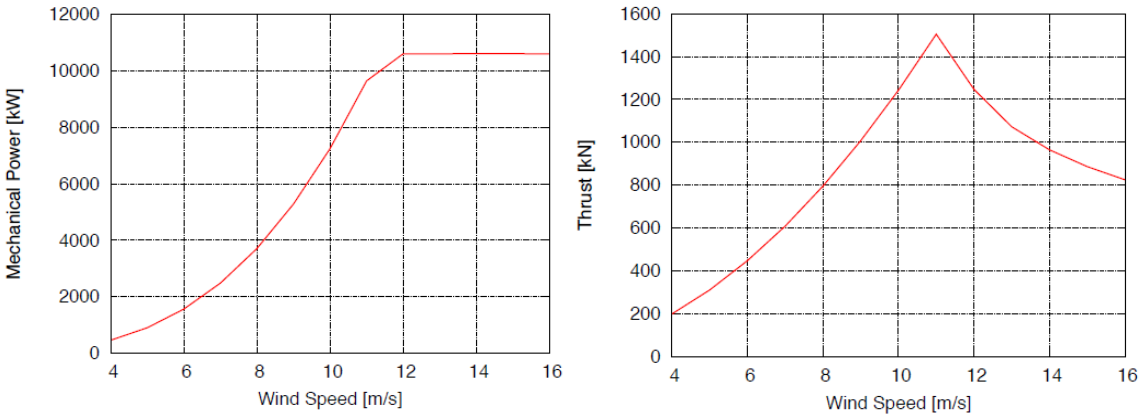

Figure 3-2: Mechanical power and thrust curves of DTU 10MW RWT based on BEM theory ([18])

3.1.3 Tower Properties of DTU 10MW RWT

All the necessary details of the DTU 10MW RWT tower can be found in the "*Description of the DTU 10 MW Reference Wind Turbine*" [18]. Some important information is shown below.

The material of tower is steel S355, as defined in the European standard DIN EN 10025-2. In order to account for the mass of secondary structures, such as paint, bolts, welds, stiffeners and flanges, the mass density was increased by approximately 8% (ρ= 8500 kg/m^3) in the calculation of the cross section mass properties [18]. The Young's Elasticity Modulus is set as 2.10E+11 Pa, and the Poisson's ratio with 0.3. The structural damping ratio for all modes of the isolated tower is specified to be 1% critical [18].

The outer diameter of the tower varies linearly from D = 8.3m at the bottom to D = 5.5m at the top. The tower was divided into 10 sections, and each section has the constant wall thickness. The wall thickness distribution is shown in *Table 3-2* [18].

Height [m]	Outer diameter [m]	Wall thickness [mm]
0.000	8.3000	38
11.500	8.0215	38
11.501	8.0215	36
23.000	7.7431	36
23.001	7.7430	34
34.500	7.4646	34
34.501	7.4646	32
46.000	7.1861	32
46.001	7.1861	30
57.500	6.9076	30
57.501	6.9076	28
69.000	6.6292	28
69.001	6.6291	26
80.500	6.3507	26
80.501	6.3507	24
92.000	6.0722	24
92.001	6.0722	22
103.500	5.7937	22
103.501	5.7937	20
115.630	5.5000	20

Table 3-2: Wall thickness distribution of the tower

Only the details of a land-based tower are listed in this section. In fact, the properties of tower for the DTU 10MW RWT will depend on the type of support structure to carry the turbine. When the land-based tower is mounted on a floater like spar, the eigenfrequency of the tower will be changed, since the support is more flexible [30]. What's more, due to the higher offshore wind speed, the required hub height for an offshore wind turbine in general will be lower than an onshore wind turbine in order to achieve the same power performance [30]. But in this thesis, the designed hub height and cross-section properties of the tower are kept as same as the land-based version. The only modification of the tower will be discussed in the next chapter.

3.2 Environment Condition

The design of offshore wind turbines needs information about the joint data of wind and wave. In this thesis, the No.14 site "Norway 5" has been chosen as the place for the analysis of floating wind turbine, as shown in *Figure 3-3*. The generic water depth of this site is 200 m, and the distance to shore is 30 km.

Figure 3-3: Location for the floating wind turbine ([33])

Lin Li has applied the contour surface method and fitted the long-term analytical joint distributions of wind and wave data in the site "Norway 5" [33]. Therefore, the operational environment conditions could be chosen based on her work. The method of choosing the condition is shown below:

1. To estimate the power of wind turbines, it's necessary to transfer the mean wind speed at hub height to the 10 m above the sea level. A power law profile with the exponent α equal to 0.1 can be used for [33]:

$$U(z) = U_{10} \cdot (\frac{z}{10})^{\alpha} \tag{3.1}$$

where z is the height, U_{10} is the mean wind speed at 10m height.

2. Then fitting a marginal distribution of mean wind speed U_w of the 1 h mean wind speed at 10 m height. Finding the most probable value of mean wind speed according to the distribution.

3. Appling the conditional distribution of significant wave height H_s for given mean wind speed, to find the most probable value of significant wave height.

4. Finally, a conditional distribution of wave peak period T_p given both U_w and H_s is used to get the most probable value of wave peak period.

Based on the procedure above, three operational conditions can be selected which are below-rated wind speed, rated wind speed and above-rated wind speed. In addition, an extreme environment condition is added, which obtained by contour surface method with a return period of 50 years [33]. All the four conditions are listed in *Table 3-3*.

Load case	Mean wind speed [m/s]	Significant wave height [m]	Wave peak period [s]	Turbulence intensity	Turbine status
1 (Below-rated)	8	2	10.3	0.17	operating
2 (Rated)	11.4	2.5	10.2	0.15	operating
3 (Above-rated)	18	4.1	10.5	0.13	operating
4 (Extreme)	40	15.6	14.5	0.11	parked

Table 3-3: Environment conditions for floating wind turbine

The turbulence intensity is a function of mean wind speed according to the IEC standard [34], and class C is used for offshore condition. Normal Turbulence Model (NTM) is used for generating wind files for operating cases while Extreme Wind Model (EWM) is for parked condition.

The operating case is the general power production case with the rotating blades and the active controller. However, in order to avoid damage in extreme conditions, all the blades are pitched to feather and the turbine need to be shut down, so the wind turbine is parked (idling). The nacelle yaw angle is kept as 0 degree in all cases.

4 CHAPTER IV: PRELIMINARY DESIGN, MODELING & ANALYSIS

A preliminary design was performed in the previous project work [42], in order to estimate weight and buoyancy, static heeling angle and natural frequencies. The data of 5MW wind turbine floater OC3-Hywind spar [9] is used as reference for the design of the 10MW wind turbine floater. Some important content of project work is introduced in this chapter.

4.1 Design Requirements for Spar Floater

In the preliminary design, the DNV's recently released standard, DNV-OS-J103 Design of Floating Wind Turbine Structures [8], is used as reference in the design.

The main objective of designing a spar WT is to create a platform which can safely generate electricity at the lowest possible cost. In order to achieve such a proper design which also could be adopted in time domain dynamic analysis later, several requirements should be fulfilled.

General Requirement

A spar floater should be designed to support this 10MW wind turbine. The floating structure consists of a steel cylinder filled with a ballast of concrete at the bottom. It may extend 120 meters beneath the sea's surface and be attached to the seabed by a three-point mooring system.

Buoyancy

The buoyancy requirement is that the floater should provide enough displacement to support the weight of the floater and the wind turbine at designed draft level. To achieve the desired draft, a proper ballast design should also be performed.

Hydrostatic Stability

Due to the presence of the wind turbine, there exist several challenges of the stability of the spar. The wind turbine will raise the center of gravity of the whole structure due to its large top mass (rotor and nacelle) high above the sea level. Besides, the large aerodynamic thrust at hub height will introduce a large overturning moment. What's more, a large heeling angle of platform will affect the rotor plane area to the wind as well as the angle of attack for all the blades sections, which might lead to a reduction of power output.

The DNV-OS-J103 [8] gives the intact stability requirements for Deep Draught Floaters (Spar), which are:

> "For deep draught floaters such as spars, the metacentric height GM shall be equal to or greater than 1.0 m. The GM is defined as the difference between the vertical level of the metacenter and the vertical level of the center of gravity and shall be calculated on the basis of the maximum vertical center of gravity VCG."

And also, there is a limit for the inclination angle under the maximum mean wind turbine thrust force, which should be the similar with the 5MW concepts, i.e. $\theta < 7°$.

Motion characteristic

The natural period is one of the most important motion characteristics of the spar platform in a design process. According to the prior study of wave spectrum on the different locations and sea states, ocean waves contain major energy in the spectral period range 5 to 25s. Therefore, to avoid the resonance problem, the natural periods of floater's motion should be kept out of this particular wave range.

Based on previous study, spar floaters for wind turbines usually have a natural period around 20 to 25s in heave motion and a natural period around 30s in pitch and roll motion. The natural periods for horizontal motions (sway, surge and yaw) are governed by the mooring system.

4.2 Floater Main Dimension

The tower is rigidly connected to the top of the floating platform at an elevation of 10m above the SWL. Between the top and bottom of the platform, the 10MW spar-buoy consists of two cylindrical regions connected by a linearly tapered conical region. The upper cylinder's diameter is 8.3m and the lower cylinder's diameter is increased to 12m. The reason for this design is to reduce hydrodynamic loads near the free surface. The linearly tapered conical region extends from a depth of 4 m to a depth of 12m below the SWL.

The heavy ballast located at the bottom provides good stability and restoring stiffness, thus limiting the platform pitch and roll motion in wind and waves. All the properties are relative to the static mean position of the platform.

Main dimensions for the new 10MW wind turbine spar floater are provided in *Table 4-1*. The thickness of spar hull is assumed as 60mm.

Main dimensions	**10MW**
Draft	120 m
Elevation of platform top above SWL	10 m
Depth to top of taper below SWL	4 m
Depth to bottom of taper below SWL	12 m
Platform diameter above taper	8.3 m
Platform diameter below taper	12 m
Hull thickness	0.06 m
Platform mass, including ballast	12,100,057 kg

Table 4-1:Platform structural properties

4.3 The Modification of Tower Properties

The loads on a wind turbine highly depend on the description of the wind flow. In reality, wind has both spatial and temporal variations due to factors like wind shear, turbulence,

wind/tower interactions, etc. Wind shear is related to how the mean wind speed increases with the height above the sea surface. A typical wind shear is shown below:

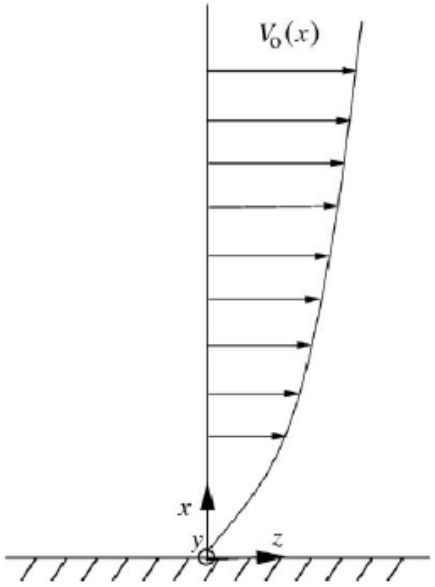

Figure 4-1: Wind shear [31]

Due to the existence of wind shear, the wind force on the wind turbine is related to the hub height. And since there is a 10-meter freeboard of the spar floater, the height of wind turbine tower need to be modified to make sure that the hub height is still 119 m. That is to say, a tower height reduction of 10 m is needed. In the project work, the tower didn't be modified, but will be done in later dynamic analysis.

4.4 Modeling of Structure

The DNV SESAM software, GeniE is used to build the 3D-model of the wind turbine and spar floater. Then the model is imported into HydroD for the corresponding analysis. The details about the software can be found in [11][19].

Two different types of finite element models were built prior to running HydroD, which are panel model and mass model shown in *Figure 4-2*.

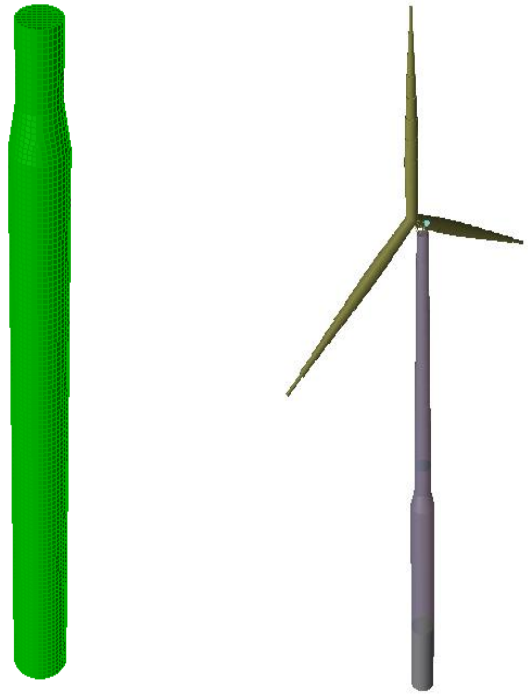

Figure 4-2: The panel model (left) and mass model (right)

Properties of Structure

The general properties of the whole structure are listed in *Table 4-2*, which read from the stability analysis result in HydroD.

Properties	HydroD
Total mass	13420.1 t
Buoyancy	13355.1 t
Center of gravity	-74.60 m
Center of buoyancy	-62.07 m

Table 4-2: Structure properties from HydroD

From the table above, it is noticed that the total mass and buoyancy are not equal in HydroD. One possible reason is that the quality of mesh for the panel model is coarse, which means that the density of mesh is still too large. As the mesh quality been refined, the difference will become smaller.

4.6 Hydrostatic Analysis

Hydrostatic and stability analysis was run for intact condition by HydroD. It could compute the draught and heel/trim angles to ensure equilibrium. A wind heeling moment should be included. In the stability analysis, the only contribution to the overturning moment is the rated thrust from the wind turbine, i.e. 193500 $kN{\cdot}m$.

The result of the stability analysis is shown in *Figure 4-3*. There are two curves denoted as righting moment and heeling moment, and the intersection point of the two curves located at 6.77°. Due to the particular geometry of spar platform, the righting moment always increases with the increasing heel angle and reaches the maximum at 90°.

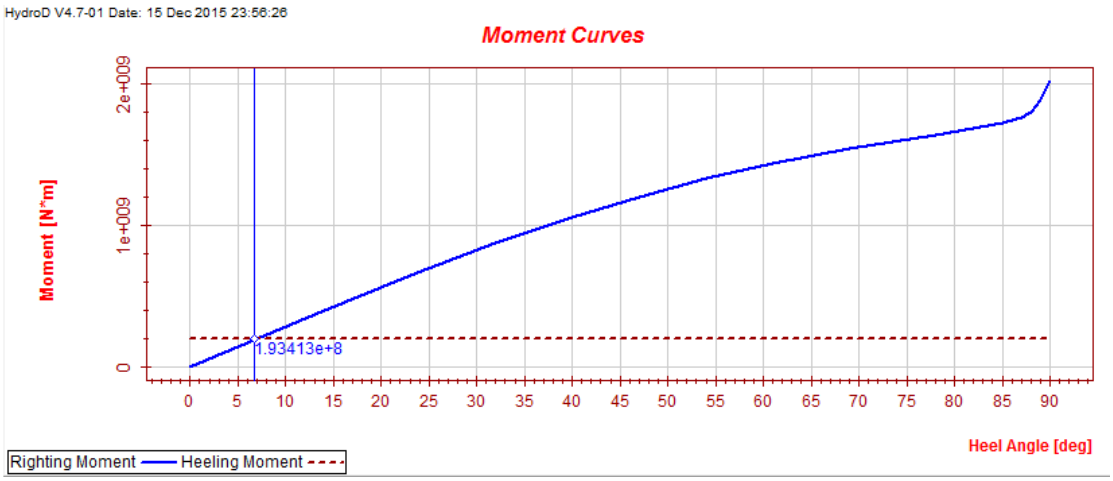

Figure 4-3: Moment curves from HydroD

Properties	HydroD
Metacentric height GM	12.54 m
Heeling angle θ	6.77°

Table 4-3: Comparison of stability parameter from HydroD and hand calculation

The result is much larger than the requirement. Therefore, the design satisfies the intact stability requirement from DNV. In general, the stability is not a big problem for spar floater concept, due to the typical large draft and correspondingly lower center of gravity.

4.7 Hydrodynamic Analysis

The hydrodynamic analysis of the spar floating wind turbine without mooring system was performed by the programs Wadam. Wadam is a hydrodynamic analysis module in HydroD, and used for calculating wave-structure interaction for fixed or floating structures of arbitrary shape. 3D potential flow theory is applied and results are presented as complex transfer functions or as deterministic results [20].

Natural Period Analysis

Since the symmetry of the spar geometry, pitch and roll motion characteristics are the same. And no mooring systems are considered in the initial design, which means horizontal motions of structure (surge, sway and yaw) cannot be calculated in analysis. Therefore, only heave and pitch motion of platform are needed to be considered.

According to the added mass from Wadam, the natural periods of heave and pitch motion could be obtained, which are shown in below:

Degree of Freedom	Heave	Pitch
Mass/Inertia [kg, kg*m2]	1.342E+07	1.273E+11
Added mass/inertia [kg, kg*m2]	5.004E+05	6.056E+10
Restoring [N/m, N*m]	5.39311E+05	1.69015E+09
Natural period [s]	31.92	38.97

Table 4-4: Natural period of heave and pitch

5 CHAPTER V: MOORING SYSTEM

Until now, all the design and analysis of the spar platform are carried out without the mooring system. However, the mooring system is essential for the time-domain simulations in the case study. In this chapter, a mooring system need to be added to the spar platform.

5.1 Theory of Mooring System

For the preliminary design, only the static analysis of mooring system is considered. The bending stiffness and dynamic effects in the line are neglected. What's more, to simplified the analysis, the effect of elasticity is also neglected. A typical case of catenary line is from Faltinsen's book [15].

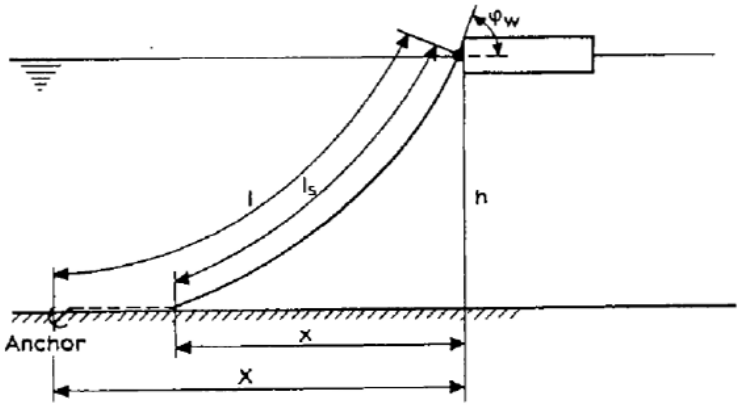

Figure 5-1: Vessel moored with one anchor line ([15])

In the figure above, h is the depth from fairlead to seabed, x is the horizontal distance between fairlead and the contact point of the mooring line with seabed, X is the horizontal distance from fairlead to anchor, φ_w is the mooring line angle at fairlead, l is the total length of mooring line and l_s is the length of the mooring line that is hanging in water.

According to Faltinsen [15]:

$$l_s = a \sinh(\frac{x}{a}) \tag{5.1}$$

$$h = a\left[\cosh\left(\frac{x}{a}\right) - 1\right] \tag{5.2}$$

$$a = \frac{T_H}{w} \tag{5.3}$$

T_H is the horizontal pretension of the mooring line, corresponding to the maximum tension T_{max} at fairlead, and *w* is the weight per unit length of the line in water.

$$T_{max} = T_H + wh \tag{5.4}$$

The horizontal distance *X* is:

$$X = l - l_s + x \tag{5.5}$$

By combining Eq. (5.1) and (5.2),

$$l_s{}^2 = h^2 + 2ha \tag{5.6}$$

According to the requirement that a gravity anchor cannot be exposed to vertical force from the mooring line, the minimum chain length l_{min} could be found. By combining Eq. (5.2), (5.4) and (5.6), the minimum length of chain is

$$l_{min} = h\left(2\frac{T_{max}}{wh} - 1\right)^{0.5} \tag{5.7}$$

When considering only linear restoring effect of anchor line, the restoring coefficient of the spread mooring system could be written into:

$$C_{11} = \sum_{i=1}^{n} k_i \cos^2\varphi_i \tag{5.8}$$

$$C_{22} = \sum_{i=1}^{n} k_i \sin^2\varphi_i \tag{5.9}$$

$$C_{66} = \sum_{i=1}^{n} k_i (x_i \sin^2\varphi_i - y_i \cos^2\varphi_i)^2 \tag{5.10}$$

Where φ_i is the angle between two adjacent lines and k_i is the restoring coefficient for anchor line number *i* which is:

$$k_i = w\left[\frac{-2}{\left(1+2\frac{a}{h}\right)^{0.5}} + \cosh^{-1}\left(1+\frac{h}{a}\right)\right]^{-1} \quad (5.11)$$

5.2 Mooring System Properties

The design of the mooring system is strongly related to the design of the platform. According to DNV-OS-E301[27], the design criteria for the mooring system are as follows:

1. Each mooring line should have adequate strength to withstand the load effects imposed by extreme environmental actions. (Ultimate Limit State)
2. The mooring system should have sufficient capacity to withstand the failure of one mooring line. (Accidental Limit State)
3. Each mooring line should have adequate capacity to withstand cyclic loading. (Fatigue Limit State)
4. No slack is permitted.
5. The limitations of the horizontal offset due to environmental loads should be considered (no vertical force on the anchor).
6. The mooring lines should be strong enough to maintain structural integrity.

In this paper, only the diameter of the spar is enhanced when compared with the appearance of the OC3-Hywind. So the configuration and hydrodynamic coefficients of the upscaled spar are similar to the OC3-Hywind concept. For convenience, the conceptual mooring system for OC3-Hywind is used directly in this case. The only change of the design is the mass per unit length of mooring line, which is triple of the original one, to reduce the spar's surge motion. Later, several tests will be performed to check whether this mooring system is acceptable for the 10MW wind turbine spar floater.

As introduced in Section 1.4, the mooring system consists of three catenary lines with multiple segments of varying properties and a clump weight. These lines are attached to

the spar via a "crowfoot" (delta line) to increase the yaw stiffness. The detailed configuration of mooring system is shown in *Figure 5-2*.

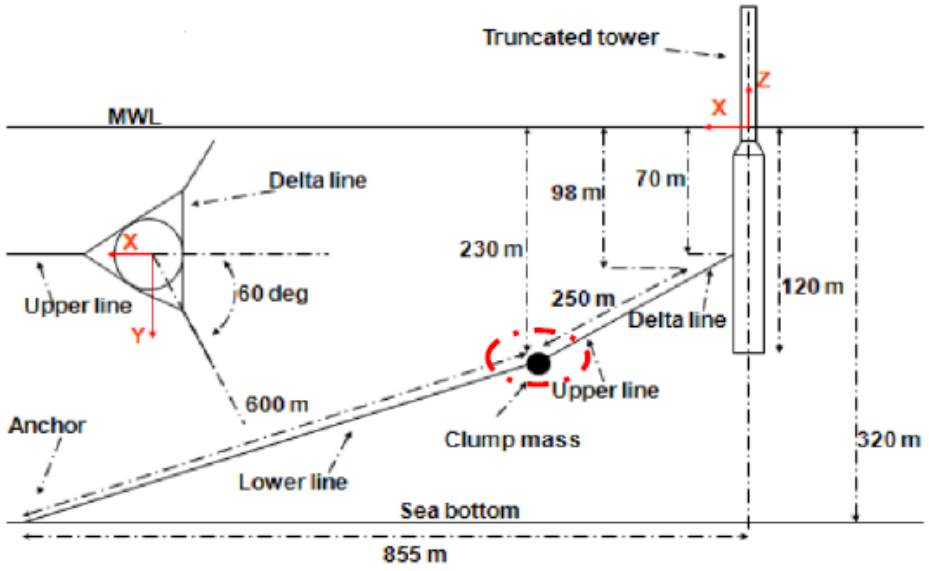

Figure 5-2: Mooring system configuration ([35])

In order to simplify the modeling and analysis of mooring system, several changes are made. First, the delta connection is eliminated, which means that an additional linear yaw stiffness should be added to the system to achieve the sufficient yaw restoring force. Second, all the catenary lines with multiple segments are replaced by a uniformly distributed line, with average values of the mass, weight, and stiffness. Third, all the damping of mooring system is neglected. To be honest, these simplifications are suitable for static analysis, but may not be appropriate in all dynamical conditions [9].

The fairleads are located at a depth of 70.0 m below the still water level (SWL) and at a radius of 6.5 m from the platform centerline. The anchors are located at a depth of 320 m below the SWL and at a radius of 855.17 m from the platform centerline. The angel between adjacent lines is 120°. Each of the three lines has an unstretched length of 902.2 m, a diameter of 0.09 m, an equivalent mass per unit length of 233.1198 kg/m and an equivalent axial stiffness of 384,243,000 N. The additional yaw stiffness is 147,510,000 Nm/rad, which is 1.5 times of original value. The properties are summarized in below:

Number of mooring lines	3	
Angel between adjacent lines	120	deg
Water depth	320	m
Depth to fairleads below SWL	70	m
Radius to fairleads from spar centerline	6.5	m
Radius to Anchors from spar centerline	855.17	m
Unstretched mooring line length	902.2	m
Mooring line diameter	0.09	m
Equivalent mooring line mass density	233.1198	kg/m
Equivalent mooring line axial stiffness	384,243,000	N
Additional yaw spring stiffness	147,510,000	Nm/rad

Table 5-1: Properties of mooring system

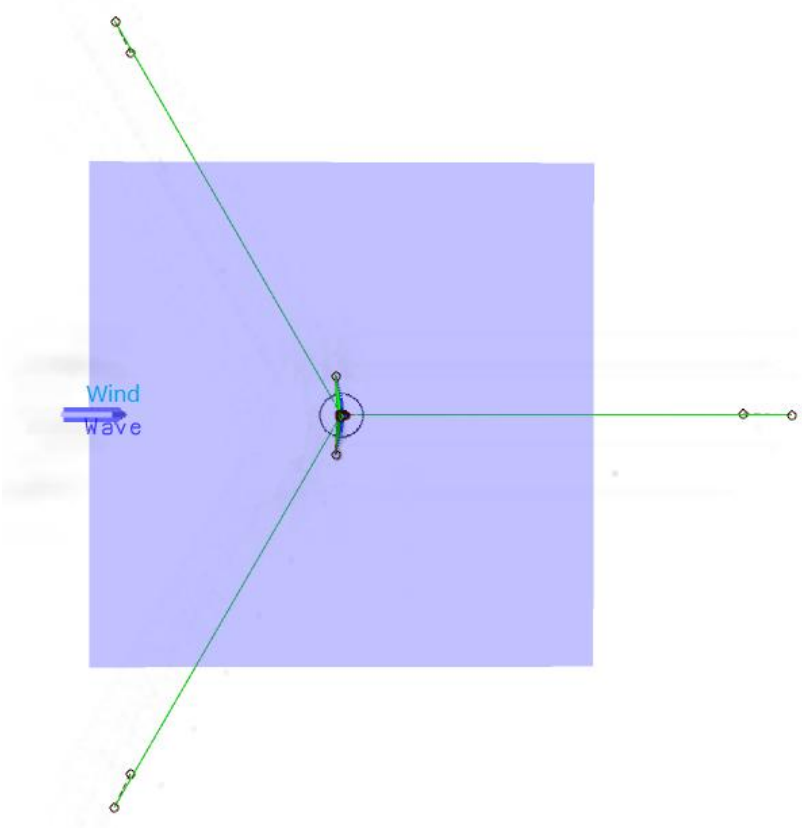

Figure 5-3: Mooring line system configuration (top-view)

5.3 Decay Tests

The aim of decay analysis is to get the natural periods and damping ratio (including linear and quadratic damping ratio) for the spar-floater with DTU 10MW RWT system. Due to the symmetry of the spar structure, only surge, heave, pitch and yaw need to be considered for the decay tests of the platform.

The test is performed at the undisturbed position. The initial displacement is achieved by applying a ramp force/moment starting at time 50s, followed by a constant force/moment, which will then be released. The system will then oscillate around the initial equilibrium position with a damped natural period until reaching equilibrium state again. The method to find the undamped natural period is shown below.

According to logarithmic decrement [36], an estimate of the system damping ratio can be found. This value will be an equivalent linear damping ratio, since our system consists of both linear and nonlinear damping mechanisms from both mooring system and body. The decrementation δ is given by,

$$\delta = \frac{1}{n}\ln\left(\frac{x_0}{x_n}\right) \tag{5.12}$$

where x_0 is initial amplitude and x_n is amplitude of *n* peaks away. The damping ratio ζ is then found by,

$$\zeta = \frac{1}{\sqrt{1+(2\pi/\delta)^2}} \tag{5.13}$$

The period of oscillation in the free decay tests are the damped natural periods. When the damping ratio is known, the undamped natural period can be calculated,

$$\omega_n = \frac{\omega_d}{\sqrt{1-\zeta^2}} \tag{5.14}$$

The decay test simulation is performed based on SIMO-RIFLEX-AeroDyn code which will be introduced in next chapter. The time series of decay tests are shown in *Figure 5-4*:

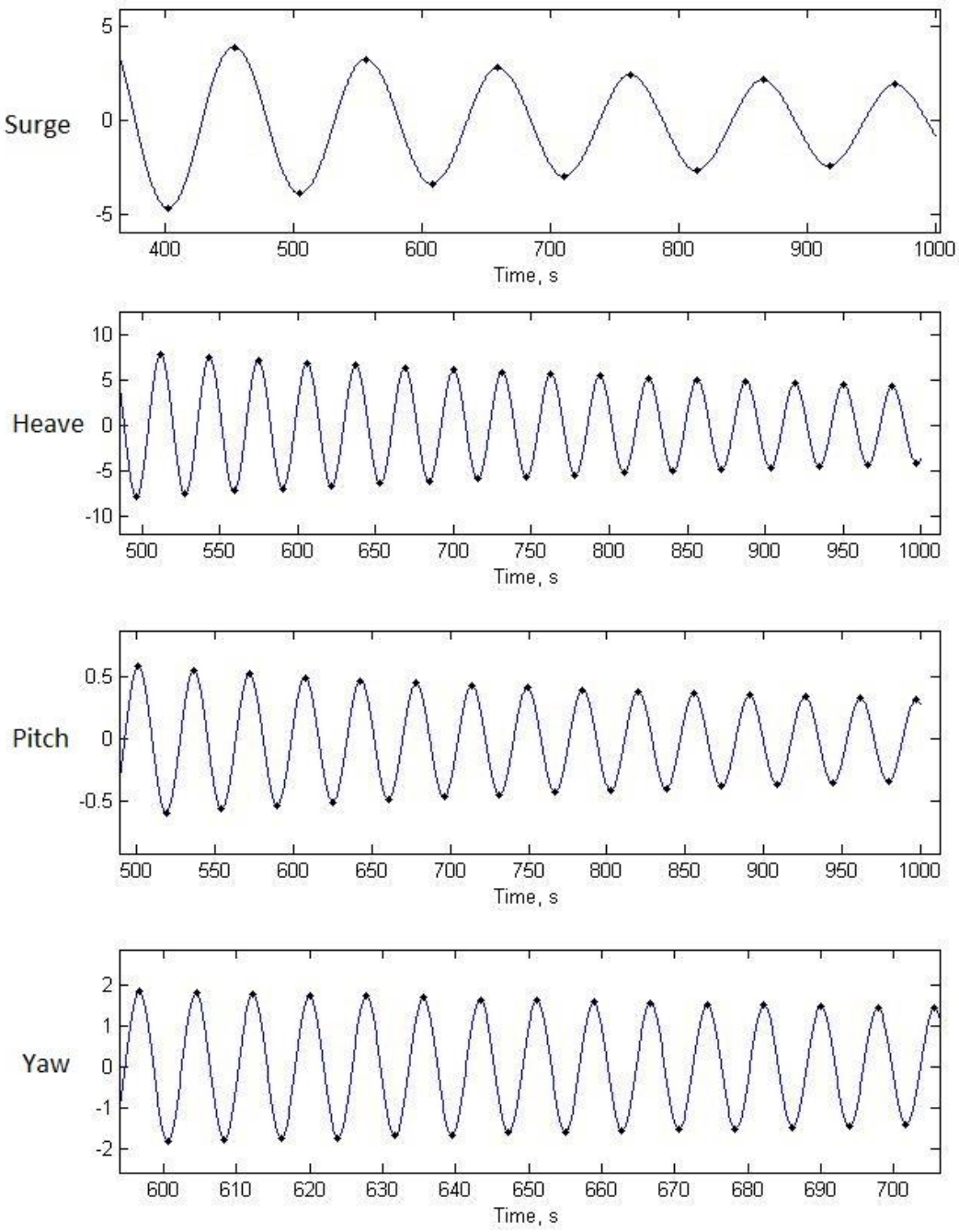

Figure 5-4: Time series of free decay tests

According to the logarithmic decrement theory above, the damped natural period, linear and quadratic damping ratio could be got by method of spline-fitting. Since the damping ratio is rather small, the undamped natural period is almost same with the damped natural period. The results are below:

Degree of freedom	Damped natural period [s]	Damping ratio	Linear damping coefficient [N·s/m]	Quadratic damping coefficient [N·s^2/m^2]
Surge	103.3	0.024	1.28E-03	1.28E-02
Heave	31.3	0.0032	1.82E-03	6.86E-04
Pitch	35.5	0.0033	2.99E-04	3.15E-02
Yaw	7.61	0.0031	4.80E-03	1.65E-04

Table 5-2: Results for decay tests

For a deep draught floater like spar, the natural periods of surge and sway are usually large, typically around 100 seconds, due to the limited restoring stiffness from mooring system. And natural periods in heave, roll and pitch of spar are usually above 20 seconds. The yaw natural period of the platform is very small, since the delta connection is used to increase the yaw stiffness. According to the performance of the decay test, the mooring system is acceptable in view of natural period.

Compared with the results from Wadam, the natural period of pitch is slightly smaller than the previous value (38.97s) due to the additional stiffness from the mooring system. Another reason could be that nonlinear restoring and elasticity of the mooring line is neglected in the test, as pointed out by Qiang Wang [30]. However, the natural period of heave is very close (31.92s), which means that the mooring system has limited restoring contribution in the heave motion.

Another interesting thing is that the quadratic damping coefficient is larger than the linear damping coefficient for the cases of surge and pitch, which means the viscous damping plays an important role in these motions since the spar is a slender cylinder.

5.4 Extreme Condition Test

Extreme condition tests are performed to check the extreme mooring line tension as well as vessel offset. As mentioned before, the platform horizontal offset should have a limitation to avoid vertical forces on the anchor, an allowable offset around 10% of the

water depth is adopted in the paper (32 m). Moreover, the mooring line should provide sufficient breaking strength to resist the maximum tension with adequate safety margins.

The load case in test is “Extreme” case as mentioned in Ch.3, which is a 50-year extreme condition for the floating wind turbine system. In these simulations the response of the platform and mooring lines are coupled, while the aerodynamic force is represented by a constant thrust force at hub height. Only head wave without current is considered.

5.4.1 Extreme Responses

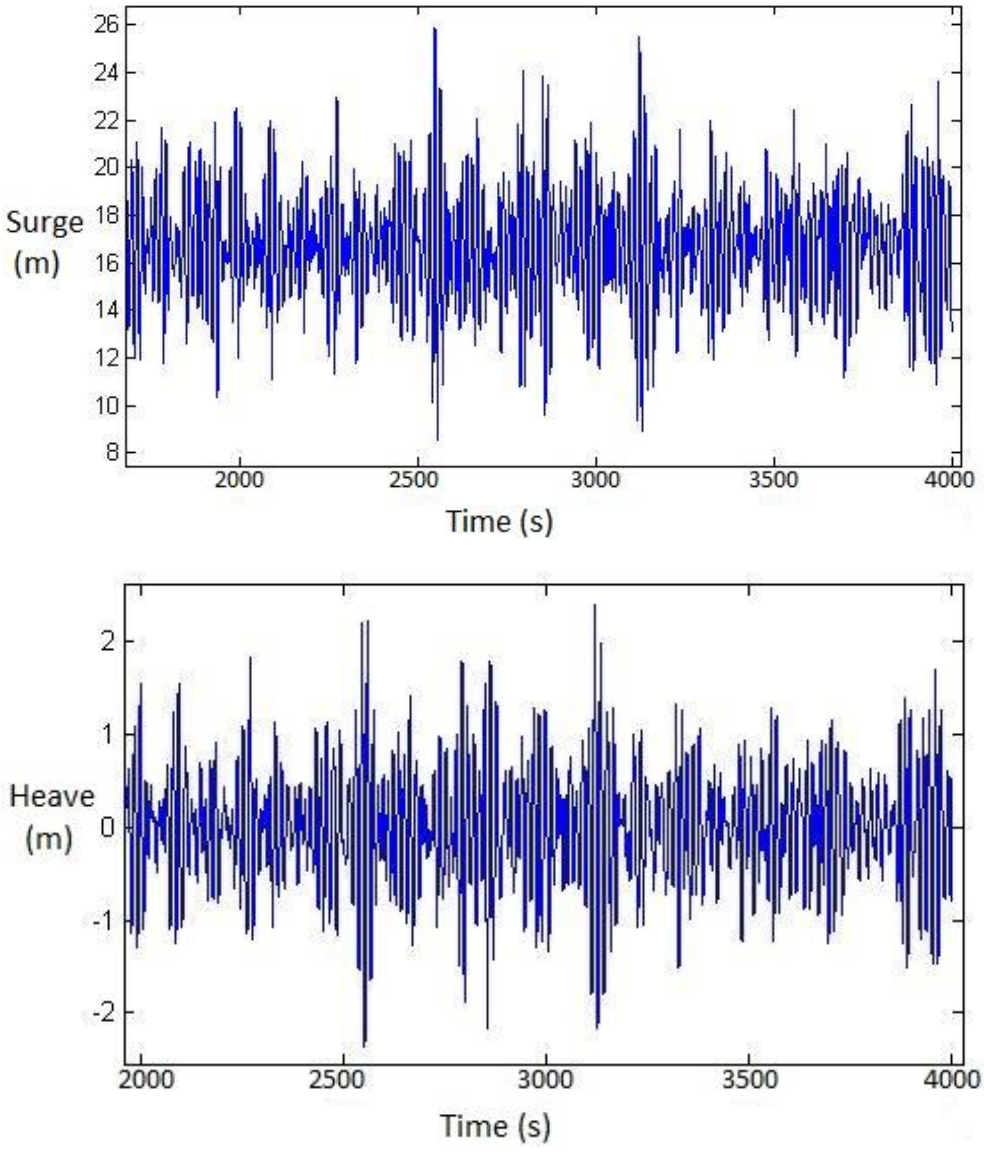

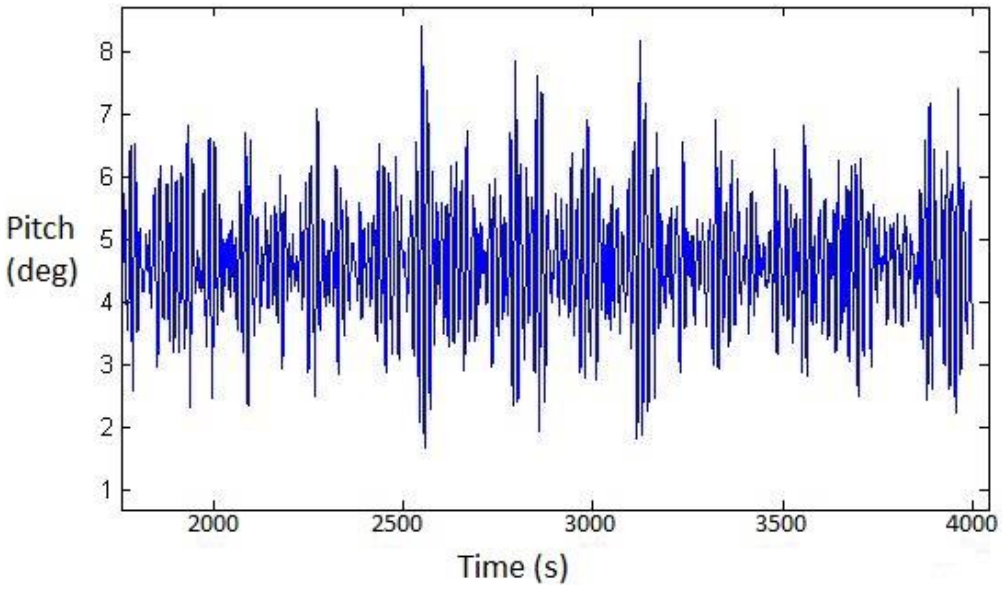

Figure 5-5: Response of the spar wind turbine under extreme condition

The extreme responses of the spar platform in surge, heave and pitch are shown in *Figure 5-5*. It is seen that the wave frequency response is dominating in all three DOFs, the period of motion is following the wave peak period (14.5 s).

Degree of freedom	Mean value	Maximum value
Surge [m]	16.7	28.1
Heave [m]	0.0	2.6
Pitch [deg]	4.6	8.9

Table 5-3: Response of the floating wind turbine under extreme condition

From *Table 5-3*, the surge and pitch have a non-zero value, while the mean value of heave is almost zero. All the maximum values of motion are within the allowable range. For the surge motion, the maximum offset is 28.1 m, which is almost 88% of the allowable offset (32 m). It means that the stiffness of the mooring system is just enough for the platform. In the future work, some modification of the mooring system may need to be applied, such as increasing the total mooring line length or changing the material properties of the catenary lines.

5.4.2 Extreme Tension

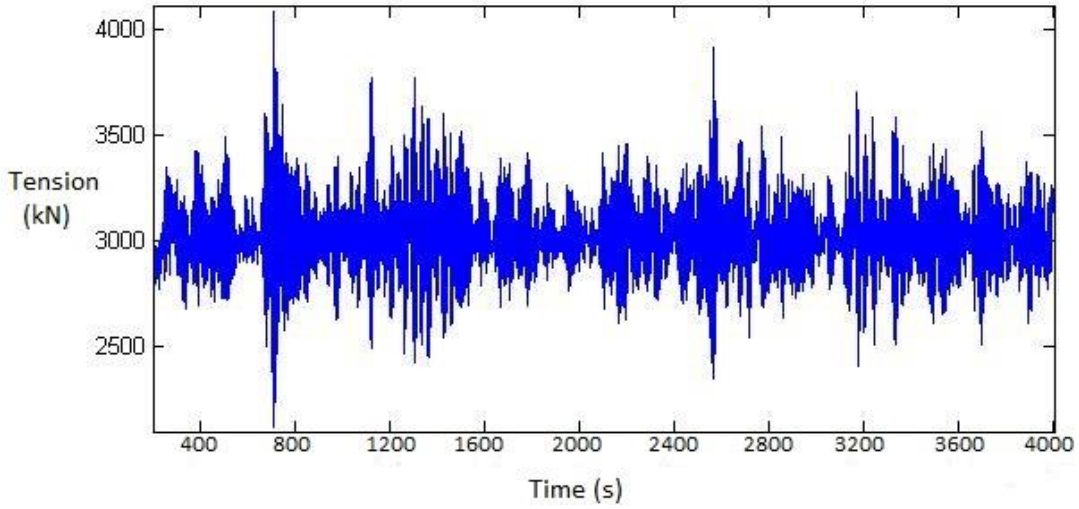

Figure 5-6: Mooring line tension response under extreme conditions

In this section, a ULS check is done based on DNV-OS-E301 [27]. The design for ULS is governed by the utilization factor:

$$u = \frac{T_{c-mean}\gamma_{mean}+T_{c-dyn}\gamma_{dyn}}{S_c} \leq 1 \qquad (5.15)$$

where, T_{c-mean} is the characteristic mean line tension, due to pretension and mean environmental; and T_{c-dyn} is the characteristic dynamic tension of the mooring line. γ_{mean} and γ_{dyn} are partial safety factors with γ_{mean} = 1.1, γ_{dyn} = 1.5. S_c is the characteristic strength of the mooring line which equals to 0.95 times of the minimum breaking strength.

In order to find T_{c-mean} and T_{c-dyn}, 10 simulations need to be performed to fit the extreme value distribution of maximum line tension. By using different wave seed number for each simulation and fitting the extreme line tension sample to a Gumbel distribution (*Figure 5-7*), the extreme value distribution is obtained. T_{c-mean} is found by averaging mean tensions of the 10 simulations. And $T_{c-dyn} = T_{MPM} - T_{c-mean}$, which T_{MPM} is the most probable max tension correspond to the 63% percentile, i.e. 37%

probability of exceedance. For conservative, the mooring line's minimum breaking strength is obtained from Hordvik's master thesis [37], i.e. 7682 kN for chain-connectors.

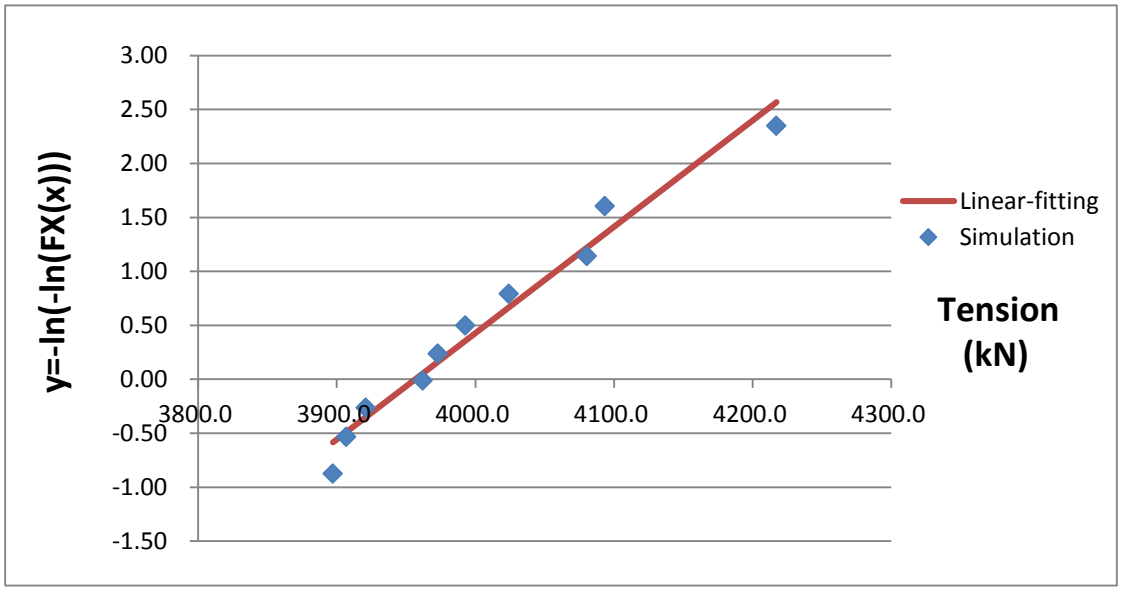

Figure 5-7: Gumbel distribution of extreme maximum tension

T_{c-mean}	γ_{mean}	T_{c-dyn}	γ_{dyn}	sum	S_c	u
3022.2	1.1	1012.6	1.5	4843.4	7297.9	0.66

Table 5-4: ULS check of the mooring line tension

The results of ULS check is summarized in *Table 5-4*. It is seen that the mooring line strength fulfill the ULS requirement. So it can be said that the OC3-Hywind mooring system is acceptable for the DTU 10MW RWT of spar floater. However, the utilization factor is less than 0.7, which means the strength of the mooring line is more than enough. The limited number (10) and time length (4000s) of simulations can be the reason for the too small utilization factor. In general, at least 20 simulations with 3-hour time length should be performed to do the Gumbel-fitting.

6 CHAPTER VI: COUPLED DYNAMIC ANALYSIS

6.1 SIMO-RIFLEX-AeroDyn Model

In this part, the coupled dynamic analysis is performed by the code SIMO-RIFLEX-AeroDyn (SRA) which is developed by Bachynski for the analysis of TLP floating wind turbine [41], as shown in *Figure 6-1*. It has several advantages, as listed below:

- It can deal with the sophisticated hydrodynamics, up to date aerodynamics, flexible control module and nonlinear beam theory which are quite useful.
- Possible to model different types of foundations and to include additional elements.
- Reasonable computational time.

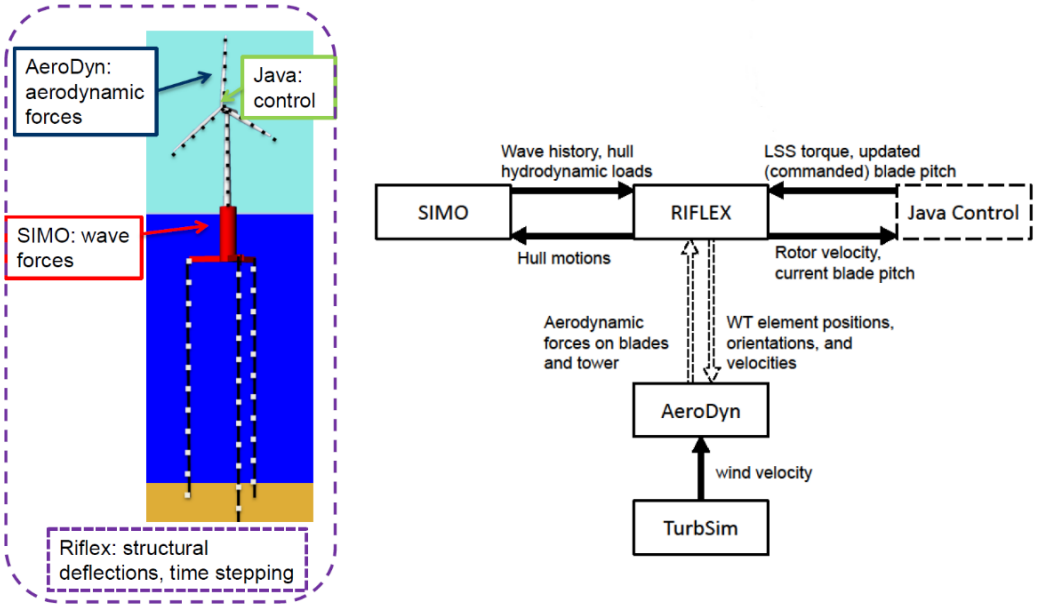

Figure 6-1: Illustration of the coupling between SIMO, RIFLEX, AeroDyn and the controller ([41])

Together with the mooring system, the complete SIMO-RIFLEX-Aerodyn model of DTU 10MW RWT spar floater now can be developed to perform the time-domain simulations. The model is built be SIMA workbench which is a software developed by MARINTEK. The configuration of the whole structure is shown in *Figure 6-2*.

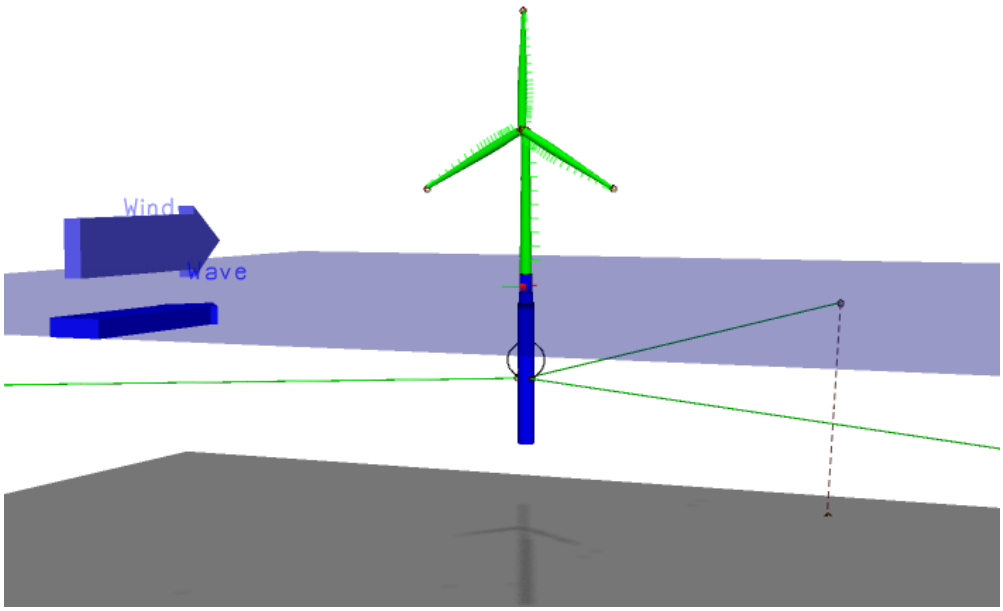

Figure 6-2:The completed SRA model in SIMA

The spar-floater, hub and nacelle are modelled as rigid SIMO bodies. The supernode at spar location acts as the master node for the fairleads (pinned) and tower bottom (fixed). Hydrodynamic loads are applied to the platform, but no external loads are applied to hub and nacelle. What's more, viscous drag force is also considered in the spar platform, as the spar is divided into three slender cylinder elements with same drag coefficient of 0.5. The platform motions are defined in the global coordinate system with Z axis along the tower and X axis parallel to the wind direction.

The mooring lines, tower, shaft and blades are modelled by flexible beam elements. Each mooring line consists of 33 uniform beam elements with the same cross sectional property from the previous chapter. Each blade has 26 beam elements (airfoils) with cross sections specified with two stiffness axes, which are then rotated according to the twist angle of the blade section. According to Section 3.1.2 & 4.3, the tower consists of 10 sections and the total height should be reduced to 105.63m, which means each section is cut by 1 meter. All the properties of blades and tower cross-sections are obtained from the DTU 10MW RWT description [18]. The illustration of the model in SRA analysis can be seen in APPENDIX A.

6.2 Constant Uniform Wind Test

In the section, constant uniform wind tests were performed in order to examine the mean offsets of the platform and check the wind turbine performance, including the controller. The constant uniform wind tests were conducted for 4 – 24 m/s with 2 m/s as increment and 11.4m/s (12 cases). And one important thing is turbine start-up takes longer for low wind speeds. The results of constant wind test are shown in figures below:

(a)

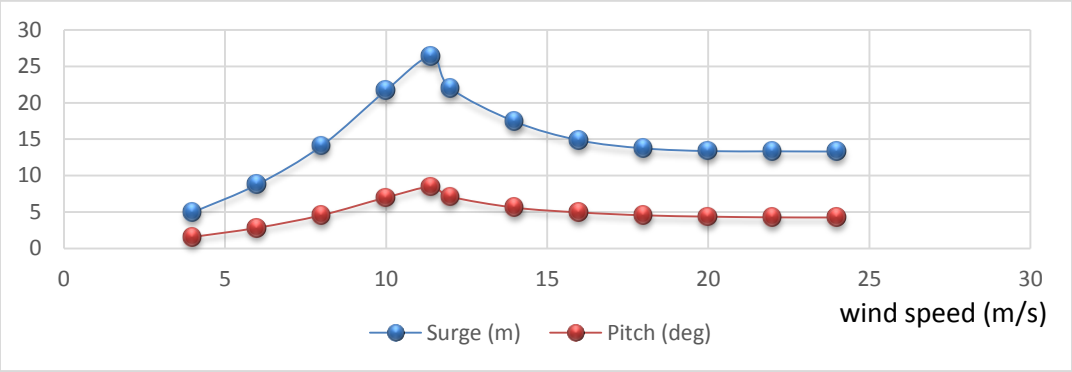

(b)

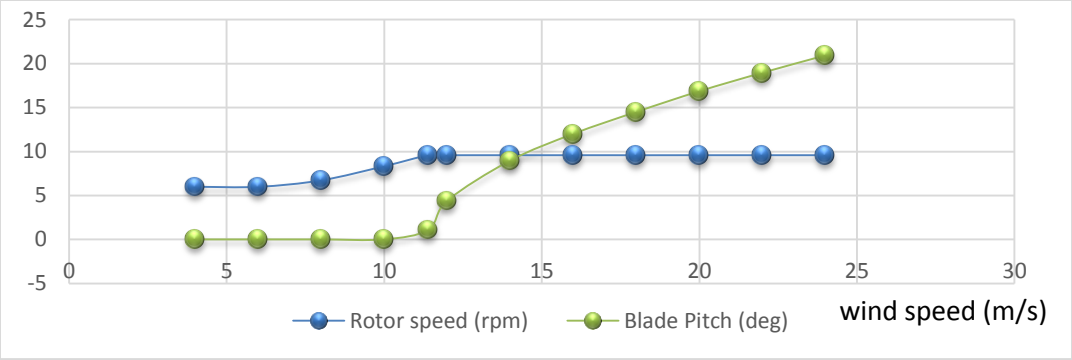

(c)

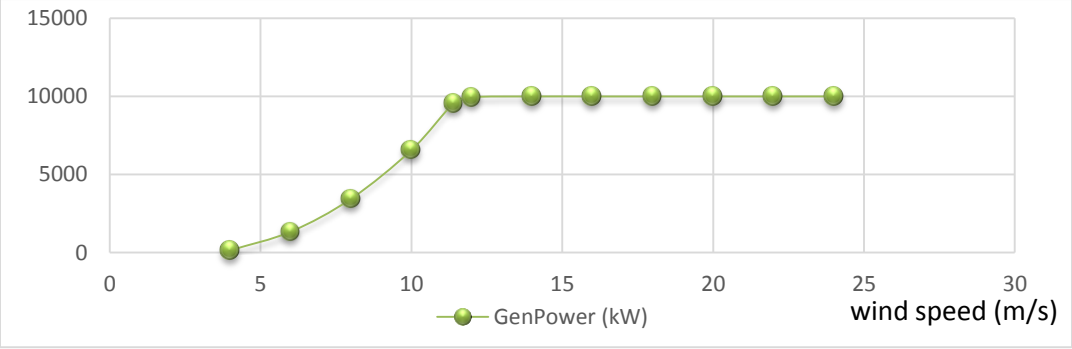

(d)

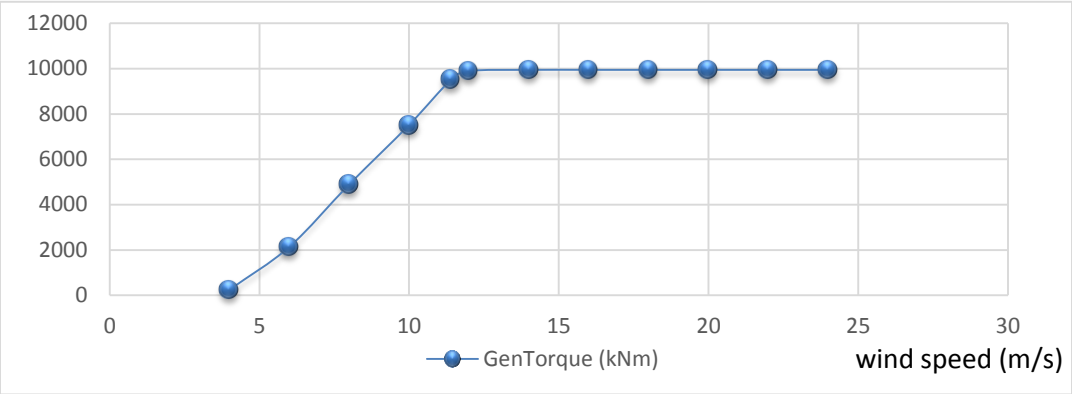

(e)

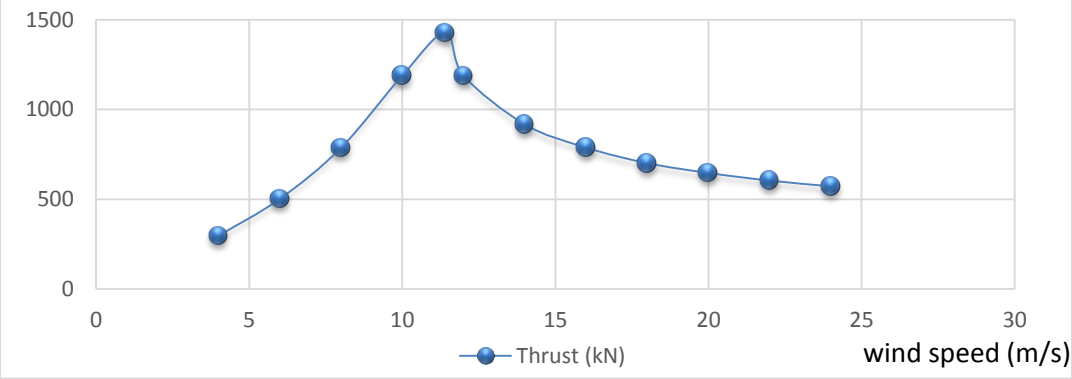

Figure 6-3: The results for constant wind test versus wind speeds : (a) Mean offset of platform in surge & pitch, (b) Mean rotor speed & blade pitch , (c)Mean generator power, (d) Mean generator torque, (e)Mean thrust

In this test, the critical point with 11.4 m/s of wind speed can divide the region between partial load region (II) and full load region (III), as introduced in Section 2.6 before. After the rated wind speed, the mean rotor speed, generator torque and power reach the maxima and are kept in constant value in the full wind load region as wind speed still increasing. Meanwhile, the mean platform displacements and thrust start to decrease as the blade pitch angle increased. It means that the blade pitch can help to keep the generated power constantly and stabilize the dynamic behavior of offshore wind turbine.

It is necessary to note that the generator power production could not reach the rated value with the original DTU 10MW land-based controller setting, so the "minimum blade pitch table" in the control file is adjusted to get a reasonable result.

6.3 Discussion of Constant Wind Test

On the whole, the performance of the spar floater wind turbine and results of the constant wind tests are reasonable. However, some interesting problems and discoveries are shown up during the tests, which will be discussed in this section.

6.3.1 Periodic Resonant Behavior at Rated Wind Speed

In general, the Generalize Dynamic Wake (GDW) method could be used for wind speed larger than 8m/s [32]. In this constant wind test, Blade Element/Momentum Theory (BEM) is applied for wind speed below 8m/s and GDW for wind speed above 8m/s. However, it is found that at rated wind speed U=11.4m/s, there are periodic resonant motions of the platform, which as shown below:

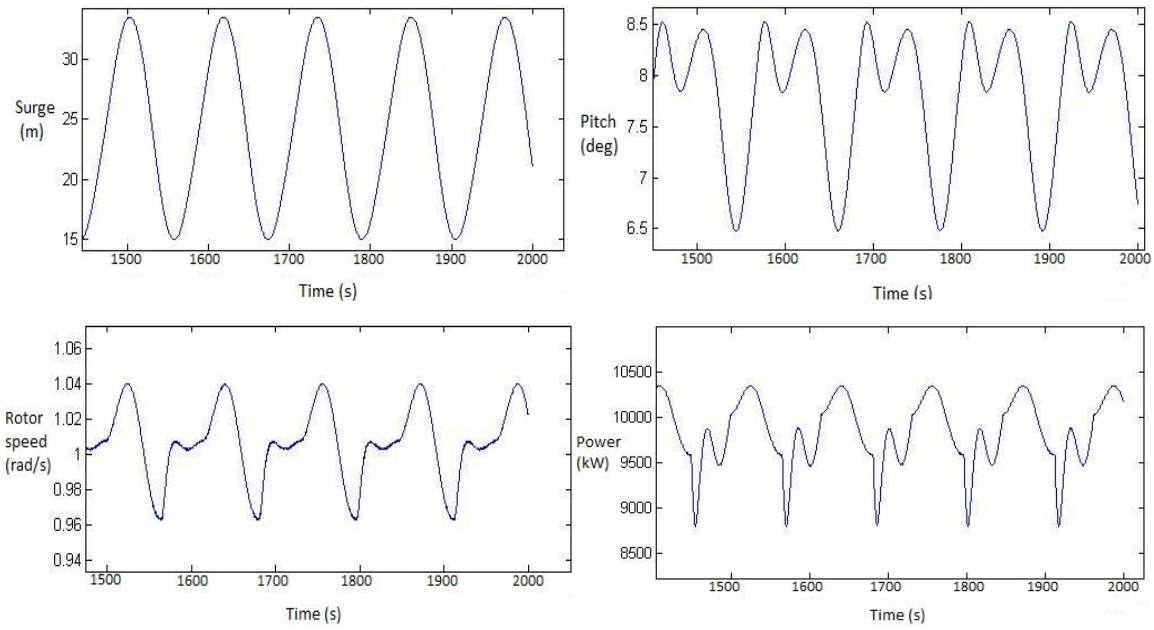

Figure 6-4: Constant wind test of U=11.4m/s with GDW method

It can be seen that when mounting the DTU 10MW RWT onto the spar platform, large resonant motion of the floater will occur at rated wind speed. It also leads to the periodic variation of wind turbine performance. The possible reason for this resonant periodic behavior will be discussed below.

Aerodynamic Theory

The possible reason is the difference between BEM and GDW theory applied in the constant wind test. Then the BEM theory is applied to the constant wind test for rated wind speed 11.4m/s. The results are shown in below:

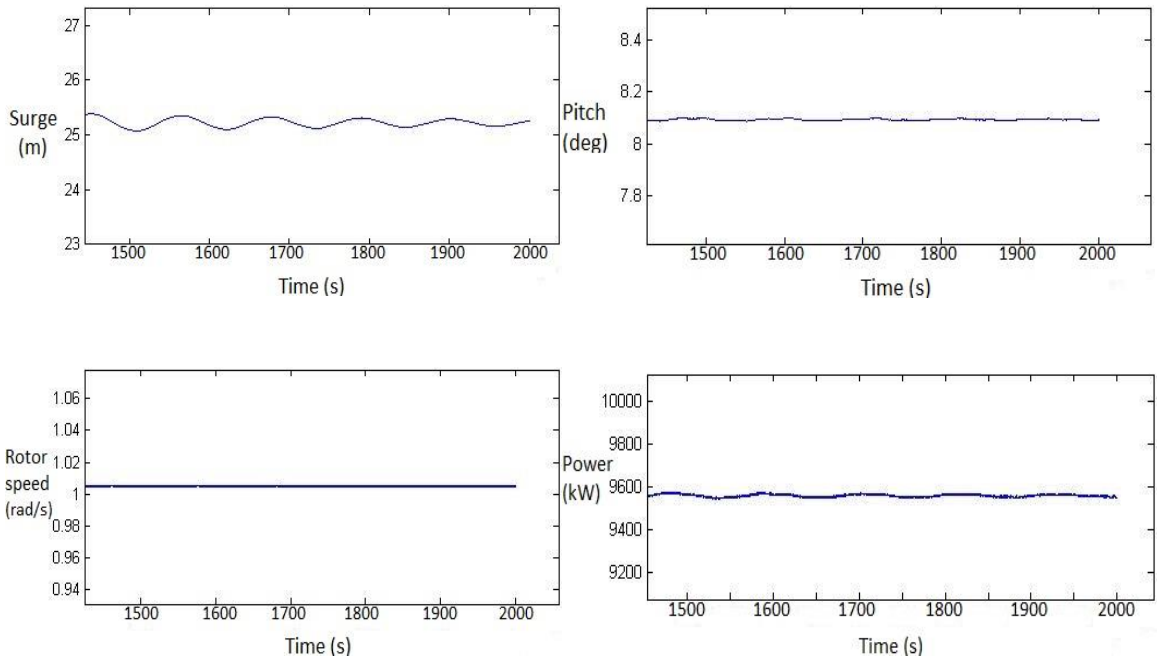

Figure 6-5: Constant wind test of U=11.4m/s with BEM method

It is seen that the results of BEM method are much better than before, and the periodic resonant motion of platform is disappeared. Compared with the difference between the BEM and GDW method, it can be concluded that the BEM method is appropriated for the rated wind speed case.

For floating wind turbines, the combination of wind and platform motions can result in low relative velocity between wind turbine and air. It is possible that at rated wind speed case, the large floater pitch motion decreases the relative velocity which makes the GDW method unsuitable. So it is important to check the results for mean wind speeds around rated wind speed to be sure that the simulation was successful.

6.3.2 The Influence of Simulation Time-Step (RIFLEX)

In the initial constant wind test, the simulation time-step in the RIFLEX was set as 0.005s. However, it is found that when constant wind speed above 14m/s or below 8m/s, an unstable yaw motion of the platform will show up. Three samples of yaw motion with 18m/s wind speed are shown below:

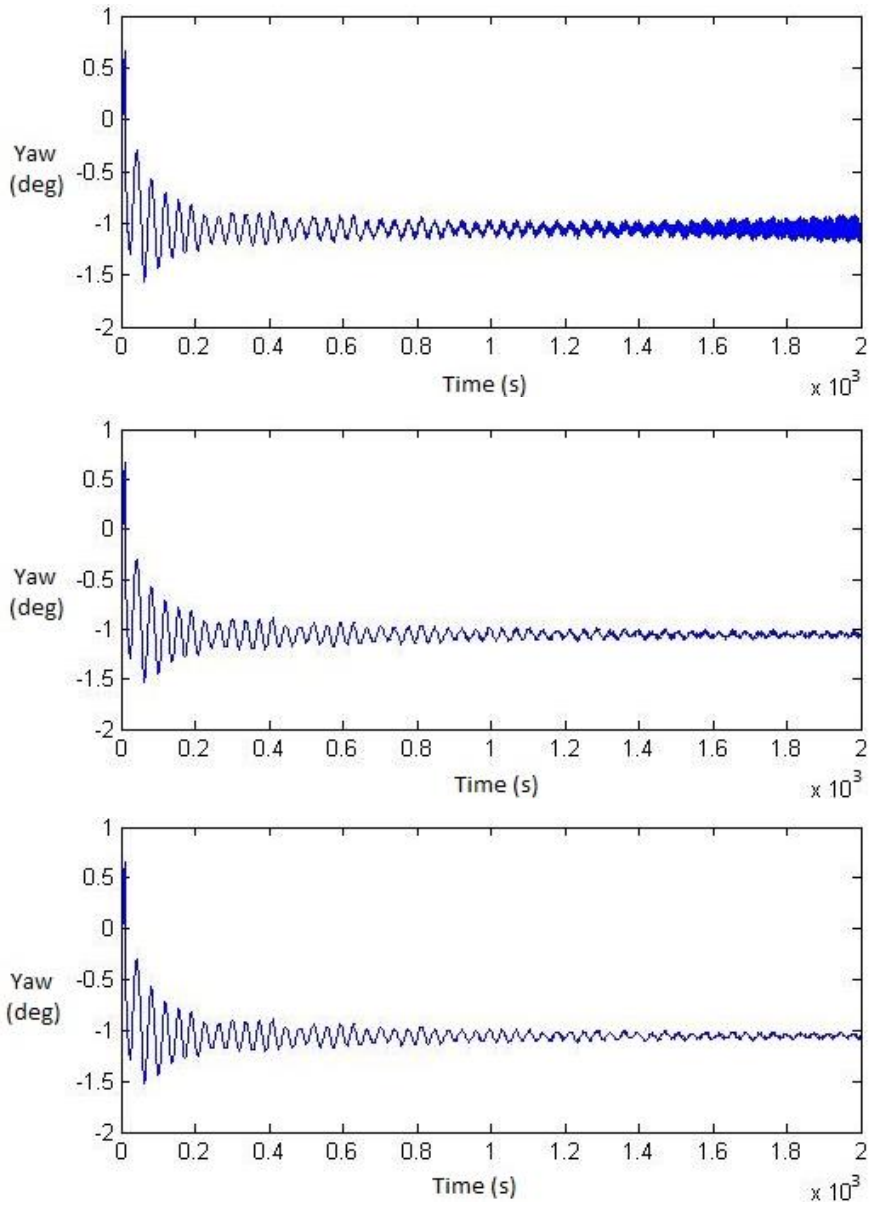

Figure 6-6: Time series of yaw motion with 18m/s wind speed. RIFLEX time-step: 0.005s(top), 0.002s(middle) & 0.001s(bottom)

From *Figure 6-6* above, it's easily seen that an unstable yaw motion appears after 1000s of simulation with time step 0.005s, and the amplitude of motion is amplified. To deal with this problem, the RIFLEX time step was modified, i.e. reduced to 0.002s and 0.001s, to check the influence of simulation time-step.

It is seen that as the simulation time-step reduced, the platform's yaw motion will become more stable, and the amplification effect disappear. In fact, a relatively small time-step is required for the RIFLEX analysis since the large velocities attained by the blades [46]. Due to the limitation of thesis scope, no further study of the phenomenon will be carried out. But the possible reason for this phenomenon is the numerical unconvergence of the analysis, since the result will be more accurate as the simulation time-step smaller.

Besides, at rated wind speed 11.4m/s and 12m/s, the generator power cannot reach the maximum value 10MW, but very close (9.6 and 9.95MW, respectively). The large pitch motion of the platform (≈9 deg) and the unfit blade pitch angle setting in the controller can be the reason for this.

6.4 Turbulent Wind Tests

Turbulent wind file is generated by the TurbSim [45] code and is used as input to AeroDyn. Three operational cases and one extreme condition from *Table 3-3* are considered in this test. The sea state is modelled by JONSWAP spectrum with a peakness factor of 3.3.

6.4.1 Control System modification

The controller for land-based DTU 10MW wind turbine is applied in all the simulations. Before the turbulent wind test, a modification of the controller is necessary. As Nielsen [43] and Jonkman [44] pointed out in their papers, the large resonant motion of the floater can be caused by negative damping from the blade pitch controller. This resonant phenomenon is more obvious in the turbulent wind test, which is shown in *Figure 6-7*.

Jonkman [9] have presented two modifications to the control systems in order to eliminate the potential for negative damping of the platform-pitch mode and improve system's response.

The first modification is a reduction of gains in the blade-pitch-to-feather control system. The DTU 10MW RWT controller is based on classical proportional-integral (PI) theory [18]. The original blade pitch controller system has a natural frequency of 0.06Hz and damping ratio of 0.7. This frequency is above the natural frequency of the floater pitch motion, i.e. 0.028Hz. According to Jonkman [9], the smallest controller response natural frequency must be lower than the smallest critical support structure natural frequency to ensure that the support structure motions of an offshore floating wind turbine with active pitch-to-feather control remain positively damped. Therefore, the controller response natural frequency was changed to 0.02Hz, to ensure that it is lower than the floater pitch natural frequency (see *Table 6-1*). The detail of how to change the controller response natural frequency can be found in Qiang Wang's thesis [30].

Item	**Default value of DTU 10MW RWT controller**	**Target value after modification**
Blade pitch controller natural frequency [Hz]	0.06	0.02
Proportional gain [-]	0.524485	0.174828
Integral gain [-]	0.141233	0.015693

Table 6-1: Modification of PI gains of the DTU blade pitch controller

The second modification is to change the generator-torque control strategy when operating at rated power. It means the control law is changed from a "constant generator power" to a "constant generator-torque" in the SRA controller input.

The time series of platform motion after modification is also shown in bottom of *Figure 6-7*. It is obvious that the resonant motion vanished, which means that the blade pitch controller is working properly this time. And there is less negative damping from the controller.

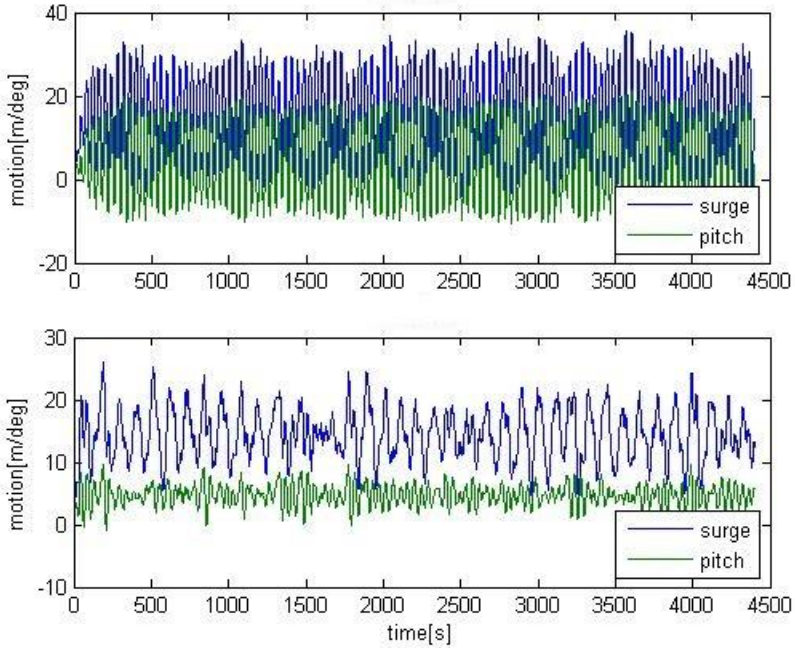

Figure 6-7: Comparison of motion under turbulent wind 18m/s. Top: before modification; Bottom: after modification

6.4.2 Result of Turbulent Wind Test

Here the result of third load case (Above-rated: 18m/s) is taken as an example. Time histories of the platform motion responses and wind turbine responses are shown in *Figure 6-8* and *Figure 6-9* respectively.

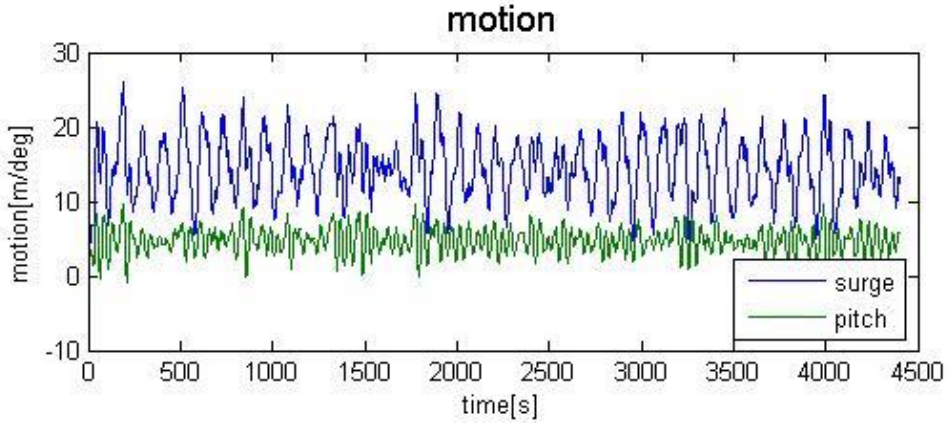

Figure 6-8: Time series of platform motion for load case 3.

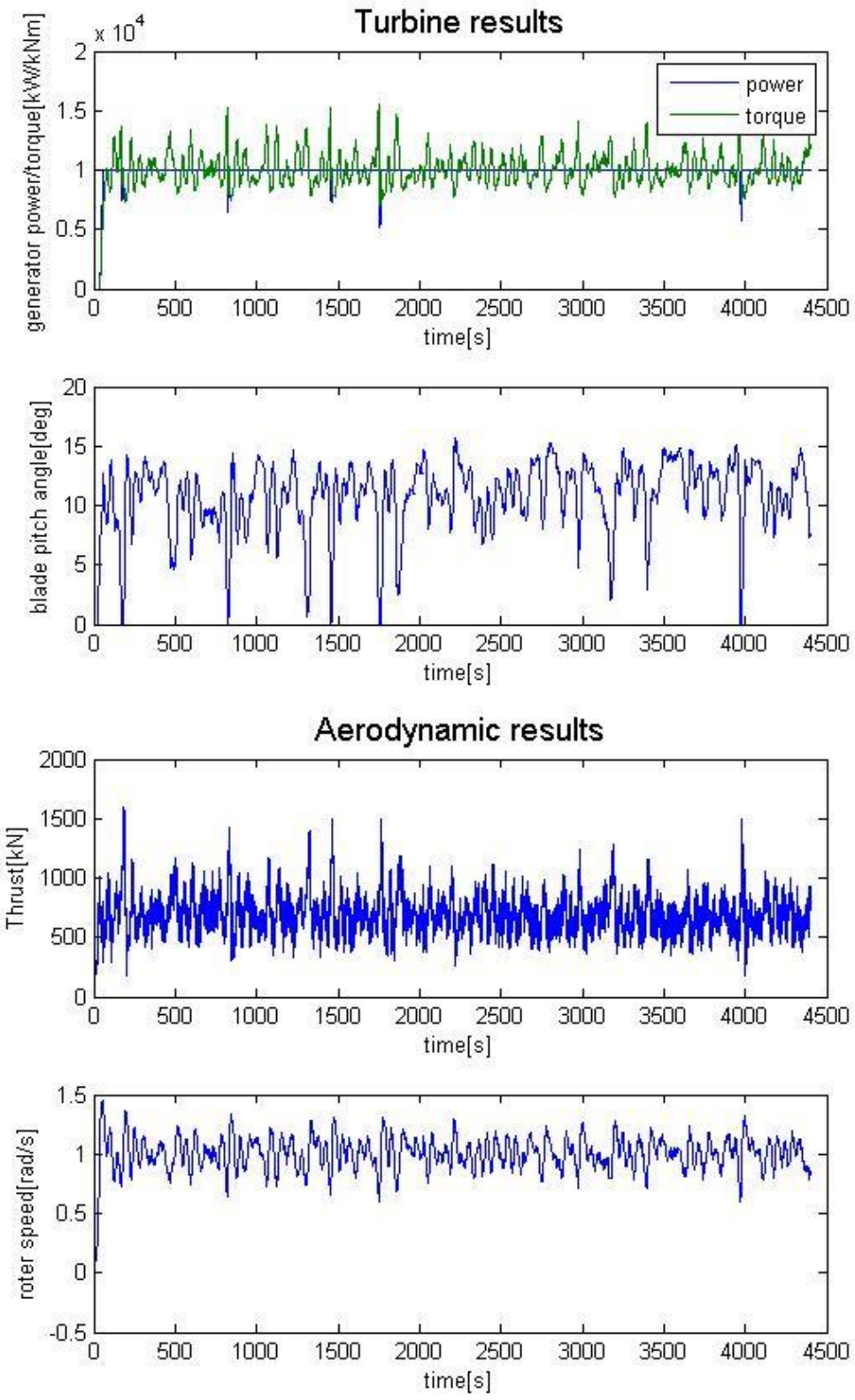

Figure 6-9: Time series of wind turbine performance for load case 3

It is seen from *Figure 6-8* that the platform motion is highly oscillating in time due to the turbulent wind and irregular wave condition, especially the surge motion. The relatively small damping effect of slender cylinder like spar and still some negative damping from the blade pitch controller may result in the large surge oscillation. It can be seen that in extreme load case (*Figure B-4*), with wind turbine parked and blade pitched to feather, the surge oscillation is much different than the operating cases, since there is no negative damping from controller and the oscillation is wave dominated.

As expected in *Figure 6-9*, there are also highly oscillation in the curves of blade pitch, thrust and rotational speed. The generator torque is oscillating in time since the "constant generator-power" control law is applied in turbulent wind tests. Meanwhile, the generator power output is almost constant and stable (10 MW), which means the controller is working properly in this case. But there are still some places on the power curve below the rated value 10MW, which means the relative wind speed on hub is dropped below the rated wind speed (11.4m/s), due to the combination of large surge and pitch oscillation of spar. The time series of other load cases can be found in APPENDIX B.

Spectral Analysis

Spectral analysis is commonly used to study the response of structure under dynamic loading. Frequency of response is treated as the only parameter without time. Maximum responses of each separate mode are got from the response spectrum, then maxima of each mode are combined in a special way to produce an estimate of maximum response of the structure.

In order to study the influence of turbulent wind further, a spectral analysis is necessary for the wind turbine response. The spectra represent the power spectral density, which are obtained by Fast Fourier Transform (FFT) of the time series and then smoothed and exported by WAFO [47] toolbox. The spectra are shown in below:

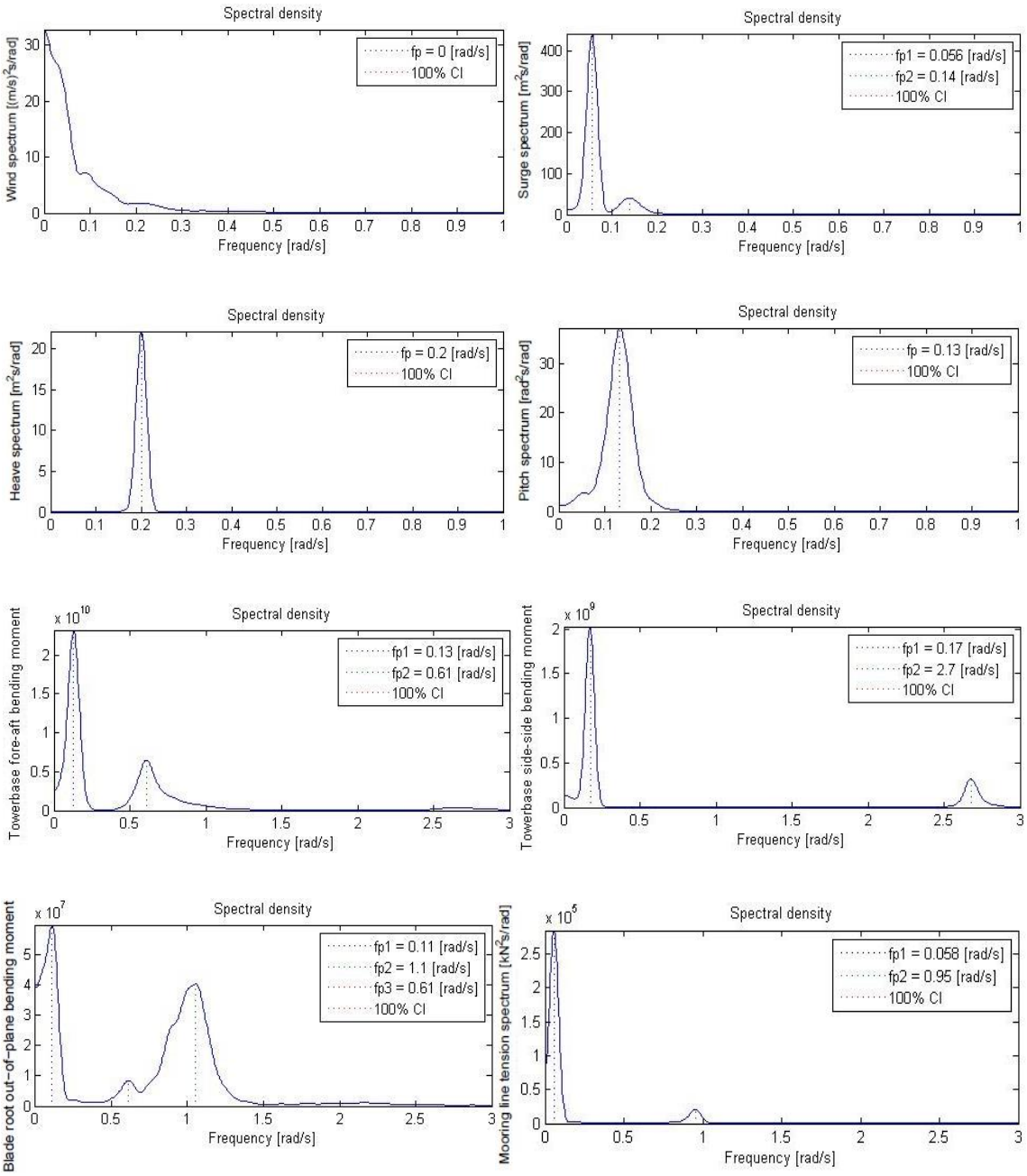

Figure 6-10: Smoothed spectra of turbulent wind (first) and floater responses: surge(second), heave(third), pitch (fourth), towerbase fore-aft bending moment (fifth), towerbase side-side bending moment(sixth), blade-root out-of-plane bending moment (seventh) and mooring line tension (last) for load case 3

In second spectrum of *Figure 6-10*, the surge motion is dominated by the low frequency responses due to the turbulent wind and surge resonant responses. The peak is at surge resonant frequency, while pitch motion and blade-pitch controller also have an influence

on the surge motion, i.e. lead to a large surge oscillation of the system. And for the pitch spectrum, the pitch resonant frequency is same with the controller's blade-pitch frequency (≈0.13 rad/s), which is smaller than the natural pitch frequency obtained from decay-test (0.17 rad/s). But the peak of heave response spectrum is at the heave natural frequency (0.2 rad/s), the controller and pitch motion have no effect on the heave motion. The turbulent wind has some effect on the surge and pitch motion, but with no influence on the heave motion. The possible reason is that no wind inclination is considered in the simulation, which means the wind direction is always horizontal. So the turbulent wind cannot excite large vertical heave motion.

In general, it can be concluded that the floating wind turbine's surge and pitch resonant motions are excited by turbulent wind combined with the blade-pitch controller, while heave motion is not affected. What's more, with the wind speed increasing, the influence from the controller becomes great, and the oscillation becomes large too. It implies that the controller from DTU 10MW land-based wind turbine may still have some problem with the spar floater.

As for the tower base bending moment, the local fore-aft bending moment results from the thrust is normal to the turbine blades. The fifth spectrum shows that the fore-aft bending moment is mostly affected by controller's frequency and turbulent wind, and the irregular wave (≈0.6 rad/s) also has some influence on it. There is a small peak in the range of 2.7 ~ 3.0 rad/s, which is possible due to the 3P-effect of the blades. Meanwhile, the side-side bending moment is because of the blades torque, and the sixth spectrum indicates that the roll resonant frequency dominates the response and the 3P-effect also exists.

The seventh figure is the spectrum of blade-root out-of-plane bending moment, and it is clear that the turbulent wind and 1P-effect (rotor speed) have important influence on the response. What's more, the wave spectrum also has a contribution to the blade-root out-of-plane bending moment.

The last one is the spectrum of mooring line tension, which is dominated by surge motion for all the load cases.

Under extreme conditions the influence of turbulent wind and blade-pitch controller is relative small since the blades are pitched to feather, all responses are wave dominated. As for the spectra of all load cases, please refer to the APPENDIX C.

Aerodynamic damping

As mentioned in spectral analysis, the pitch resonant frequency is 0.13 rad/s, which is smaller than the natural pitch frequency obtained from decay-test (0.17 rad/s). What's more, the surge resonant frequency is also a little smaller than surge natural frequency. Besides the influence from the controller, the aerodynamic damping is another reason for this phenomenon. As shown in Eq. (5.14), if the damping ratio is large enough, the resonant frequency will be reduced effectively.

Under operational condition, there is very large thrust force acting on the rotor which is the main source of aerodynamic damping. A detailed derivation for the aerodynamic damping of constant speed wind turbines is given by Garrad [48]. The aerodynamic damping term is:

$$C_{damping} = \frac{1}{2}\rho V_{rot} c \frac{dC_L}{d\alpha} \tag{6.1}$$

Where $\frac{dC_L}{d\alpha}$ is the rate of change of the lift coefficient with angle of attack α, c is the chord length and V_{rot} is the blade tip speed.

According to Eq. (6.1), it is clear that the aerodynamic damping depends on the blade tip speed, i.e. the rotor speed for a specified turbine. Therefore, the large aerodynamic damping under operational conditions can be the possible reason for the reduction in surge and pitch resonant frequency.

CHAPTER VI: COUPLED DYNAMIC ANALYSIS

7 CHAPTER VII: COMPARISON OF THREE CONCEPTS

There are another two master students also studying offshore floating wind turbines, but with different floater concepts. These concepts include a semi-submersible (SS) and a tension leg platform (TLP).

All concepts are designed to support the DTU 10MW RWT, and have been modeled in the same manner by using the same software. So the results are based on the same theory and hence easily to compare. The environment conditions for the simulation are also same, which are listed before.

7.1 General Information of Three Concepts

Semi-submersible (SS)

The semi-submersible (SS) is based on the Principle powers "Windfloat" design. The platform is composed of three columns, with heave plates at each column for additional damping in heave, pitch and roll. The wind turbine structure is located at one main column as shown in *Figure 1-2*.

Three catenary mooring lines are attached to the three columns to provide horizontal restoring stiffness. Good stability is achieved by the large waterplane area moment of inertia to limit the pitch and roll motion in wind and waves. The Windfloat design also included an active ballast system which is not considered here. The main parameters of the concept and mooring configuration are summarized in *Table 7-1* & *Table 7-2*. The detail of this semi-submersible platform is on master thesis of Touhidul Islam.

Tension Leg Platform (TLP)

The TLPWT concept (*Figure 7-1*) is based on SeaStar deepwater mini-platform. The TLP floater consists of two central columns and three spokes. The three spokes spread evenly (120deg) around the central columns. Since the spokes are all connected to the

bottom central column, the bottom column is designed as twice thicker than the upper one to provide sufficient strength. Besides, there is a concrete ballast (4456 t) locating inside the bottom column. The mooring system consists of 3 vertical tendons mounted at the ends of two spokes at the bottom of the structure. The detail of this concept can be found in the master thesis of Xiaoshuang Tian. The main parameters of the concept and mooring configuration are summarized in the following tables.

Floater	**Spar**	**SS**	**TLP**
Draft [m]	120	19.15	35.3
Water Depth [m]	320	200	200
Column Diameter [m]	12	12.8	19.8
Number of columns/pontoons	1	3	3
Total Mass [t]	13405.2	7708	9293
Displacement [m^3]	13078.2	7520	17362
COG from SWL [m]	(-0.3, 0, -74.53)	(0, 0, 4.9)	(-0.04, 0, -9.83)
COB from SWL [m]	(0, 0, -62.07)	(0, 0, -9.576)	(0, 0, -22.67)
Hub location from SWL [m]	(-2.7, 0, 119)	(27.6, 0, 119)	(-2.7, 0, 119)

Table 7-1: Main dimensions of three concepts

Floater	**Spar**	**SS**	**TLP**
Mooring Configuration	3×Catenary line	3×Catenary line	3×tension leg
Fairlead depth [m]	-70	-18.5	-35.3
Anchor depth [m]	-320	-200	-200
Unstretched mooring line length [m]	902.2	861.2	164.67
Mooring line diameter [m]	0.09	0.153	2.7
Equivalent mooring line mass density [kg/m]	233.12	466.0	5737
Equivalent mooring line axial stiffness [kN]	384,243	2,000,000	931,845

Table 7-2: Mooring system properties of three concepts

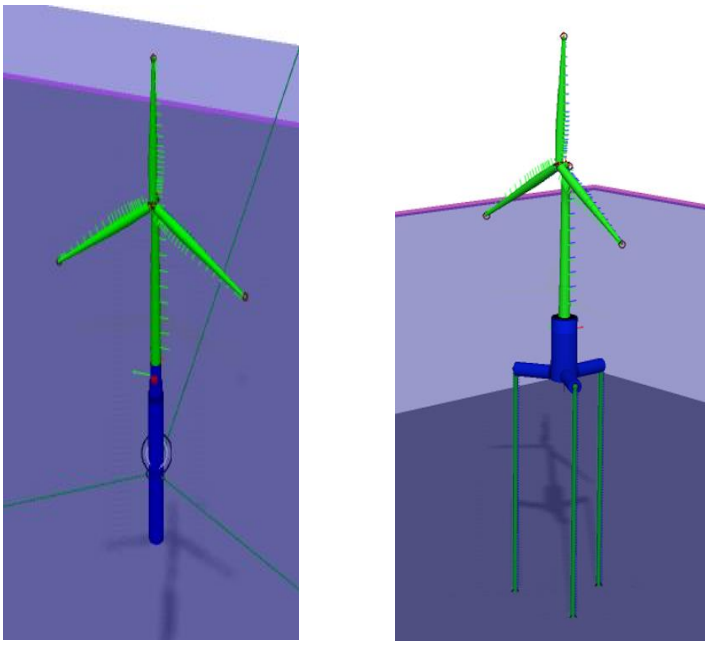

Figure 7-1: The spar(left) & TLP(right) as modelled in SIMA (no figure of SS in SIMA)

7.2 Results & Discussion

Free Decay Test

The three floaters considered here are designed to support the DTU 10MW reference wind turbine. The natural periods of the three concepts are given in *Table 7-3*.

Floater	**Spar**	**SS**	**TLP**
Surge/Sway [s]	103.3	62.6	45.23
Heave [s]	31.3	21.93	0.55
Roll/Pitch [s]	35.5	41.1	0.6
Yaw [s]	7.61	51.09	20.87

Table 7-3: Natural periods of the three concepts obtained by free decay tests.

In surge and sway, the spar has large natural periods due to the relative small surge and sway restoring stiffness from the catenary mooring system. In heave, the natural periods

of the spar and the TLP are located outside the typical wave excitation range (5~25s), while the natural period of the semi is still within this range, implying that large heave motion for the semi can be excited. In roll and pitch, the natural periods of all three concepts also are not within the wave periods range, so the wave-induced pitch motion will be small. However, the yaw natural period of the spar is within the wave period range, which may lead to significant yaw motion.

Wind Turbine Performance

Figure 7-2 shows the mean generator power production of the three concepts under the constant wind and calm water conditions. It is seen that the power behavior of the three concepts has the similar trend:

The mean generator powers of the three concepts increase as the wind speed increases. When reach a certain wind speed, the mean generator powers are kept in constant value as wind speed still increasing. The controller implemented is designed to keep the rotational speed constant when the rated operating point is reached, the mean generator powers are therefore constant at above rated wind speeds.

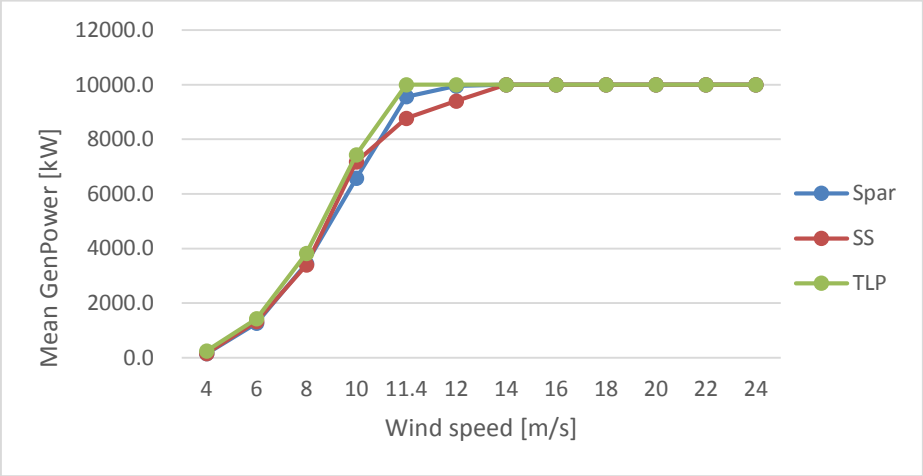

Figure 7-2: Mean generator power production for the three concepts under constant wind test

However, it is noticed that for spar and SS, the mean generator power could not reach the maximum value when wind speed at 11.4m/s and 12m/s. The possible reason is the relatively large pitch motion of spar and SS ($\approx 9^{\circ}$ and 11°, respectively). For TLP, this phenomenon is vanished due to the very small pitch motion (0.0056°).

Platform Motion

The dynamic responses are studied under the turbulent wind and irregular wave conditions, including the global platform motion, tower base fore-aft bending moment, blade root out-of-plane bending moment and mooring line tension. The same four environmental load cases are applied in the one-hour simulation, and the mean value and standard deviation of dynamic responses are obtained by averaging the one-hour ensembles.

Figure 7-3 & *Figure 7-4* compares the mean values and standard deviations of the global motions of the three concepts. Here only the results of surge and pitch motion are presented.

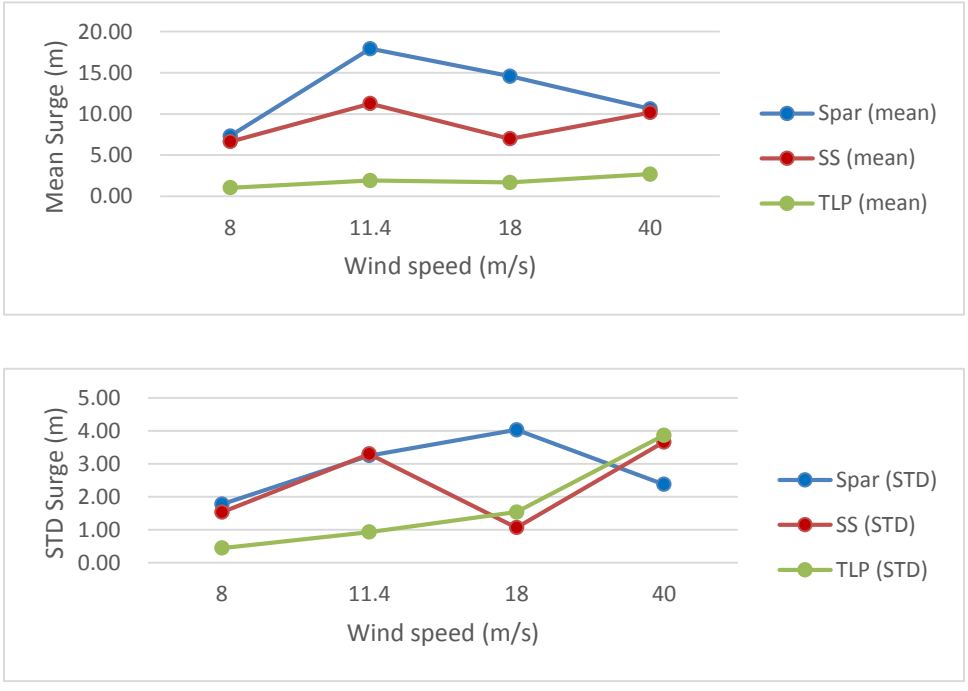

Figure 7-3: Mean value and standard deviation of surge motion for the three concepts

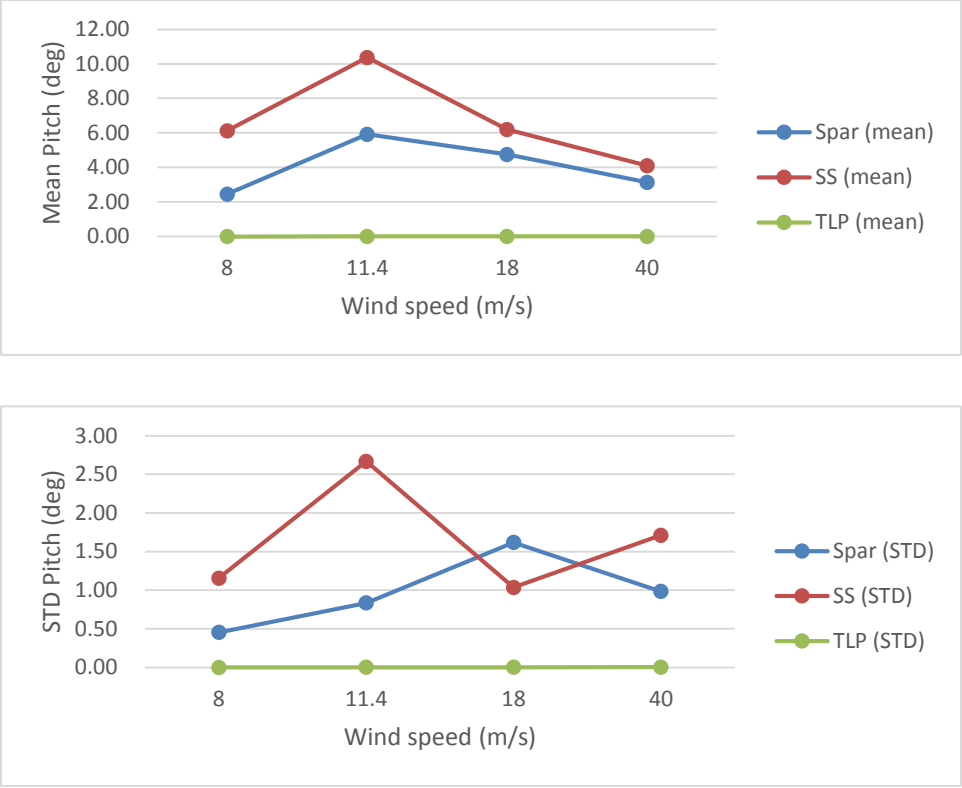

Figure 7-4: Mean value and standard deviation of pitch motion for the three concepts

Because of the differences in structural and hydrodynamic properties and in mooring systems, the three floater wind turbine concepts have different global motions. But at rated wind speed, all three concepts have the relatively large surge and pitch motions.

As the center of gravity of the spar is 74.53 m below SWL, which is much larger than the semi and TLP, the mean value and standard deviation of surge motion for the spar are therefore larger than others. For pitch motion, the semi has larger mean value and standard deviation than others. And due to the taut mooring system, all the motions for the TLP is much smaller as compared to the spar and the semi.

As mentioned before, since the negative damping from the controller when wind speed above rated, the oscillation of spar, i.e. the standard deviation of motion, is larger than other two cases when the wind speed is 18m/s. But the mean value of spar is reasonable in the case of 18m/s.

Tower Base Bending Moment & Blade Root Bending Moment

The tower base bending moment and blade root bending moment are caused by the large aerodynamic force acting on the rotor and blades. The tower base fore-aft bending moment and blade root out-of-plane bending moment are chosen for comparison.

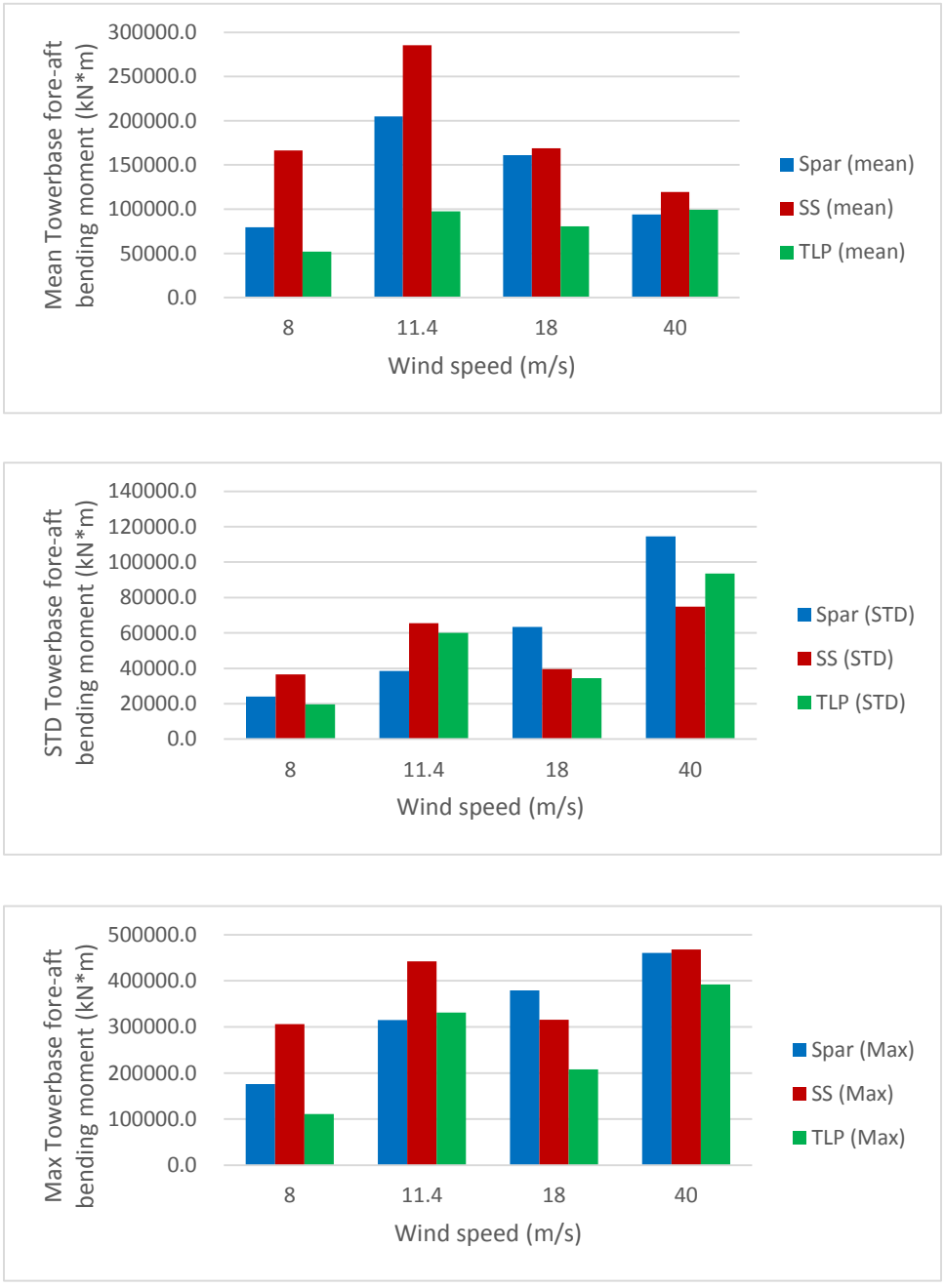

Figure 7-5: Mean value, standard deviation & max value of tower base fore-aft bending moment for the three concepts

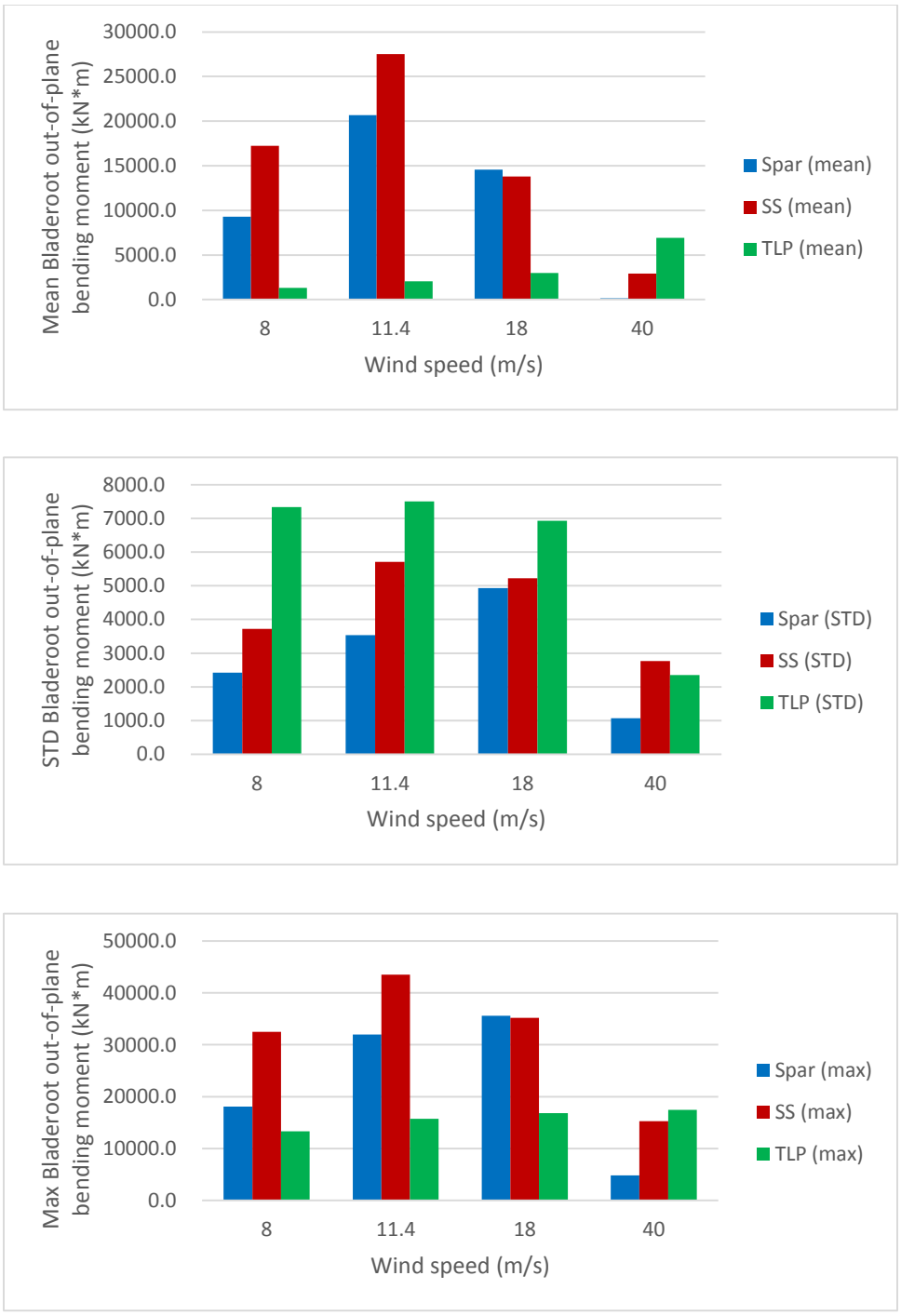

Figure 7-6: Mean value, standard deviation & max value of blade root out-of-plane bending moment for the three concepts

Figure 7-5 shows the comparison of tower base fore-aft bending moment for the three concepts. It is noticed that the mean value of moment reaches its largest value at rated

wind speed, which is consistent with the thrust performance of wind turbine. The standard deviation and maximum value of spar is increasing with wind speed increasing, also due to the large oscillation behavior of the structure. These large variations of bending moments under high wind speed can cause large stress fluctuations, thus leading to great fatigue damage to tower base.

Figure 7-6 shows the comparison of blade root out-of-plane bending moment for the three concepts. Firstly, it is noticed that the mean value of moment reaches its largest value at rated wind speed for spar and semi, which is also consistent with the thrust performance of wind turbine. Besides, for the extreme load case, the blade bending moment reduces dramatically, especially for spar, which is caused by the fact that all blades are pitched to feather. The blade root out-of-plane bending moment of spar and semi have the similar behavior, yet the TLP has a different trend.

The figure above also shows that the most dangerous condition for the tower response is the condition at rated wind speed rather than the condition at the 50-year extreme condition.

Mooring Line Tension

In this part, the mooring line tensions at the fairlead are studied. The comparison of three concepts is shown in *Figure 7-7*.

As presented before, the three concepts used different mooring systems which lead to different behaviors of the mooring line tension. The mean value, standard deviation and maximum values of the semi are all larger than that of the spar. And the TLP applied the three pretension tendons, which results in very large tension in the tendons. The tension of TLP's tendon is almost 8 times higher than the mooring tension of spar and semi. The trend of mean value, standard deviation and maximum values of all three concepts are similar. The maximum tension value appears at the extreme condition for all concepts.

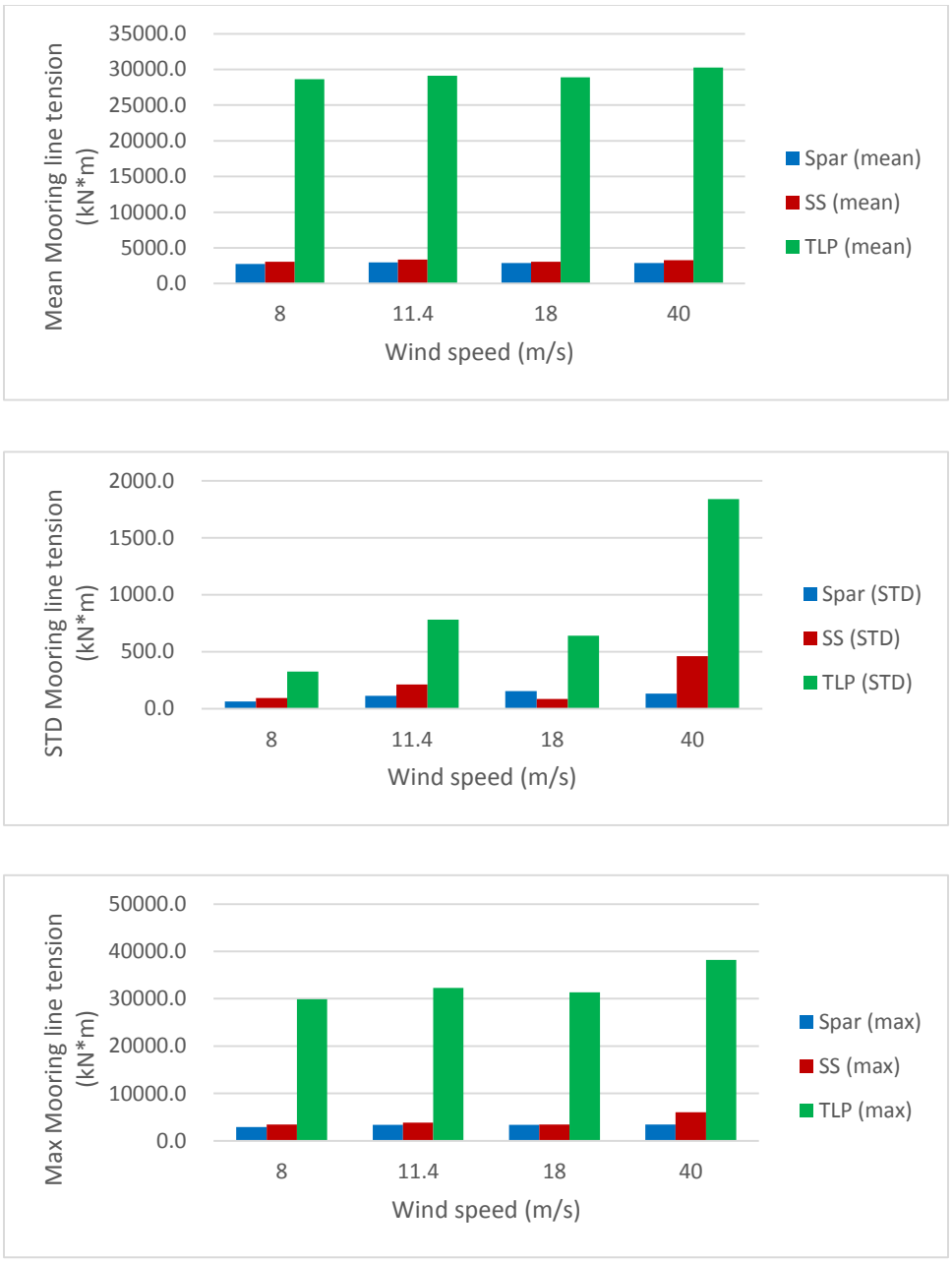

Figure 7-7: Mean value, standard deviation & max value of mooring line tension for the three concepts

8 CHAPTER VIII: CONCLUSION & FURTHER WORK

8.1 Conclusion

A preliminary design of a spar-type floater combined with a catenary mooring system to support the DTU 10MW reference wind turbine has been successfully performed. The hydrostatic and hydrodynamic behaviors of the spar platform are studied in details. Then the coupled dynamic analysis of the spar floater wind turbine is performed by the following process:

1. The aerodynamic and structural models are developed in AeroDyn and RIFLEX (SIMA) for the DTU 10MW wind turbine.
2. Then a complete spar wind turbine model (including mooring system) is developed in SIMO-RIFLEX-AeroDyn based on the preliminary design data.
3. Perform time-domain simulations of the spar wind turbine for specific wind and wave conditions.
4. Compare the dynamic responses of the spar concept with the other two concepts (TLP and semi-submersible).

It can be concluded from the thesis that it's theoretically feasible to use a spar-type platform to support the DTU 10MW RWT. More detailed conclusions are listed below:

- The floater design satisfies the intact stability requirement from DNV. In general, the stability is not a big problem for spar floater concept, due to the typical large draft and correspondingly lower center of gravity.
- The heave, roll and pitch natural periods of the spar are within a certain range to avoid the resonance problem and keep the wind turbine operating in a relatively stable condition. Due to the limited restoring stiffness from mooring system, the surge natural period obtained from free decay test is very large. The difference of pitch natural periods between Wadam and free decay test is due to the additional stiffness from the mooring system.

- According to extreme condition tests, the extreme mooring line tension as well as vessel offset are within a relatively safe range.

- In constant wind test, the application of Generalize Dynamic Wake (GDW) method can result in periodic resonant motions of the platform under rated wind speed, which will vanish by using the Blade Element/Momentum Theory (BEM).

- The controller in the SRA code was designed based on the land-based DTU wind turbine. For floating wind turbine at above rated wind speed, the blade pitch controller will excite the resonant motion of the platform, which could be reduced by changing the PI gains of the controller. However, for spar concept, the resonant oscillation cannot be avoided completely when wind speed is above rated, which means negative damping from the controller exists.

- The floating wind turbine's surge and pitch resonant motions are excited by turbulent wind combined with the blade-pitch controller, while heave motion is not affected. What's more, with the wind speed increasing, the influence from the controller becomes great, and the oscillation becomes large too. Under extreme conditions the influence of turbulent wind is relative small, all responses are wave dominated.

- The floater's motion has limited influence on the aerodynamic performance of the wind turbine, but will lead to larger blade and tower bending responses (mainly due to the platform pitch motion). Both blade and tower have the largest structural responses under operational condition with rated wind speed rather than the extreme condition.

- At rated wind speed the TLP has the largest mean power production, followed by spar and then SS.

- Spar has the largest surge oscillations among three concepts, so the spacing between spar-floater wind turbines should be greater in a wind farm. For pitch motion, the semi has larger mean value and standard deviation than others. And due to the taut

mooring system, all the motions for the TLP is much smaller as compared to the spar and the semi.

- The tension of TLP's tendon is almost 8 times higher than the mooring tension of spar and semi.

8.2 Further Work

Due to limitation of time, several phenomena have not been fully discussed or studied. In addition, some assumptions have been made during the study. Therefore, some further work may need to be done in future:

1. The tower used in this design is initially designed for land-based wind turbine, besides the tower height, more appropriate hub height and tower property should be adjusted for the floating wind turbine.

2. The yaw natural period of spar is 7.6 s, which is located in the wave excitation range and may lead to significant yaw motion. More studies of the spar yaw motion under different irregular wave conditions should be performed.

3. The limited number (10) and time length (4000s) of simulations can be the reason for the too small utilization factor in the ULS check of mooring tension. To get a more accurate result, at least 20 simulations with 3-hour time length should be performed to do the Gumbel-fitting.

4. During the constant wind test, the periodic resonant behavior at rated wind speed with Generalize Dynamic Wake (GDW) method is an interesting phenomenon. A further study of it can be performed.

5. For the turbulent wind test, the large oscillation of spar cannot be avoided entirely, even the PI gains of the controller is modified. However, for another two concepts, this phenomenon is less obvious. More detailed studies of it should be conducted in the future work.

CHAPTER VIII: CONCLUSION & FURTHER WORK

REFERENCES

[1] Twidell, J., and Gaudiosi, G., eds., 2009. *Offshore Wind Power*. Multi-Science Publishing Co. Ltd.

[2] Butterfield, S., Musial, W., Jonkman, J., Sclavounous, P., and Wayman, L., 2005. *Engineering challenges for floating offshore wind turbines*. In 2005 Copenhagen Offshore Wind Conference, no. NREL/CP-500-38776.

[3] Musial, W., Butterfield, S., and Ram, B., 2006. *Energy from offshore wind. Tech. Rep*. NREL/CP-500-39450, National Renewable Energy Laboratory.

[4] Laskow, Sarah (13 September 2011). *Hope Floats for a New Generation of Deep-Water Wind Farms*. Good Environment. Retrieved 12 October 2011.

[5] UMassAmherst. Early Offshore Wind Research. URL: http://www.umass.edu/windenergy/about/history/earlyresearch

[6] Musial, W.; S. Butterfield; A. Boone (November 2003). *Feasibility of Floating Platform Systems for Wind Turbines* (PDF). NREL preprint (NREL) (NREL/CP-500-34874): 14. Retrieved 10 September 2009.

[7] Dominique Roddier, Antoine Peiffer, Alexia Aubault, and Joshua Weinstein. *A Generic 5 Mw Wind float for Numerical Tool Validation & Comparison Against a Generic Spar*. In ASME 2011 30th International Conference on Ocean, Offshore and Arctic Engineering OMAE 2011, Rotterdam, The Netherlands, 2011.

[8] DNV-OS-J103. *Design of Floating Wind Turbine Structures*. Det Norsk Veritas, 2013.

[9] Jonkman, J. M. (2010). *Definition of the Floating System for Phase IV of OC3*. Golden, CO, USA: National Renewable Energy Laboratory.

[10] MARINTEK. *SIMO Theory Manual Version 4.0 rev 1*. Norwegian Marine Technology Research Insitute, Trondheim, Norway, 2012.

[11] *SESAM User Manual, GeniE v6.4. Concept design and analysis of offshore structures*. Det Norsk Veritas, 2013.

[12] Lindemark, T., Kamsvåg, F. & Valsgård, S. *Fatigue analysis of gas carriers*. RINA conf. on Design and Operation of Gas Carriers, London UK, 2004

[13] Torgeir Kirkhorn Vada. *Hydrodynamic analysis of offshore structures* (PDF). DNV Software, April 2013. URL: http://www.offshorenorway.no/business_presentation/Hydrodynamic%20analysis%20of%20offshore%20structures.pdf

[14] Munson, B. R., Young, D. F., and Okiishi, T. H., 2006. *Fundamentals of Fluid Mechanics*. Wiley.

[15] Faltinsen, O., 1990. *Sea Loads on Ships and Offshore Structures*. Cambridge University Press.

[16] DNV-OS-C301. *Stability and watertight integrity*. Det Norske Veritas, 2012.

[17] Marilena Greco. *Lecture Notes to TMR 4215: Sea Loads*. Department of Marine Hydrodynamics, NTNU, 2012.

REFERENCES

[18] C. Bak, et al. *Description of the DTU 10 MW Reference Wind Turbine*. DTU Wind Energy Report-I-0092 (2013)

[19] *SESAM User Manual, HydroD v4.7. Wave load & stability analysis of fixed and floating structures*. Det Norsk Veritas, 2014.

[20] DNVGL. *Frequency domain hydrodynamic analysis of stationary vessels – Wadam.* URL: https://www.dnvgl.com/services/frequency-domain-hydrodynamic-analysis-of-stationary-vessels-wadam-2412?gclid=Cj0KEQiAtMSzBRDs7fvDosLZmpoBEiQADzG1vGDuS3jIupq_eKAK2WCzpiclMa-hLp5zm9-cLbG3sW4aAqzk8P8HAQ

[21] A. Arapogianni and et. al. *Deep water - the next stop for offshore wind energy*. Technical report, EWEA, 2013.

[22] A. Ho, A. Mbistrova & G. Corbetta. *The European offshore wind industry - key trends and statistics 2015*. The European Wind Energy Association, EWEA.

[23] Qing Yu & Xiaohong Chen. *Floating Wind Turbines.* American Bureau of Shipping, May 2012.

[24] Johan M. J. Journee and W. W. Massie. *Offshore Hydrodynamics*. Delft University of Technology, 2001.

[25] J. Jonkman & W. Musial. *IEA Wind Task 23 Offshore Wind Technology and Deployment*. Golden, CO, USA: National Renewable Energy Laboratory, 2010

[26] Z. Gao and T. Moan. *Mooring system analysis of multiple wave energy converters in a farm configuration*. In Proc. of the 8th European Wave and Tidal Energy Conference (EWTEC), Uppsala, Sweden, 2009.

[27] DNV-OS-E301. *Position Mooring*. Det Norsk Veritas, 2013.

[28] Richard D'Souza. *State-of-the-art of spread moored systems for deepwater floating production platforms*. Offshore Magazine, 2002.

[29] J. Jonkman, S. Butterfield, W. Musial, and G. Scott. *Definition of a 5-MW Reference Wind Turbine for Offshore System Development*. Technical Report NREL/TP-500-38060, National Renewable Energy Laboratory, 2009.

[30] Qiang Wang. *Design of a Steel Pontoon-type Semi-Submersible Floater Supporting the DTU 10MW Reference Turbine.* Master of Science Thesis, European Wind Energy Master – EWEM, 2014.

[31] Matrin O.L. Hansen. *Aerodynamics of Wind Turbines*. *2nd edition*. Earthscan, London, 2008.

[32] Erin Bachynski. *Basic aerodynamics for wind turbines.* Lecture notes.

[33] Lin Li, Zhen Gao, and Torgeir Moan. *Joint Environmental Data at Five European Offshore Sites for Design of Combined Wind and Wave Energy Devices*. In 32nd International Conference on Ocean, Offshore and Arctic Engineering, OMAE2013, Nantes, France, 2013.

[34] IEC 61400-1. *Wind turbines - Part 1: Design requirements*. International Electrotechnical Commission, 2005.

[35] Karimirad M, Moan T. *Feasibility of the application of a spar-type wind turbine at a moderate water depth[J]*. Energy Procedia, 2012, 24: 340-350.

[36] Gao, Z. *Logarithmic decrement*. 2010.

REFERENCES

[37] T. Hordvik. *Design analysis and optimisation of mooring system for floating wind turbines*. M.Sc. THESIS of Department of Marine Technology, NTNU, 2011.

[38] Madjid Karimirad. *Stochastic Dynamic Response Analysis of Spar-Type Wind Turbine with Catenary or Taut Mooring Systems*. PhD thesis, Norwegian University of Science and Technology, Trondheim, Norway, 2011.

[39] MARINTEK. *SIMO User Manual Version 4.0 rev 0*. Norwegian Marine Technology Research Insitute, Trondheim, Norway, 2012.

[40] MARINTEK. *RIFLEX User Manual Version 4.0 rev 3*. Norwegian Marine Technology Research Insitute, Trondheim, Norway, 2013.

[41] Erin Elizabeth Bachynski. *Design and Dynamic Analysis of Tension Leg Platform Wind Turbines*. PhD thesis, Norwegian University of Science and Technology, 2014.

[42] Wenfei Xue. *Design and analysis of a spar floater supporting the DTU 10MW wind turbine*. Project work, Norwegian University of Science and Technology, 2015.

[43] F. G. Nielsen, T. D. Hanson, and B. Skaare. *Integrated dynamic analysis of floating offshore wind turbines*. In Proceedings of OMAE2006 25th Inter-national Conference on Offshore Mechanics and Arctic Engineering, 49 June 2006, Hamburg, Germany, 2006.

[44] Jason Mark Jonkman. *Influence of control on the pitch damping of a floating wind turbine*. Technical report, National Renewable Energy Laboratory, 2008.

[45] B. J. Jonkman and L. Kilcher. *TurbSim User's Guide: Version 1.06.00*. Technical report, National Renewable Energy Laboratory, 2012.

[46] Erin Elizabeth Bachynski. *SIMO-RIFLEX-AeroDyn (64-bit) and NRELControl_fixpitch.jar User Manual*. July, 2013.

[47] WAFO-group. WAFO - A Matlab Toolbox for Analysis of Random Waves and Loads - Tutorial for WAFO version 2.5. Math. Stat., Center for Math. Sci., Lund University, Lund, Sweden, 2011. URL: http://www.maths.lth.se/matstat/wafo

[48] Freris, LL. *Wind Energy Conversion Systems*. Prentice-Hall, New York, 1990.

REFERENCES

APPENDIX A

Illustration of the model in SRA analysis

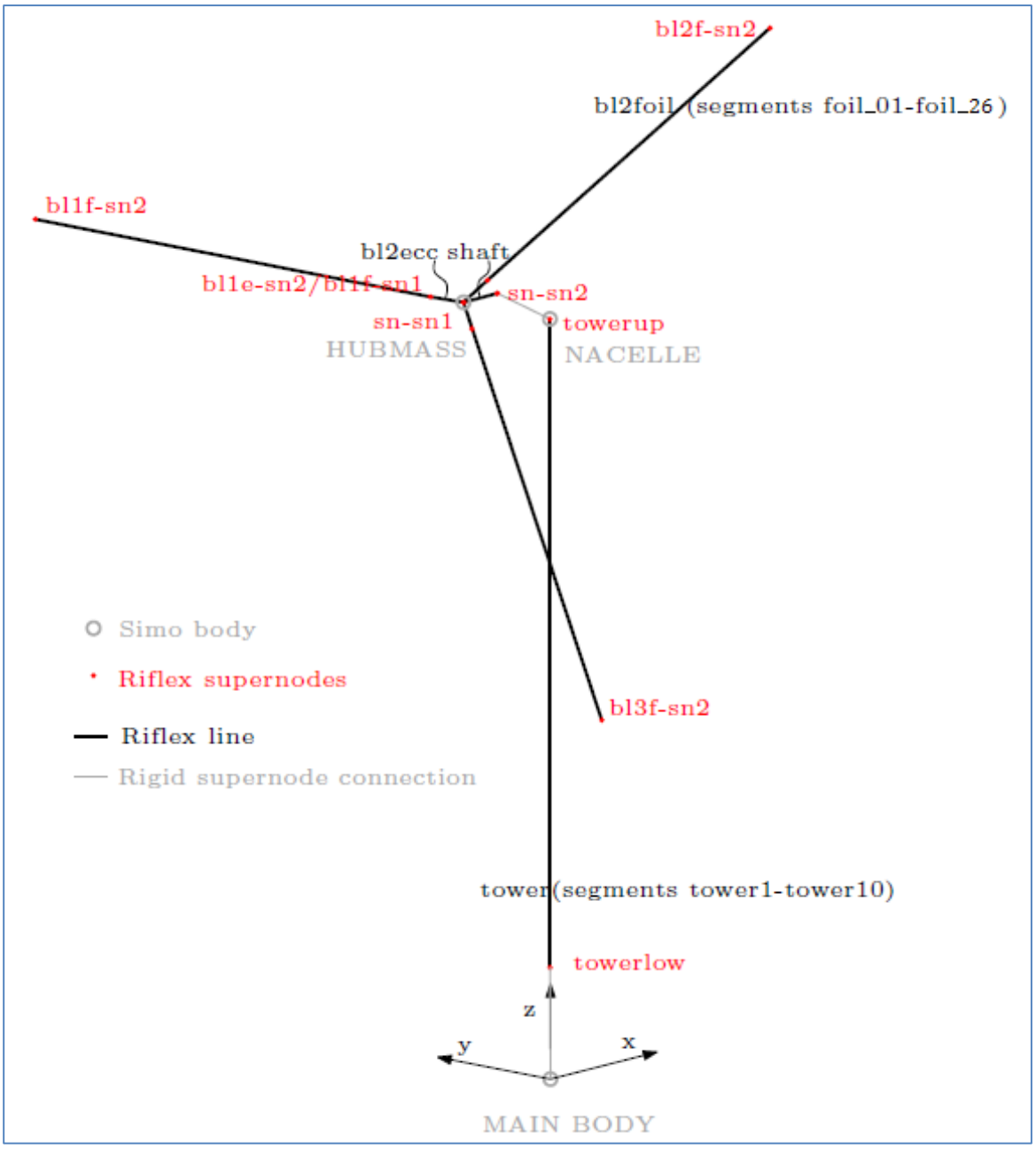

Figure A-1: RIFLEX lines, supernodes and SIMO bodies for spar-floater wind turbine. (Without mooring system) ([46])

APPENDIX A

APPENDIX B

Time series of turbulent wind test for all load cases

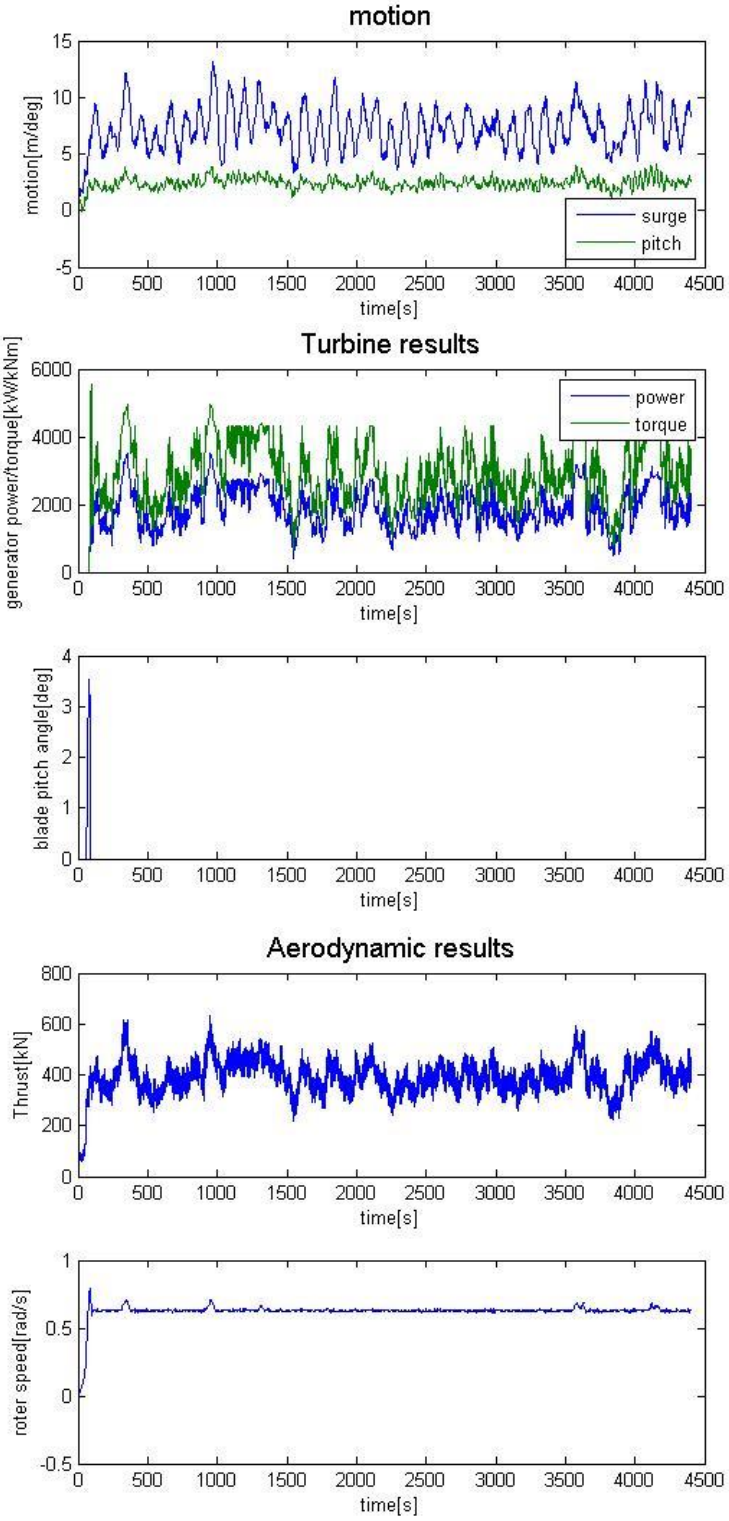

Figure B-1: Time series of turbulent wind test for load case 1

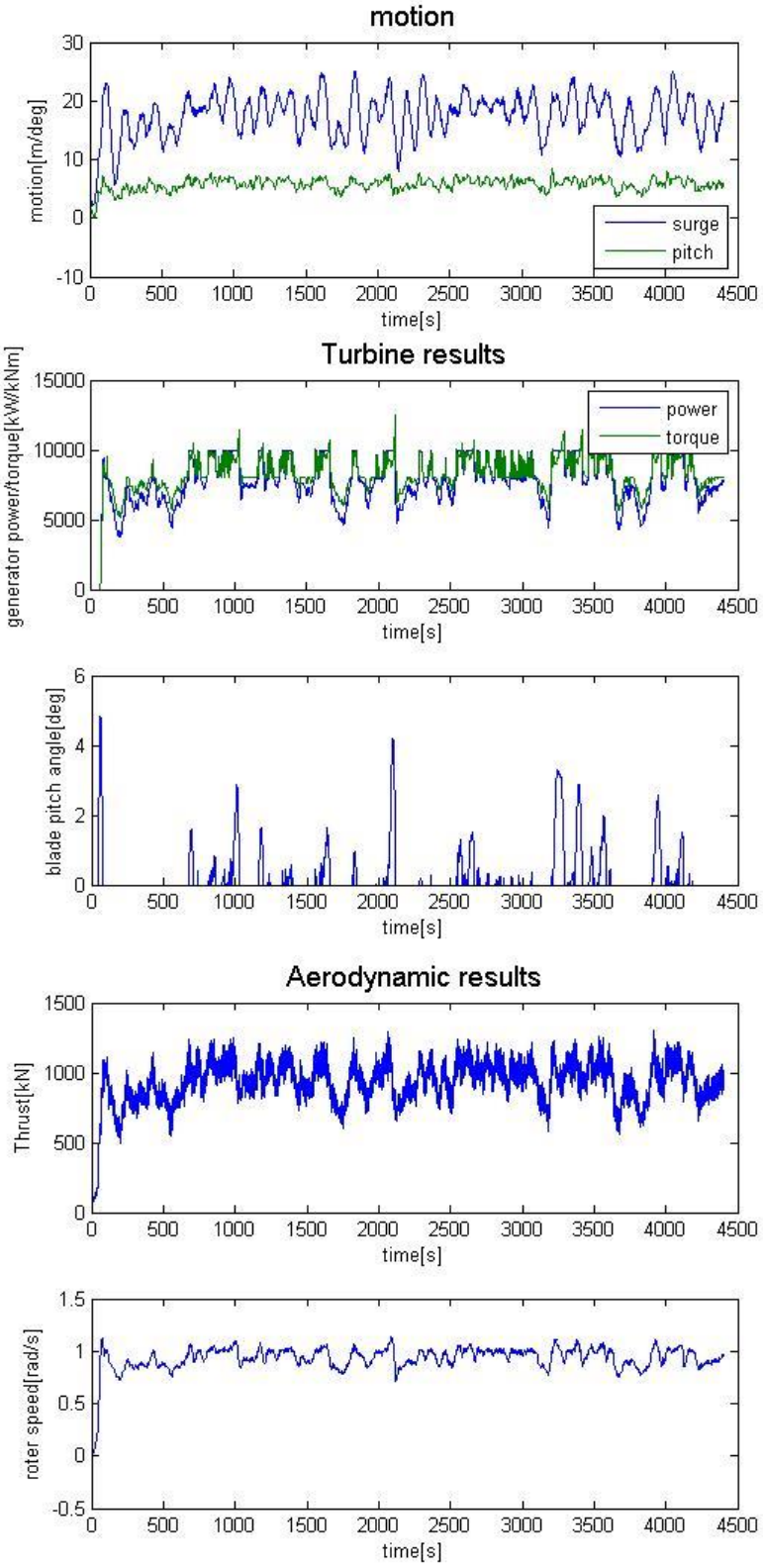

Figure B-2: Time series of turbulent wind test for load case 2

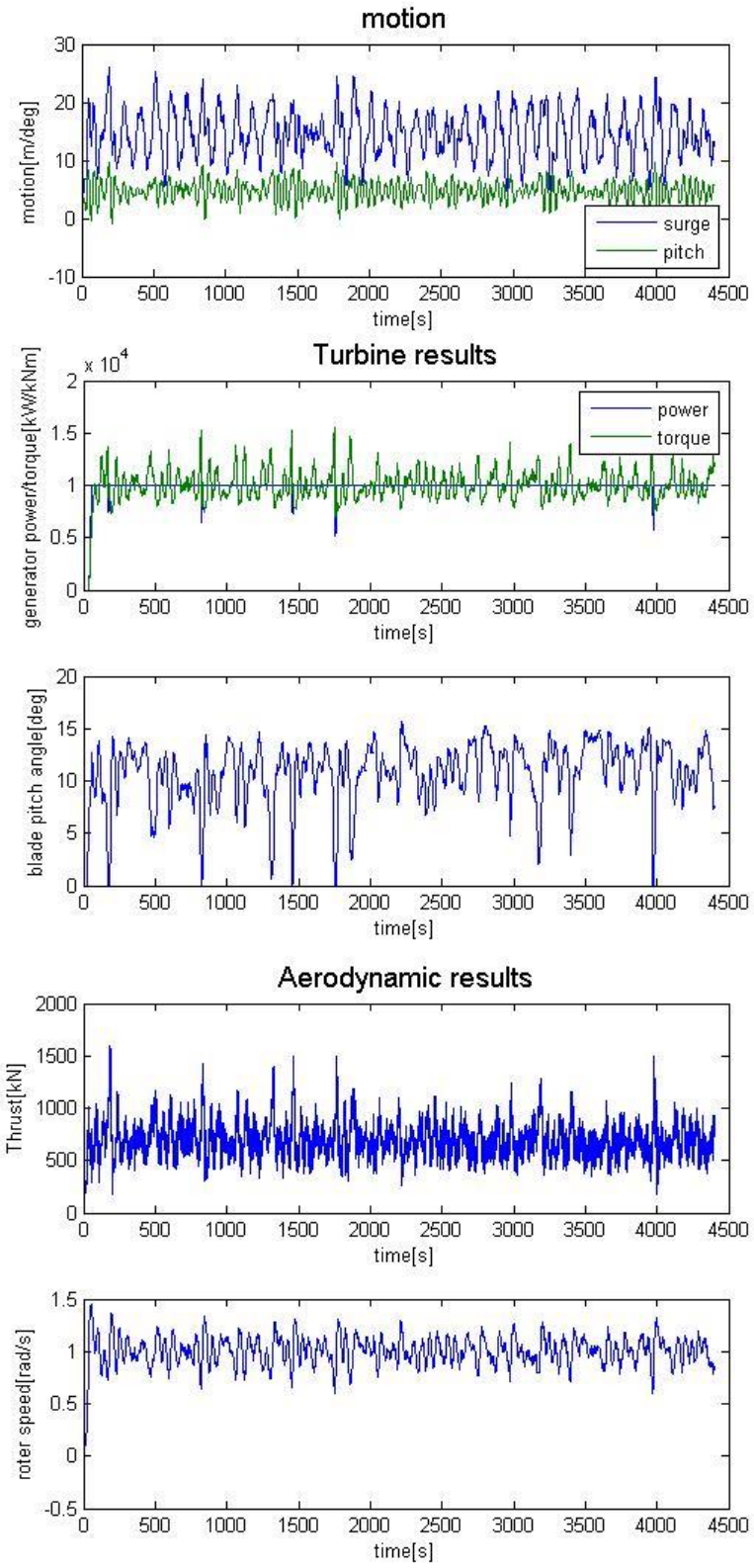

Figure B-3: Time series of turbulent wind test for load case 3

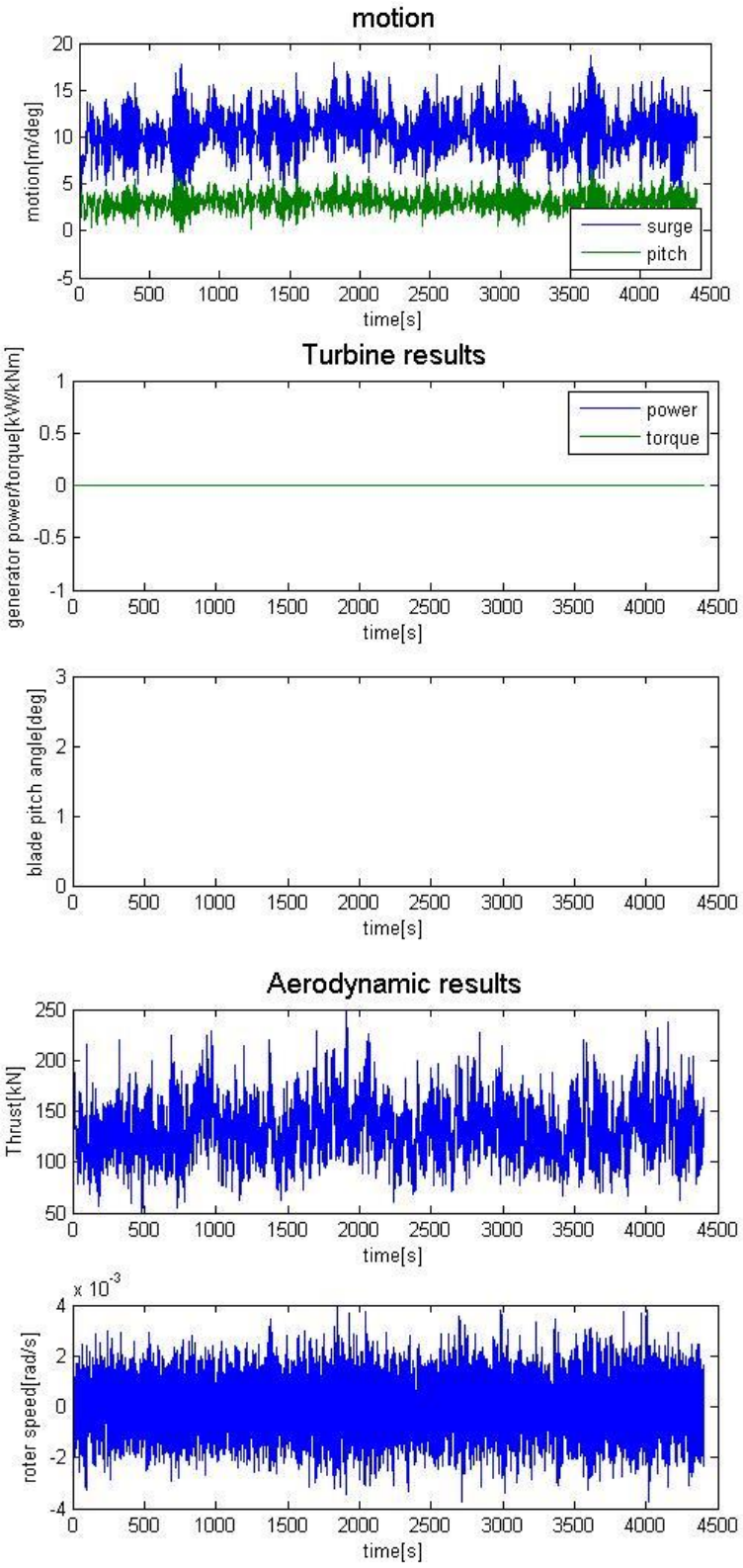

Figure B-4: Time series of turbulent wind test for load case 4

APPENDIX C

Response spectrum of all load cases

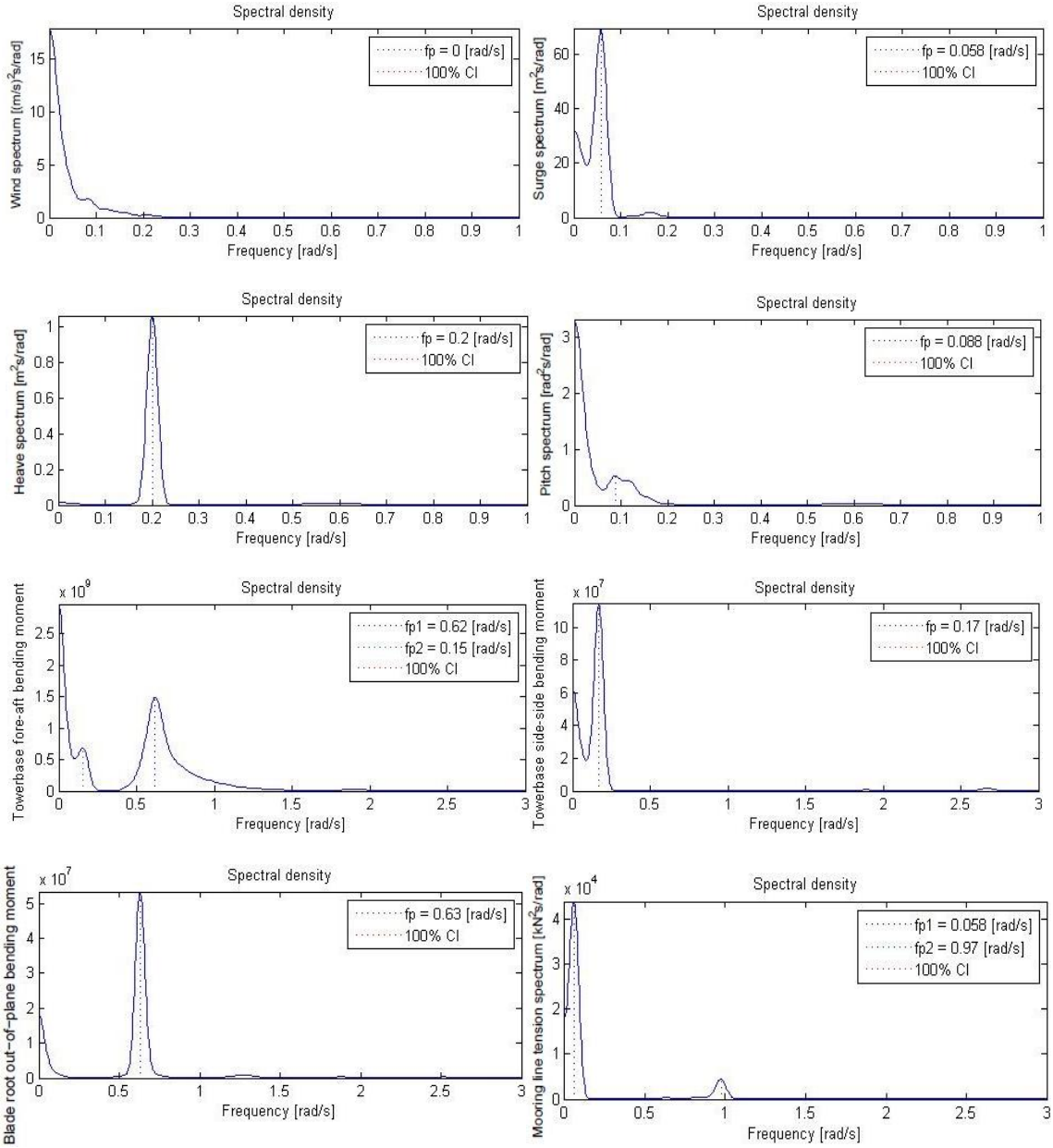

Figure C-1: Smoothed spectra of turbulent wind (first) and floater responses: surge(second), heave(third), pitch (fourth), towerbase fore-aft bending moment (fifth), towerbase side-side bending moment(sixth), blade-root out-of-plane bending moment (seventh) and mooring line tension (last) for load case 1

APPENDIX C

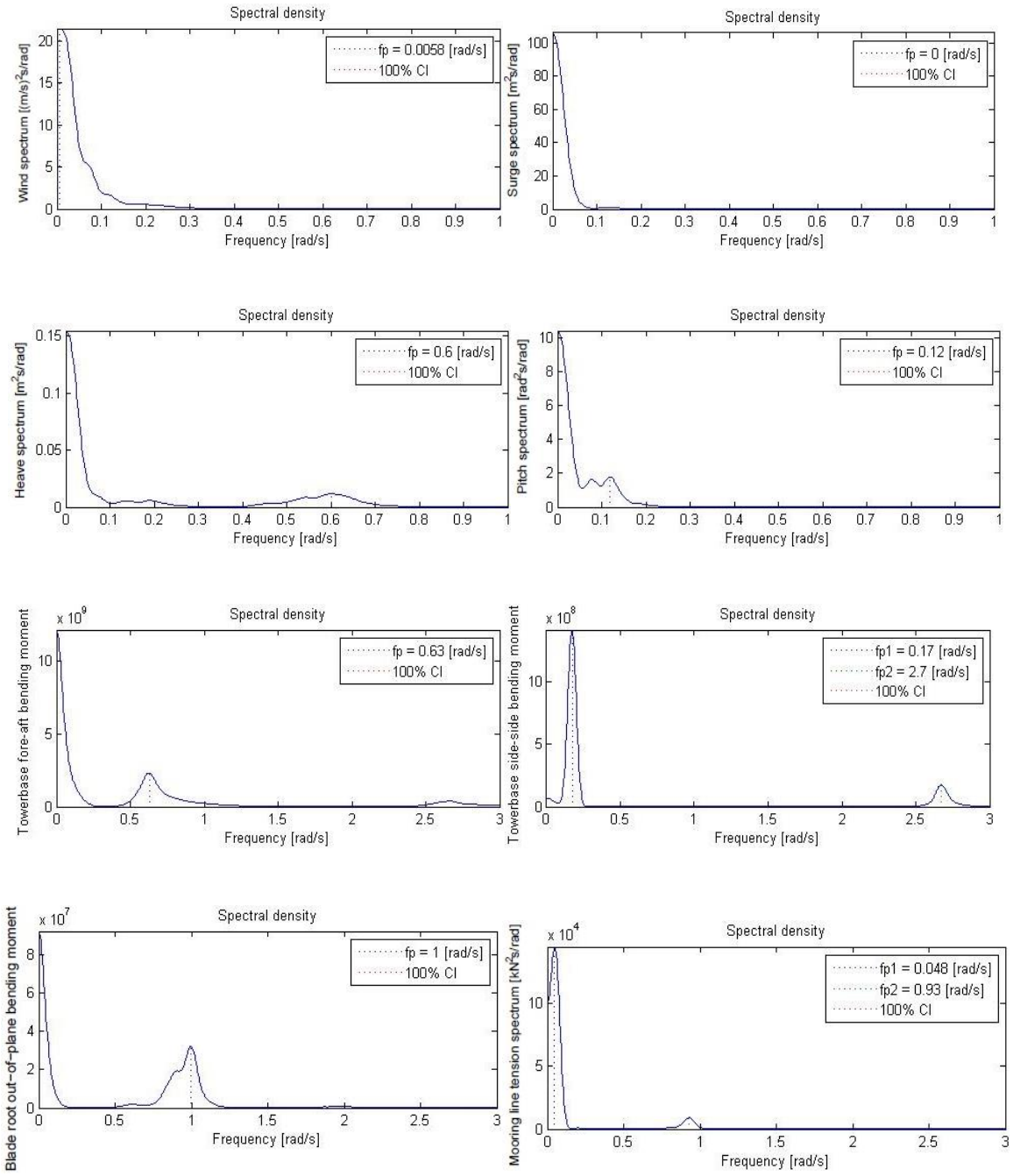

Figure C-2: Smoothed spectra of turbulent wind (first) and floater responses: surge(second), heave(third), pitch (fourth), towerbase fore-aft bending moment (fifth), towerbase side-side bending moment(sixth), blade-root out-of-plane bending moment (seventh) and mooring line tension (last) for load case 2

APPENDIX C

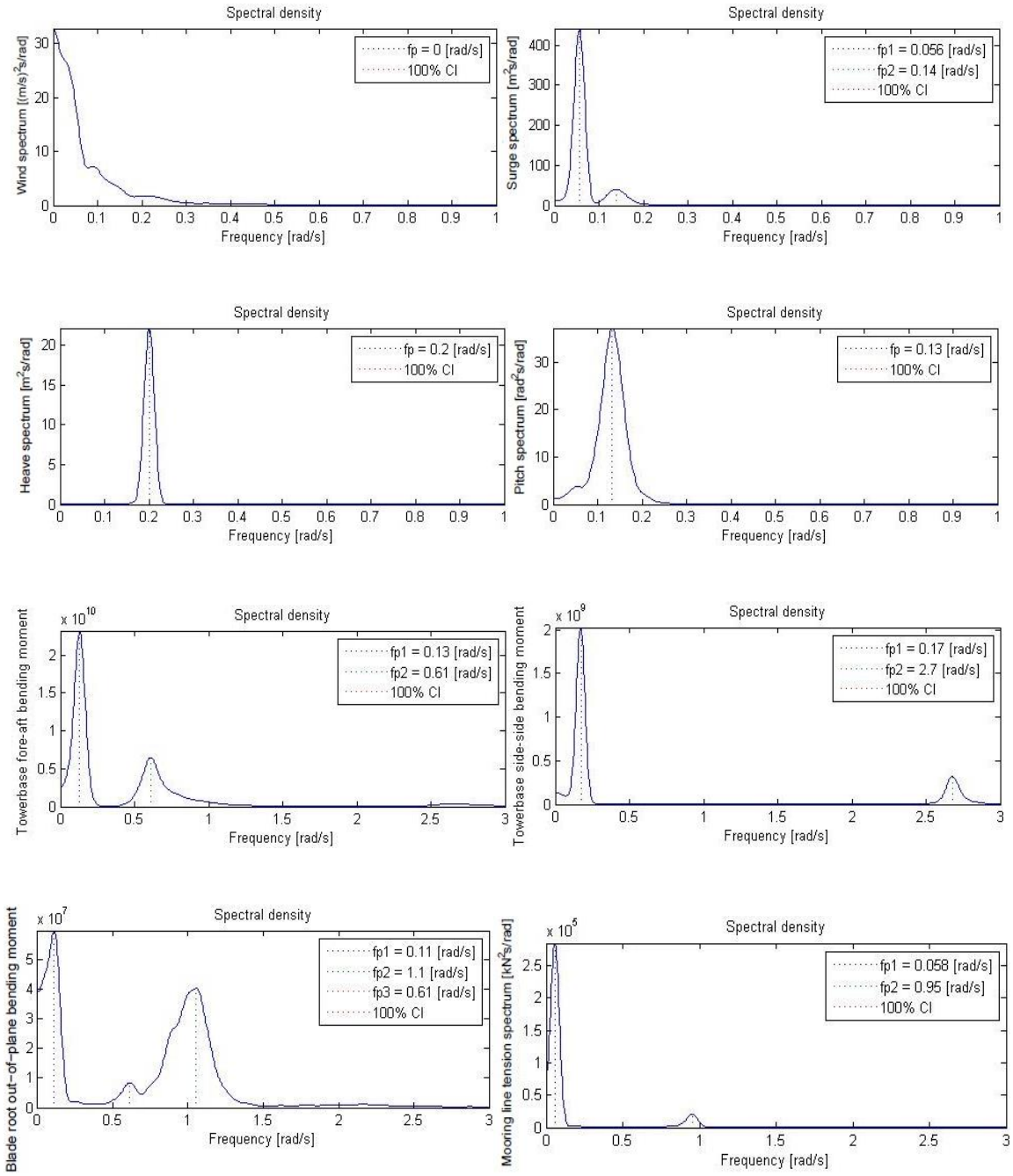

Figure C-3: Smoothed spectra of turbulent wind (first) and floater responses: surge(second), heave(third), pitch (fourth), towerbase fore-aft bending moment (fifth), towerbase side-side bending moment(sixth), blade-root out-of-plane bending moment (seventh) and mooring line tension (last) for load case 3

APPENDIX C

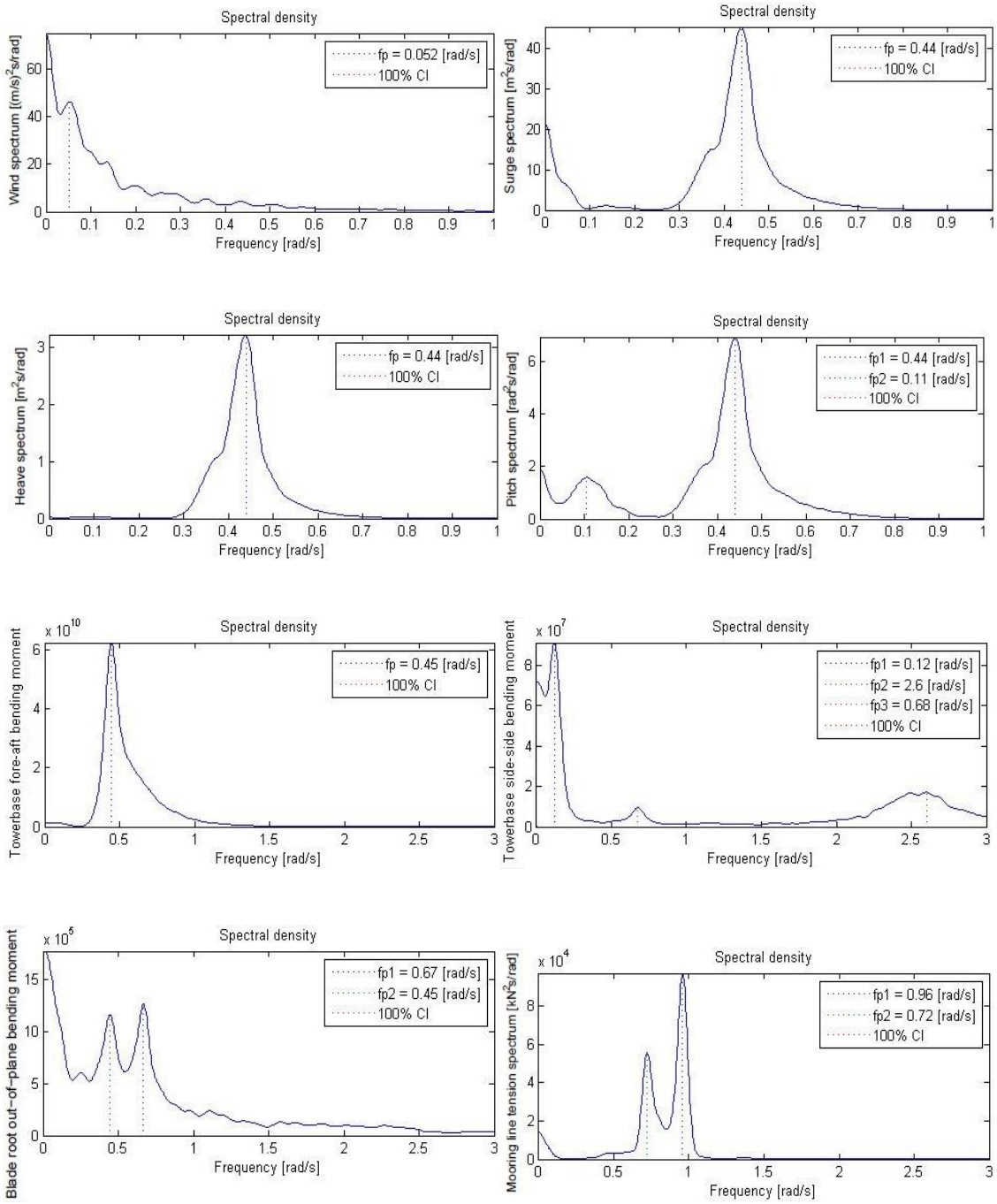

Figure C-4: Smoothed spectra of turbulent wind (first) and floater responses: surge(second), heave(third), pitch (fourth), towerbase fore-aft bending moment (fifth), towerbase side-side bending moment(sixth), blade-root out-of-plane bending moment (seventh) and mooring line tension (last) for load case 4